



UNIVERSITÀ DEGLI STUDI DI PALERMO

Denominazione Dottorato – Medicina molecolare e biotecnologie
Denominazione del Dipartimento di riferimento - Dipartimento di fisica e chimica
Settore Scientifico Disciplinare – Biofisica Molecolare e Bio-Imaging

Biophysical investigation on therapeutic proteins
(Chaperonins, Hsp60 and CCT/TRiC)
involved in human diseases

IL DOTTORE
DARIO SPIGOLON

IL COORDINATORE
CALOGERO CARUSO

IL TUTOR
MAURIZIO LEONE

EVENTUALE CO TUTOR
DONATELLA BULONE
PIER LUIGI SAN BIAGIO

Chapter I

Molecular chaperones	1
1.1- Introduction	1
1.1.1 Heat Shock Proteins.....	3
1.1.2 Group I and group II chaperonins (Cpns)	5
1.1.3 Working Mechanism of molecular chaperones	6
1.1.4 Modes of substrate binding.....	7
1.1.5 General principle of molecular chaperones in preventing aggregation	9
1.2- GroEL/Hsp60: Oligomeric structure and allosteric states	10
1.3- TRiC: The protein folding machine in Eukaryotes.....	12
1.4- Chaperonins as nanocarriers for intracellular drug delivery	17
1.5- Chaperone-like systems: Caseins.....	19
1.5.1 Structural features of caseins	20
1.5.2 Alpha-Casein as a Molecular Chaperone.....	21

Chapter II

Molecular chaperones involved in human diseases	23
2.1- Molecular Chaperones and protein misfolding diseases	23
2.1.1 Mechanisms of toxicity in aggregation diseases	26
2.1.2 Role of molecular chaperones in Alzheimer's disease	28
2.1.3 Mutations in molecular chaperones as the cause of human diseases	31
2.2- Molecular Chaperones and Oncogenesis	34
2.1.1 Hsp60: Contribution to oncogenesis	34
2.1.2 TriC/CCT: Contribution to oncogenesis	37
2.3- Molecular chaperones as potential drug targets	41

Chapters III

Materials and Methods	40
3.1- Materials	40
3.1.1 Chaperonins (Group I and II).....	40
3.1.2 Abeta amyloid.....	41
3.2-Methods & Characterization.....	42
3.2.1 Differential Scanning Calorimetry, DSC	42
3.2.2 Isothermal Titration Calorimetry, ITC	43
3.2.3 Circular Dichroism, CD	46
3.2.4 High Performance Liquid Chromatography, HPLC	47
3.2.5 Light Scattering, LS	48
3.2.6 Fluorescence Spectroscopy, FS	48
3.2.7 Atomic Force Microscope measurements, AFM	49

Chapter IV

(Dis)assembly and Structural Stability of chaperonins group I GroEL/Hsp60)	50
4.1 Aim and introduction	50
4.2 Results & Discussion	51
4.3 Conclusions	74

Chapter V

Hsp60, amateur chaperone in amyloid-beta fibrillogenesis75

5.1 Aim and introduction 75

5.2 Results & Discussion 76

5.3 Conclusions 84

Chapter VI

Diseases caused by defective molecular chaperones: Quantitative analysis of the impact of a pathogenic mutation on the CCT5 chaperonin subunit using a proxy archaeal ortholog (Dis)assembly and Structural Stability .86

6.1 Aim and introduction 86

6.2 Results & Discussion 88

6.3 Conclusions 99

Chapter VII

α -Casein Inhibits Insulin Amyloid Formation by Preventing the Onset of Secondary Nucleation Processes 100

7.1 Aim and introduction 100

7.2 Results & Discussion 101

7.3 Conclusions 109

Conclusions.....110

Acknowledgements	113
Papers and contributions during PhD	115
References	118
Appendix	147
A-1 FASTA sequences	147
A-2 Nucleotide effect on Pf-CD1, Pf-H, Pf-R	149
Figures	
Fig. 1.1 Cellular processes scheme regulated by molecular chaperones	2
Fig. 1.2 Schematic representation of the modes of substrate binding in Hsps	7
Fig. 1.3 Folding pathway of a typical oligomeric enzyme	9
Fig. 1.4 Structure of the GroEL oligomer and subunit	11
Fig. 1.5 GroEL functions as chaperone by collaborating with GroES	12
Fig. 1.6 Backbone alignment of the thermosome and GroEL apical domains	13
Fig. 1.7 Molecular architecture of TRiC/CCT	14
Fig. 1.8 Cryo-EM study of TRiC conformational cycle	16
Fig. 1.9 Scheme Models for the chaperone-assisted folding of newly synthesized polypeptides in the cytosol.	16
Fig. 1.10 Scheme of the basic strategy for ATP-responsive intracellular drug deliver	18
Fig. 1.11 Putative mechanism of action of α S-casein	21
Fig. 2.1 A scheme depicting common features of misfolding and aggregation in neurodegenerative misfolding diseases	24
Fig. 2.2 Protein misfolding and aggregation in different neurodegenerative diseases.	27
Fig. 2.3 Role of molecular chaperones in Alzheimer's disease	30
Fig. 4.1 Human Hsp60s compared to bacterial homolog GroEL	51
Fig. 4.2 Thermal unfolding of GroEL at different protein concentrations	54
Fig. 4.3 CD results for GroEL unfolding	55

Fig. 4.4 Thermal unfolding of p-mtHsp60 followed by DSC and CD	56
Fig. 4.5 Thermal unfolding of p-mtHsp60 at different protein concentrations	56
Fig. 4.6 Thermal unfolding of mtHsp60 followed by DSC and CD	57
Fig. 4.7 GroEL chromatographic separations at HPLC	58
Fig. 4.8 P-mtHsp60 chromatographic separations at HPLC	59
Fig. 4.9 Mt-Hsp60 chromatographic separations at HPLC at 25°C.....	59
Fig. 4.10 GroEL tetradecamer complex obtained by Pymol.....	62
Fig. 4.11 DSC thermograms for GroEL, fit with Tetradecamer-Heptamer-Monomer Dissociation/Unfolded Model	63
Fig. 4.12 DSC thermograms for p-mtHsp60, fit with Tetradecamer-Heptamer- Monomer Dissociation/Unfolded Model	63
Fig. 4.13 DSC thermograms for mtHsp60, fit with Tetradecamer-Heptamer-Monomer Dissociation/Unfolded Model	64
Fig. 4.14 Experimental DSC thermograms and best fit with Tetradecamer-Heptamer- Monomer Dissociation/Unfolded Model	66
Fig. 4.15 DSC thermogram for a sample of GroEL.....	67
Fig. 4.16 Thermal unfolding of GroEL subunits after thermally induced dissociation of oligomers.	70
Fig. 4.17 Thermal unfolding of Hsp60 subunits after dissociation thermally induced.	71
Fig. 4.18 GroEL ITC profiles.	72
Fig. 4.19 Hsp60 ITC profiles	72
Fig. 5.1 Simplified scheme of A β 1-40 amyloid aggregation in the absence and in the presence of Hsp60.....	76
Fig. 5.2 ITC Binding curves	79
Fig. 5.3 : Influence of Hsp60 on A β aggregation kinetics	80
Fig. 5. Morphology of A β species formed in the presence of Hsp60 under amyloid aggregation conditions	81
Fig. 5.5 Investigation on the influence of Hsp60 on oligomeric distribution of A β after incubation under amyloid aggregation conditions	82
Fig. 6.1 Differential scanning calorimetry thermograms for Pf-CD1 (red), Pf-H (green), and Pf-R (blue).....	88
Fig. 6.2 Differential scanning calorimetry at different protein concentrations	90
Fig. 6.3 Analysis of oligomer components by size-exclusion chromatography	91
Fig. 6.4 Circular dichroism. CD spectra	92
Fig. 6.5 Isothermal titration calorimetry of the oligomer assembly process; Isothermal titration calorimetry of ATP binding to the chaperonins	95
Fig. 6.6 Isothermal titration calorimetry for ATP binding to the chaperonins	96

Fig. 6.7 ATP effect on DSC thermograms.....	97
Fig. 7.1 ThT and tyrosine fluorescence intensity as a function of time	102
Fig. 7.2 Near UV CD spectra during fibril formation of insulin w and w/o α -cas .	104
Fig. 7.3 CD spectra at different T and DSC scan for insulin w and w/o α -cas	105
Fig. 7.4 ThT fluorescence intensity as a function of time	107

Tables

Table 2.1 Examples of human diseases caused by protein misfolding	23
Table 2.2 Different heat shock proteins, their localization, functions, and involvement in different neurodegenerative diseases	29
Table 4.1 Parameters of GroEL, mt and p-mtHsp60 heat denaturation	52
Table 4.2 Thermodynamic parameters obtained by fitting DSC thermograms of GroEL with THMDU model.....	62
Table 4.3 Thermodynamic parameters obtained by Fit with THMDU model for p-mtHsp60	65
Table 4.4 Thermodynamic parameters obtained by Fit with THMDU model for mtHsp60.....	65
Table 4.5 Comparison of the Thermodynamic parameters obtained by Fit with THMDU model for the three proteins	66
Table 4.6 BIC of different models for GroEL	73
Table 5.1 Binding parameter for $\alpha\beta$ and mtHsp60	78
Table 6.1 Thermodynamic parameters for heat denaturation	89
Table 6.2 Secondary structure composition and assignments from CD spectra for native and unfolded protein	92
Table 6.3 Thermodynamic parameters for the hexadecamer-monomer equilibria	95
Table 6.4 ATP-binding parameters obtained by the “one set of sites” model	97
Table 6.5 Thermodynamic parameters for heat denaturation in the presence of nucleotide.....	98

Abstract

Molecular chaperones are indispensable cellular components that assist folding and assembly of newly synthesized proteins, translocation of proteins across membranes, as well as refolding and degrading of misfolded and aggregated proteins. In the last few years, innovative therapeutic strategies targeting stability and functionality of chaperones have received great attention, particularly in the field of neurodegenerative diseases. Moreover, the growing number of diseases found linked to chaperone mutations, testifies to the importance of their role in the cellular protein-quality control mechanism. The investigation of the biophysical interactions between chaperones and specific proteins involved in diseases, including their structural and functional properties, are therefore a crucial step for both validating the chaperones' role in physiological and pathological state, and developing effective chaperones-based treatment approaches.

In the present PhD thesis work, we studied two representative examples of human molecular chaperones, Hsp60 and CCT/TRiC, appertaining to the class of the so-called "chaperonins" (Cpns). They are large, hollow, ATP-dependent nanomachines that promote correct folding of a wide range of proteins.

Heat shock protein (Hsp60) is a molecular chaperone that assists protein folding in mitochondria. Hsp60 can accumulate in the cytosol, in various pathological conditions (i.e., cancer and chronic inflammatory diseases). Here we studied its functional oligomeric equilibrium as compared to that of its well-known bacterial homolog GroEL. We also show that Hsp60 is capable of inhibiting the fibrillogenesis of A β peptide (the protein involved in Alzheimer's disease). The probable inhibition mechanism operating at molecular level is discussed.

CCT/TriC is a chaperon universally found in Archaea and eukaryotes. Several chaperonopathies linked to CCT loci are clinically well characterized and, for those due to non-lethal genetic mutations, there is considerable information on their mode of inheritance.

A protein model has been recently developed to investigate the mechanism of a crippling hereditary sensory neuropathy, due to a point mutation (His147Arg) in CCT5, one of the eight subunits of the human CCT. Here we report quantitative information on the loss of structural stability impaired by the pathogenic mutation.

Finally, we tested if an efficient inhibition of amyloid formation can be achieved by chaperone-like systems, like as α -Caseins, which is known to exert a stabilizing function through direct interaction (similar to small Hsps). In fact, the evaluation of the mechanism of chaperone-like activity proved helpful for better understanding the structural basis of the substrate binding in sHsps.

Chapter I

“Molecular chaperones”

1.1 Introduction

About 60 years ago, Anfinsen demonstrated that a polypeptide chains fold spontaneously to form native, compact protein structures whose three-dimensional conformation is determined by the amino acids sequence. This result was the basis of a fundamental principle of biology, the Anfinsen's paradigm [1.1], stating that the native structure of a protein is encoded in its primary structure. In vitro unfolding/refolding experiments of different proteins confirmed the general validity of the paradigm and led to the assumption that spontaneous self-assembly also happens inside the cell. A first caveat to this assumption was added in the 1980s when it was observed that new synthesized polypeptide chains bind transiently to a preexisting protein before they fold (Barraclough et al., 1980; Haas, 1983). Later it became clear that, in the cell, a large numbers of newly synthesized proteins requires the assistance of helper proteins that prevent aggregation and assist folding *in vivo*. In fact, cellular conditions of high protein concentration, temperature and ionic strength, are greatly different from the artificial environment of the test-tube, and may often favour protein aggregation over correct folding. A large group of unrelated protein families, named collectively “molecular chaperones, carry out several tasks: assisting a successful folding, signal transduction, assembling, targeting, transporting and degrading proteins within the cell [1.2 -1.8] (Figure 1.1). Their activities increase the yield of protein-folding reactions and aid recovery from cellular stress. In some particular conditions, they can also promote protein unfolding.

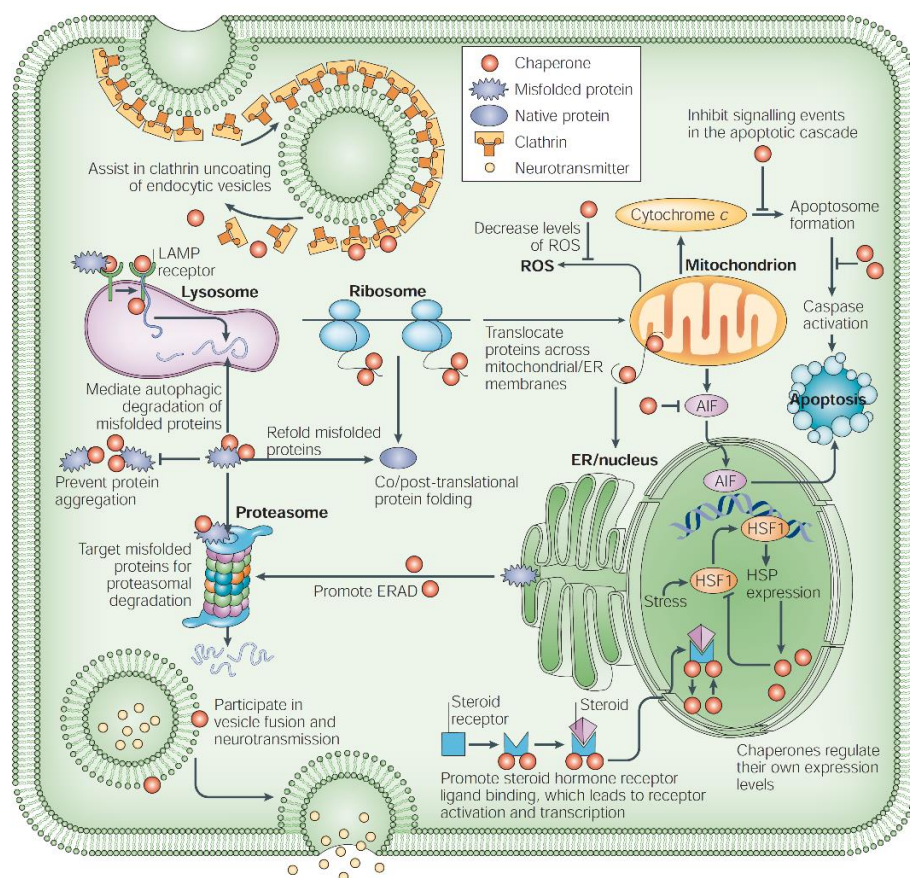


Figure 1.1 Scheme of cellular processes regulated by molecular chaperones. Besides facilitating protein folding and preventing protein aggregation, the molecular chaperones regulate several other cellular processes, such as autophagy, vesicle fusion, signal transduction, apoptosis and proteasomal degradation. Abbreviation/acronyms: AIF, apoptosis-inducing factor; ER, endoplasmic reticulum; ERAD, endoplasmic reticulum-associated degradation; HSF1, heat shock transcription factor 1; HSP, heat shock protein; LAMP, lysosomal-associated membrane protein; ROS, reactive oxygen species.

In addition to molecular chaperones, cells have evolved two mechanisms for the degradation of misfolded proteins, the ubiquitin-proteasome pathway and lysosome-mediated autophagy. Under certain conditions, when chaperones cannot repair misfolded proteins, chaperone-mediated targeting to the ubiquitin-proteasome system or to lysosomes results in selective degradation [1.2 – 1.5].

1.1.1 Heat Shock Proteins

Conditions of stress, including (but not limited to) temperature elevation, activate a cellular programme known as the heat shock response. It is characterized by a robust increase in the synthesis of some proteins that are crucial for recovery from stress-induced damages. These proteins, named “heat shock proteins” (Hsps), contribute to guarantee cell proteostasis by avoiding protein misfolding and aggregation. Further, they are involved in protein degradation and disaggregation of toxic aggregates by clearance mechanisms. As proteins, chaperones can be affected by mutations. The growing number of diseases found to be linked to chaperone mutations (see chapter 2), testifies the importance of their role in the cellular protein-quality control mechanism.

Almost all Hsps function as molecular chaperones, and they have been classified into six main families on the basis of their approximate molecular mass (in kDa): Hsp100, Hsp90, Hsp70, Hsp60, Hsp40 and the smallest Hsps (sHsps) with weight less than 40 kDa (See Paragraph 1.1.2). The main features of different members of Hsps family are briefly described in the following.

Hsp100

Heat shock protein 100 (Hsp100) chaperones are members of the AAA+ protein family (adenosine triphosphatases with diverse activities). They share a common ATPase domain and form large ring-shaped structures. In yeast, Hsp104, the best-characterized Hsp100, regulates protein aggregation, disaggregation and thermotolerance, but no mammalian homologue has been identified so far [1.9, 1.10].

Hsp90

Hsp90 chaperones are an essential component of the eukaryotic cytosol, where they stabilize misfolded proteins and regulate the activity of various signaling proteins, including steroid hormone receptors, tyrosine kinases, nitric oxide synthase and calcineurin [1.11, 1.12].

Hsp60

Hsp60 chaperones are heptameric complexes of identical subunits stacked back to back in a double-ring structure that contains a large central cavity in which protein folding is thought to occur. In eukaryotes, Hsp60 family members (also called Group I chaperonins) are found in the mitochondria, and cooperate with a cofactor of the Hsp10 family. A second class of chaperonins (Group II chaperonins) is found in the eukaryotic cytosol but has no Hsp10 cofactor. The best-characterized Group II chaperonin is TRiC, which comprises eight subunits per ring encoded by different genes. TRiC is thought to be crucial for the folding of actin and tubulin in the eukaryotic cytosol (we will focus on it in the next paragraph) [1.13].

Hsp70

Hsp70 chaperones (with Hsp40s, their co-chaperones) assist in the stabilization and folding of many substrates and are found in most cellular compartments. In humans, 11 genes that encode Hsp70 family members have been identified, including the constitutive cytosolic member heat shock cognate 70 (HSC70), the stress-induced cytosolic Hsp70, the endoplasmic reticulum-localized glucose-regulated protein 78 (GRP78) and the mitochondrial GRP75 (REF. 104). All Hsp70 proteins have a conserved amino-terminal ATPase domain that binds and hydrolyses ATP, and a carboxy (C) - terminal substrate-binding domain [1.14].

Hsp40

Hsp40 co-chaperones bind Hsp70 through a conserved J-domain and stimulate ATP hydrolysis, resulting in a conformational switch that closes the substrate-binding pocket of Hsp70 and facilitates the capture of non-native protein substrates. Hsp40s also bind protein substrates and target these substrates to Hsp70, enhancing the efficiency of the Hsp70/Hsp40 refolding cycle. Higher eukaryotes have many Hsp40 family members, whose differential expression or localization might regulate the substrate specificity of conserved Hsp70 family members [1.15–1-17].

Small heat shock proteins

sHsps have a molecular mass of less than 40 kDa and assemble into large, oligomeric structures that resemble a hollow ball. All sHsps contain a conserved,

C-terminal α -crystallin domain of about 100 residues that mediates oligomeric assembly. Similar to Hsp90 chaperones, sHsps transiently interact with and stabilize misfolded substrates, conceivably until the Hsp70/Hsp40 system can actively refold them [1.18].

1.1.2 Group I and group II chaperonins (Cpns)

The term chaperonin has been often used interchangeably with heat shock protein 60 (hsp60). In fact, the chaperonins (Cpns) are a ubiquitous family of sequence-related molecular chaperones, comprising oligomeric proteins of approximately 60 kDa subunit mass that are essential for protein folding either under normal or stressful conditions [1.19-1.21].

The Cpns are large, hollow, ATP-dependent nanomachines that promote correct folding of a wide range of proteins. They are involved in the ATP dependent folding and refolding of a wide variety of structurally unrelated proteins [1.22] and are essential for cell viability at all temperatures [1.23].

The Cpns are divided into 2 subgroups: group I and group II. Members of the GroEL family (or group I Cpns, Fig. 1.4) are found in eubacteria, mitochondria, and chloroplasts. The group II or TRiC (TCP-1 ring complex, see Fig. 1.7) protein family is found in the eukaryotic cytosol and in archaeobacteria (reviewed by Gutsche et al 1999). Of the group II members, only the archaeobacterial Cpns are heat shock inducible [1.24].

Although the two subfamilies have a similar cage-like structure, there are some important differences in the regions that bind substrate proteins (see Fig. 1.9). GroEL works with its co-protein GroES and uses an ATPase cycle to transiently create an enclosed, enlarged cavity in which protein folding takes place. No co-protein has been identified for the TCP1 subfamily, but an extra structural element built into the apical domain of TCP1 (see Fig. 1.8) may fulfil a similar role to GroES [1.25, 1.26]. GroEL (hsp60, cpn60) is a 14-mer of 58 kDa subunits in two rings, and its co-protein GroES (hsp10, cpn10) is a heptameric ring of 10 kDa subunits. The related eukaryotic cytosolic chaperonin, CCT (TCP1, TRiC), contains two rings of eight subunits, derived from eight related, but distinct, gene products [1.27]. In the archaeobacteria, the thermosome, or TF55, has two rings of eight or nine subunits, each composed of one or two subunit types [1.28]. The human CCT

(chaperonin containing TCP1) is a complex assembly of eight similar but non-identical [1.29-1.31] subunits which functions to fold non-native proteins through the alternative opening and closing of the two chambers. By contrast, many hyperthermophilic Archaea, including *Pyrococcus furiosus* and several groups such as *Pyrodictium*, *Methanopyrus*, and *Pyrobaculum spp* have a single group II Cpn subunit. The double ring of these archaea is therefore composed of 16 identical subunits and is minimally complex. Hyperthermophile Cpns are exceptionally stable in vitro [1.32, 1.33], affording a suitable model for studying oligomerization of group II Cpn such as the human CCT complex (see chapter 4, 4.3).

1.1.3 Working Mechanism of molecular chaperones

Although playing similar jobs, the structures and modes of action of the molecular chaperone families are remarkably diverse. Some families are very specific in their action, whereas others are very general. Some, but not all, use the binding and hydrolysis of ATP to control the release and binding of substrate proteins. Based on their mechanism of action, molecular chaperones have been divided into three functional subclasses [1.8]:

- **Folding chaperones** (e.g., DnaK and GroEL in prokaryotes, and Hsp60 and Hsp70 as well as the HspB group of Hsps including Hsp27 and HspB1 in eukaryotes) rely on adenosine triphosphate (ATP)-dependent conformational changes to mediate the net refolding/unfolding of their substrates.
- **Holding chaperones** (e.g. Hsp33 and Hsp31) bind partially folded proteins and maintain their substrates on their surface to await availability of folding chaperones.
- **Disaggregating chaperones** (e.g. ClpB in prokaryotes and Hsp104 in eukaryotes), which promote the solubilization of proteins that have become aggregated as a result of stress

1.1.4 Modes of substrate binding

Though few models of modes of substrate binding of the Hsps are available, the detailed information obtained so far are strongly interesting. The diversity of chaperone-polypeptide interactions is illustrated schematically in Figure 1.2.

The small Heat Shock Protein (sHsps) have an enormous capacity for substrate binding, but the structural basis of their binding remains unknown. Denatured proteins could bind sHsps by coating their surface, or perhaps could be encased inside a shell formed by the sHsp subunits. The latter possibility would require disassembly and reassembly of the sHsp oligomers. This sHsp class is not known to have ATPase activity and seems to act as a passive binder of non-native protein in response to cellular stress [1.34, 1.35].

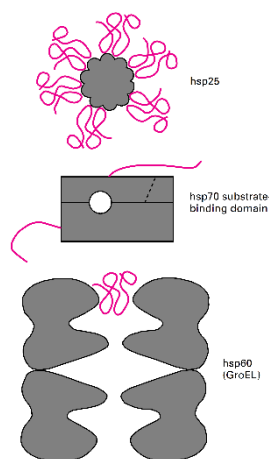


Figure 1.2 Schematic representation of the possible modes of substrate binding in Hsps (Hsp25, Hsp70 and Hsp60). Nonnative polypeptide is shown in pink and the various chaperone architectures in grey. For hsp25, the location of substrate binding is unknown. The substrate could be enclosed in a shell of protein subunits rather than coating the outside, as shown here.

DnaK (Hsp70, BiP) is the *Escherichia coli* homologue of a large and important class of Hsps present in the cytosol, endoplasmic reticulum, mitochondria and chloroplasts [1.36]. It acts in concert with co-proteins DnaJ (involved in substrate binding and presentation) and GrpE (a nucleotide-exchange factor). Crystal structures of both the ATPase domain, which is structurally related to actin and hexokinase [1.37], and the substrate-binding domain [1.38] are separately known. The latter shows a remarkable brick-shaped domain permeated by a hole through

which the bound peptide runs. A α -helix running across the top of this hole is proposed to serve as a hinged lid, allowing entry and exit of the polypeptide-chain segment that binds in a completely extended conformation. ATP binding and hydrolysis control release and binding of the substrate by an unknown mechanism involving interactions between the two domains and DnaJ.

In contrast with the previous two examples, hsp60 (GroEL, cpn60) forms a large cage-like structure with two rings of seven subunits, each surrounding a central cavity.

The protein-folding intermediate binds to hydrophobic sites lining these cavities. The hsp100 family has a hexameric ring structure [1.39, 1.40] and it seems plausible that the unfolded substrate might also bind in the central cavity in this case. Some of these ATPases associate with multi-subunit proteases and play a role in protein degradation, as well as in thermos-tolerance. They have the capacity to dissociate protein aggregates; expression of yeast hsp104 at normal levels is required for conversion and maintenance of the psi^+ phenotype, a prion-like phenomenon involving the aggregation of the translation termination factor sup35 [1.41]. Hsp90 interacts with a range of steroid receptors and kinases by an as-yet-undetermined mechanism. The recent crystal structure of the N-terminal domain has revealed an ATP-binding site and an unexpected similarity to the fold of DNA gyrase [1.42].

The endoplasmic reticulum proteins calnexin and calreticulin are chaperones that act more specifically by binding to given oligosaccharides and performing quality control during the processing of glycoproteins [1.43]. Peptidylprolyl isomerase (PPI) and protein disulphide-isomerase (PDI) catalyse the *cis-trans* isomerization of proline residues and the isomerization of disulphide bonds, respectively. These are potentially rate-limiting steps in the folding process and several examples are now known in which their activities are required for successful protein folding [1.44, 1.45].

Finally, the pro-sequences of certain proteins act as intramolecular chaperones, facilitating the acquisition of the native state before being removed by processing to yield the active protein [1.46]. It should be noted that this is a case of specific catalysis of a folding step, as presumably the pro-sequence has evolved to stabilize the transition state in the folding reaction of the main protein chain. This is very

different from the concept of a general molecular chaperone, where stabilization of transition states is implausible for a wide range of substrates with different folds.

1.1.5 General principle of molecular chaperones in preventing aggregation

As stated above, one of the common features of the molecular chaperone family is an interaction with non-native proteins, but how can this basic affinity be translated into an increase in the efficiency of a typical folding reaction (see Scheme Fig. 1.3). If the intermediates of a protein-folding reaction are sequestered by the addition of a molecular chaperone, this passive binding event alone can improve the yield of that folding reaction as long as two criteria are met: first, that the stability of the interaction between chaperone and folding intermediate is not greater than the free energy of folding, and secondly, that the loss of yield in the folding reaction is due to aggregation.

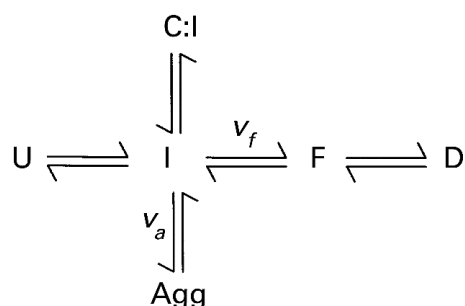


Figure 1.3 Folding pathway of a typical oligomeric enzyme. Unfolded polypeptide chains (U) undergo a rapid hydrophobic collapse to form a compact folding intermediate (I). This folding intermediate folds productively (with a rate v_f) to form a folded, native-like monomer (F), which then dimerizes to give the native active enzyme complex (D). However, losses in the productive folding reaction arise from non-specific association (with rate v_a) of I to form aggregates (Agg). In the presence of a molecular chaperone (C), a third possible fate for the folding intermediate exists: it can form a complex with the molecular chaperone (C:I) with an affinity defined by the dissociation constant (K_d) for this interaction.

If the rate of a multimolecular aggregation process (v_a) is more dependent on the concentration of intermediate [I] than the rate of productive unimolecular protein folding (v_f), the yield of folding is increased by the reversible formation of a chaperone-intermediate (C-I) complex that lowers the concentration of folding

intermediate in solution, i.e. if $v_f=k_f[I]$ and $v_a=k_a[I]^n$, then α , the partition coefficient between folding and aggregation, is given by:

$$\alpha = v_f/v_a = k_f/k_a \cdot [I]^{n-1}$$

If the value of $[I]$ is high, then $\alpha \rightarrow 0$ and aggregation is favoured. Conversely, if $[I]$ is low, then $\alpha \rightarrow 1$ and folding is favoured. Implicit in this analysis, however, is the fact that there must be a concomitant decrease in the observed rate of folding because of this drop in folding intermediate concentration [1.47]. If an equilibrium between bound and free states exists, then under conditions of heat shock or other cellular stress the amount of denatured protein will increase and the equilibrium will be shifted towards the bound state. Thus proteins would be stabilized by molecular chaperones in these conditions. When conditions improve, any non-native proteins that are released will have a better chance of reaching the native state, and the equilibrium will shift toward the free state.

Chaperones also deliver proteins to proteolytic complexes [1.48], presumably a mechanism for disposing of damaged proteins that cannot reach the native state, or proteins that have been targeted for proteolysis as part of programmed turnover or cell death.

1.2 GroEL/HSP60 oligomeric structure and allosteric states

The best known molecular chaperone is *Escherichia coli* GroEL. It is formed by two back-to-back stacked rings of seven subunits that alternately serve as containers for the folding of other proteins subunits. The structures of the GroEL oligomer and its various complexes have been determined by X-ray crystallography [1.49, 1.50] and by electron cryo-microscopy [1.51]. Figure 1.4 shows the crystallographic structure of both the oligomer and a single subunit. The oligomer is cylindrical and formed from two heptameric rings stacked back-to-back. Each ring encloses a central cavity and there are holes in the sides of the structure. The interface between the two rings is flat, except for the two contacts (numbered 1 and 2) formed by the base of each subunit with its neighbours in the opposite ring. On the right is shown the backbone structure of the outlined subunit with the three domains colour-coded. The termini are located close together in the equatorial domain (blue), which forms the inter-

ring and most of the intra-ring contacts. The inter-ring contacts are formed by salt bridges, labelled C1 and C2. This domain also contains the nucleotide-binding site, and an adenosine 5'-[γ -thio-triphosphate (ATP[S]) molecule is shown bound in the site [1.50]. An exposed region of anti-parallel chains connects the equatorial domain to the intermediate domain. This connecting region is a site of hinge rotation, labelled hinge 1. At the top of the intermediate domain, another hinge region (hinge 2) connects to the apical domain, which contains the binding sites for polypeptide substrates and for GroES [1.52].

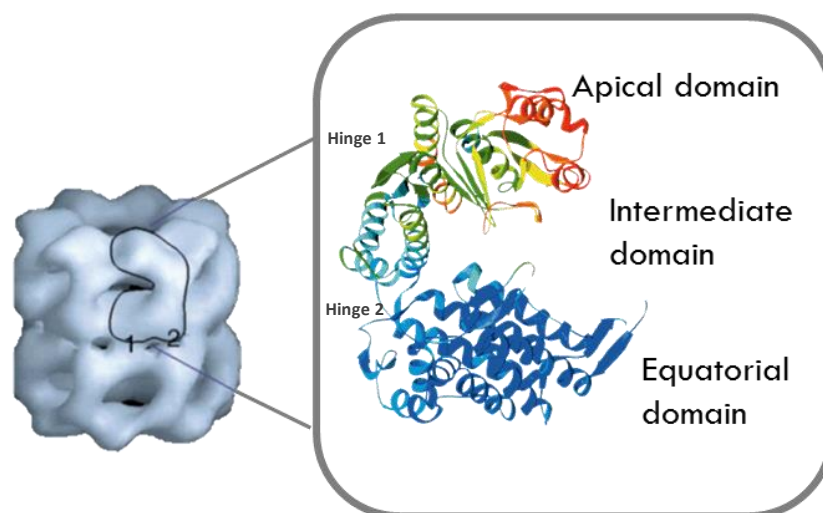


Figure 1.4 Structure of the GroEL oligomer and subunit: Shown on the left is the crystal structure of GroEL filtered to 2.5 nm resolution, showing the double-ring structure and the location of an individual subunit within the oligomer. Shown on the right is the backbone trace of the GroEL subunit as described in the text.

Together with ATP and a co-protein GroES, it constitutes a molecular machine that binds non-native polypeptides and facilitates their refolding in an ATP-dependent manner (Fig. 1.5). The action of the ATPase cycle causes the substrate-binding surface of GroEL to alternate in character between hydrophobic (binding/unfolding) and hydrophilic (release/folding). ATP binding initiates a series of dramatic conformational changes that bury the substrate-binding sites, lowering the affinity for non-native polypeptide [1.7].

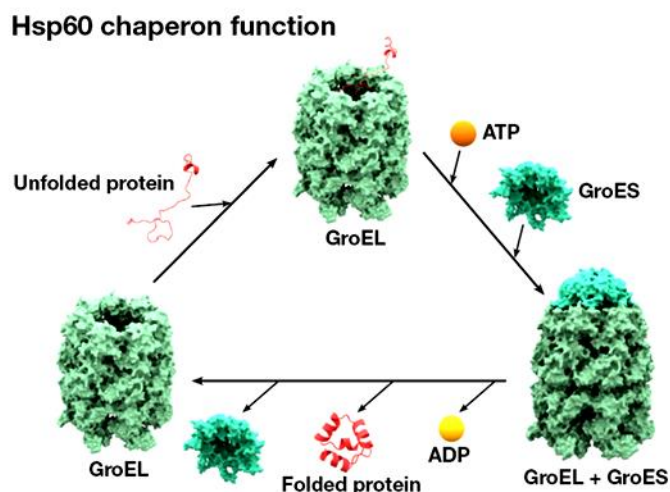


Figure 1.5 GroEL functions as chaperone by collaborating with GroES. (1) Non-native protein binds to the trans ring of a GroEL-GroES complex. End-to-end exchange of GroES (possibly through a symmetric complex with a GroES molecule bound to each of the GroEL rings) results in the encapsulation of the protein substrate in the cis cavity. (2) In the presence of ATP, productive folding of protein substrates can occur in the cis cavity. (3) Release of GroES and substrate protein (whether folded or not) results in the regeneration of the acceptor complex for non-native protein.

1.3 TRiC: The protein folding machine in Eukaryotes

An interesting variant of the GroEL structure is seen in the CCT subfamily, exemplified by the archaeobacterial thermosome. This chaperonin has two rings of eight subunits each, and rather low sequence homology with GroEL. The only detectable homology is in the equatorial domain, particularly around the ATP-binding site, whereas the apical domain appears to be quite divergent [1.53]. However, the crystal structure of the apical domain reveals that, despite the lack of sequence homology, it has a similar overall fold except for one unique and prominent feature (Figure 1.6) [1.54]. In the region that forms the hydrophobic binding site in GroEL, the thermosome apical domain has a long extension, which forms a α -helical protrusion. This extension is highly conserved in the TCP1 family and contains hydrophobic residues proposed to act as substrate-binding sites. The extensions would arch over the central channel to form a substrate-binding surface very different from that in GroE chaperonins [1.54]. In fact, the formation of a

closed lid has been observed in the recently determined crystal structure of the intact thermosome hexadecamer [1.55]. This difference is consistent with the observed differences in specificity of TCP1 and GroE chaperonins, for example, in the folding of luciferase. Figure 1.6 shows an overlay of the GroEL and thermosome apical domain folds.

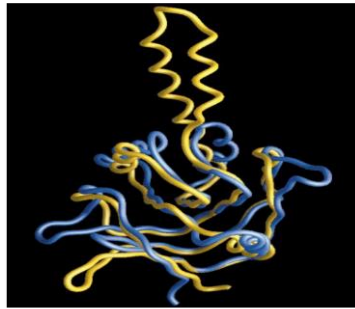


Figure 1.6 Backbone alignment of the thermosome and GroEL apical domains. The thermosome (gold) and GroEL (blue) apical domains are aligned, highlighting the helical extension present in the thermosome. The fold homology is clear in the β -sheet core of the domain. The structures were aligned by selecting equivalent residues in the conserved β -strands and performing a rigid body fit with Quanta (Molecular Simulations). The Figure was produced with GRASP [1.55].

TRiC (T-complex protein-1 ring complex, also known as CCT) is an essential 1 MDa eukaryotic chaperonin. It has a double-ring structure with a central cavity in each ring [1.56]; each ring is composed of eight homologous but distinct subunits (CCT 1–8) [1.57, 1.58], arranged in a specific order [1.59, 1.60] (Figure 1.7A).

Each subunit is ~60 kDa and consists of three domains—apical, intermediate, and equatorial (Figure 1.7B). While the sequence of the equatorial and intermediate domains is conserved, that of the apical domains is highly diverged among the eight subunits [1.61]. Multiple structures have been reported for TRiC [1.62- 1.64] using x-ray crystallography (Figure 1.7A) and single particle cryo-EM.

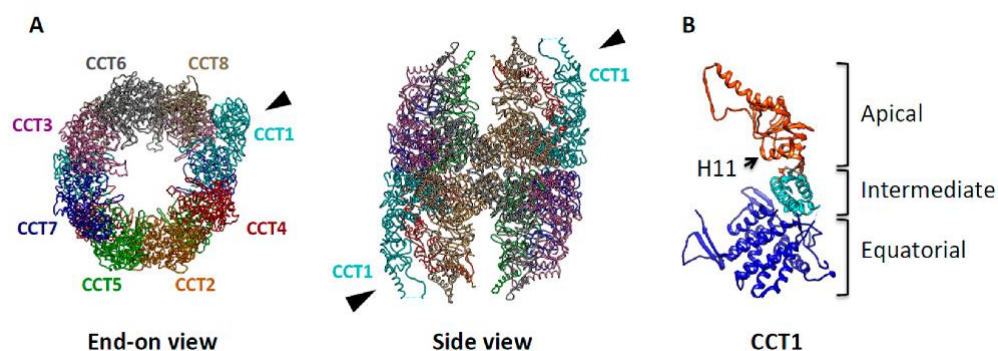


Figure 1. 7 Molecular architecture of TRiC/CCT. (A) The end-on and side views of the X-ray crystal structure of TRiC, modified from PDB ID 2XSM, show that TRiC is a double-ringed structure composed of eight homologous but distinct subunits (CCT1–8). Each subunit is shown having a different color with the specific subunit order indicated. The black arrowhead indicates CCT1, which has unique asymmetrical features; (B) The X-ray structure of CCT1 is shown as a representative subunit. Helix-11 (H11), the putative substrate recognition site is indicated by the arrow.

TRiC assists productive folding of substrate proteins by undergoing conformational changes that are ATP-dependent [1.65-1.68]. The structures of the TRiC in the presence of varied nucleotide conditions have been solved using cryo-EM at intermediate resolution, which have led to an improved understanding of the large conformational changes that occur upon nucleotide binding and hydrolysis [1.69, 1.70]. The conformational cycling begins with the binding of ATP and a transition of the complex to the closed conformation required for ATP hydrolysis to bring the lid helices into close proximity. Opening of the lid occurs in conjunction with releasing ADP from the active site. The complex can exist in an asymmetrical conformation with one ring closed and one open even during ATP cycling conditions, suggesting an inter-ring allosteric model mediated through a two-stroke mechanism (see Fig. 1.8) [1.71]. However, the allosteric communication that occurs between the rings is not well understood.

Although the mechanisms of TRiC-substrate recognition, binding, and folding still remain under investigation, it is known that each of the subunits can recognize different polar and hydrophobic motifs within substrate proteins [1.72]. TRiC

interacts with approximately 10% of the proteome and its function is absolutely essential for viability [1.73]. TRiC substrates have been identified by multiple groups [1.74, 1.75] and, recently, Yam and colleagues determined ~200 cellular TRiC substrates using proteomic global approaches based on immunoprecipitation and mass spectroscopy [1.73]. From the secondary structure analysis of the substrates, TRiC has been shown to mediate the folding of a number of β -sheet rich proteins, including telomerase cofactor TCAB1 [1.76], the cell cycle regulators CDC20 and CDH1, as well as members of the STAT family of transcription factors [1.77].

However, the full repertoire of TRiC substrates remains underdetermined, in part, because specific motifs characteristic of TRiC substrates have not been identified. As a general principle, TRiC substrates have a higher potential to aggregate. Substrate proteins also are often large, have extended hydrophobic stretches, or are involved in multi-protein complexes [1.78]. The ability to assist such a wide range of proteins with diverse folds and sequence properties raises the potential for multiple mechanisms through which TRiC can recognize substrates and promote their folding.

Recent *in vitro* work has illuminated the molecular determinants of substrate interaction with the apical domains of TRiC subunits. Using known subunit-substrate pairs, Joachimiak and colleagues have demonstrated that substrate motifs are recognized by a cleft formed between Helix 11 (H11) and a proximal loop in the TRiC apical domains (Figure 1.7B). In addition, the subunit arrangement recently has been identified with a combinatorial approach that employed X-ray crystallography and chemical crosslinking mass spectrometry as well as bioinformatics [1.79] (Fig. 1.7A). The subunit arrangement of TRiC leads to the spatial partitioning of subunits with different chemical properties. Specifically, subunits are segregated by their ATP-binding affinities (High affinity subunit: CCT1,2,4,5, Low affinity subunit: CCT3,6,7,8) [1.80]. Thus, the hetero-oligomeric nature of TRiC generates chemically asymmetric features, which likely provide the basis for the unique ability of TRiC to fold specific substrates [1.81]. The meaning of this asymmetric nucleotide usage and allosteric mechanism in the context of protein folding remains an area of ongoing research [1.82].

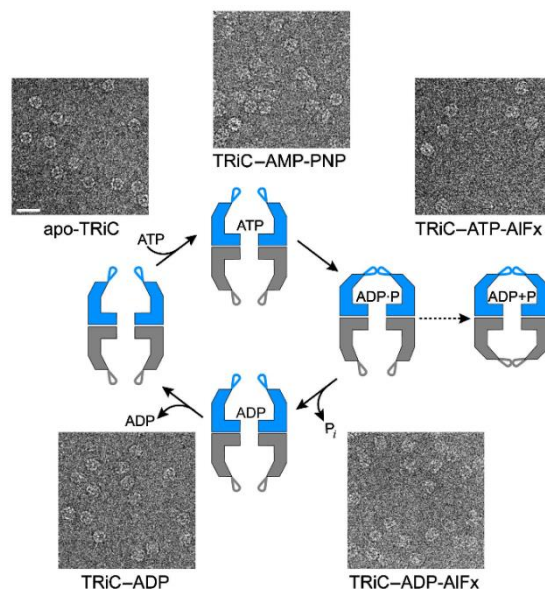


Figure 1.8 Cryo-EM study of TRiC conformational cycle. Cartoon diagram illustrates the TRiC conformational transitions in the apo state and four distinct nucleotide biochemical states throughout the ATPase cycle. In addition, a representative micrograph of ice-embedded TRiC in each state is shown. Scale bar is 320 Å.

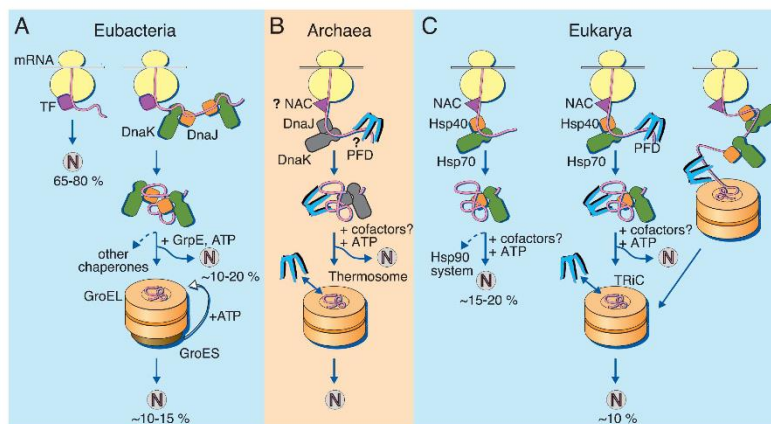


Figure 1.9 Model of the Models for the chaperone-assisted folding of newly synthesized polypeptides in the cytosol. (A) Eubacteria. TF, trigger factor; N, native protein. Nascent chains probably interact generally with TF, and most small proteins (65 to 80% of total) fold rapidly upon synthesis without further assistance. Longer chains (10 to 20% of total) interact subsequently with DnaK and DnaJ and fold upon one or several cycles of ATP-dependent binding and release. About 10 to 15% of chains transit the chaperonin system – GroEL and GroES – for folding. GroEL does not bind to nascent chains and is thus likely to receive an appreciable fraction of its substrates after their interaction with DnaK. (B) Archaea. PFD, prefoldin; NAC, nascent chain-associated complex. Only some archaeal species contain DnaK/DnaJ. The existence of a ribosome-bound NAC homolog, as well as the interaction of PFD with nascent chains, has not yet been confirmed experimentally. (C) Eukarya – the example of the mammalian cytosol. Like TF, NAC probably interacts generally with nascent chains. The majority of small chains may fold upon ribosome release without further assistance. About 15 to 20% of chains reach their native states in a reaction assisted by Hsp70 and Hsp40, and a fraction of these must be transferred to Hsp90 for folding. About 10% of chains are co- or post translationally passed on to the chaperonin TRiC in a reaction mediated by PFD. Image and caption taken from Hartl and Hayer-Hartl (2002).

1.4 Chaperonins as nanocarriers for intracellular drug delivery

The realization of ‘surgical nanomachines’ (which detect particular biological signals and accordingly evaluate which tasks are required to cure wounded tissues), envisaged by Feynman, is undoubtedly an ultimate scientific challenge. However, at present, there is still a long way to go before we are able to synthesize such intelligent, tailored nanomachines [1.83, 1.84].

Biomolecular machines are elegant nanoscale devices formed by the elaborate assembly of protein subunits, and play crucial roles in a range of biological events including cell division, intra/intercellular transportations, cellular movements and signal transductions [1.85–1.86]. In biological systems, these machines operate using a mechanical force, generated by conformational changes of constituent protein subunits, and chemically fuelled by adenosine-5'-triphosphate (ATP) and its analogues. The chemomechanical forces generated are tiny (5–60 pN) [1.87], but can cleave non-covalent interactions that form at nanoscale biointerfaces. We therefore envisioned that it might be possible to assemble an intelligent nanocarrier based on proteins, and tailor it to break up to release drugs in ATP-rich domains, under chemomechanical forces similar to those that occur in biological systems. Endogenous ATP, produced during inflammation [1.88], is considered an essential immunogenic signalling molecule. Although various stimuli-responsive synthetic carriers have already been reported [1.89–1.92], ATP-fuelled nanocarriers composed of integrated biomolecular machines are quite attractive, because it is possible to take full advantage of their sophisticated stimuli-specific operations.

Recently has been reported ([1.83]) a prototype of such intelligent nanocarriers, nanotubes assembled by supramolecular polymerization of a chaperonin GroEL mutant that has an extra-large molecular mass of ~800 kDa ([1.93]; Fig. 1.10). In biological systems, GroEL captures denatured proteins into its cavity and promotes their refolding. To release guest proteins after refolding, GroEL undergoes conformational changes induced by the hydrolysis of ATP into ADP that lead to the opening and closing of its cavity [1.93]. In the same work [1.83], was demonstrated how this nanotubular carrier (NT, Fig. 1.10a) indeed also breaks up into short-chain oligomers according to the expected mechanism, triggered by ATP. They also found that ^{BA}NT (a surface-modified version of the nanotube with a boronic acid (BA) derivative; Fig. 1.10b) can enter into human epithelial carcinoma (HeLa) cells

and respond to intracellular ATP. Finally, it was shown that this nanocarrier possibly provides a general strategy for intracellular delivery of drugs, when these are suitably anchored onto an irreversibly denatured guest protein such as α -actalbumin (α -LAdenat) through an enzymatically cleavable linker (Fig. 1.10c). This scission occurs with a sigmoidal dependence on ATP concentration, which means that the nanocarrier can differentiate biological environments in terms of the concentration of ATP for selective guest release. Furthermore, biodistribution tests reveal preferential accumulation of the nanocarriers in a tumour tissue.

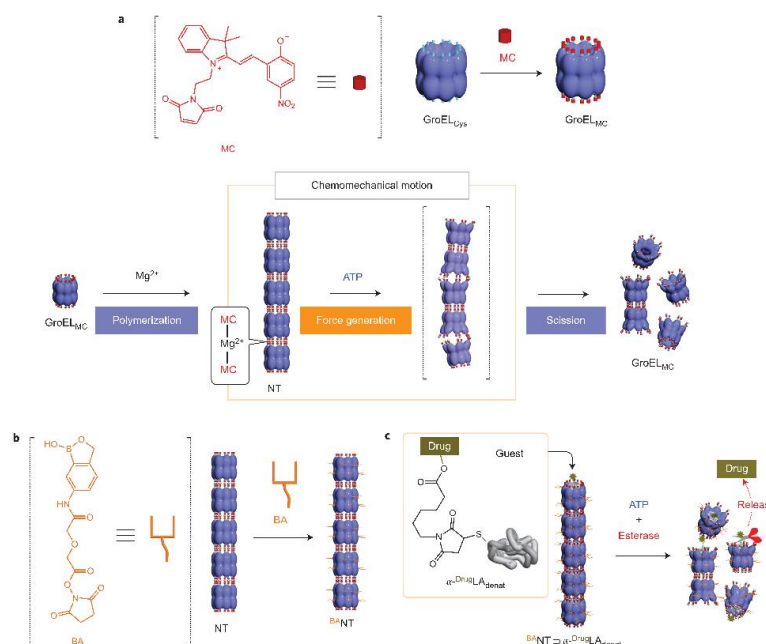


Figure 1.10 Schematics of the basic strategy for ATP-responsive intracellular drug delivery. **a**, Schematics of the preparation from mutant GroELCys and Mg²⁺-mediated supramolecular polymerization of GroEL_{MC}, forming a nanotube (NT), and its scission by ATP-fuelled chemomechanical conformational changes of the GroEL_{MC} building units. In the nanotube, the GroEL_{MC} monomer units are tightly connected together at their apical domains through multiple MC–Mg²⁺–MC bridges (MC, merocyanine). However, a mechanical force, generated by the ATP-fuelled conformational changes, is large enough for this multivalent GroEL_{MC} connection to break. **b**, Schematic illustration of the preparation of cell-penetrable ^{BA}NT by modification of the surface amine moieties of the nanotube with a 2-(hydroxymethyl)phenylboronic acid cyclic monoester derivative (BA). **c**, Schematic illustration of the basic strategy of ATP-responsive intracellular drug delivery with cell-penetrable ^{BA}NT, using as the guest irreversibly denatured α -lactalbumin (α -Drug_{LAdenat}) appended with drugs through an enzymatically cleavable ester linker (^{BA}NT \cap α -Drug_{LAdenat}). Chemomechanical scission of ^{BA}NT \cap α -Drug_{LAdenat}, triggered by binding with intracellular ATP, results in admission of esterase into the open cavity of chain-broken GroEL_{MC} \cap α -Drug_{LAdenat}, thereby allowing for ester-bond cleavage and subsequent release of drugs.

1.5 Chaperone-like systems: Caseins

The caseins are a heterogeneous group of dairy proteins constituting 80% of the protein content of bovine milk. The operational definition of casein is that proportion of total milk protein which precipitates on acidification of milk to a pH value of 4.6 [1.94-96]. The remaining dairy proteins, known collectively as whey proteins, do not precipitate. Caseins are synthesized in the mammary gland and are found nowhere else among the plant and animal kingdoms [1.97]. The casein family of proteins comprises α -, β - and k -caseins, all with little sequence homology [1.98]. As their primary function is nutritional, binding large amounts of calcium, zinc and other biologically important metals, amino acid substitutions or deletions have little impact on function. The caseins also lack well-defined structure and as a result their amino acid sequence is less critical to function than in many 'classic' globular proteins. Hence, the caseins are one of the most evolutionarily divergent protein families characterized in mammals. Alpha-casein, α_S -casein, is in fact two distinct gene products, α_{S1} - and α_{S2} -casein, with the 'S' denoting a sensitivity to calcium. Of all the caseins, α_{S1} - and β -casein are predominant in bovine milk, representing 37 and 35% of whole casein respectively, whereas α_{S2} - and k -casein make up 10 and 12% of whole casein, respectively [1.97].

The casein proteins and their derivatives have been used by the food industry as important nutritional and stabilising proteins for many years [1.99]. Early studies showed that whole casein (i.e. α_S -, β - and k -casein) prevented heat induced aggregation of whey proteins, even in calcium-containing systems [1.100 - 1.103]. It was proposed that the stabilizing action of the caseins on heat-denatured target proteins occur through non-specific interactions. This opened up a new avenue of uses for casein proteins in stabilizing both milk and non-milk proteins and thereby contributing to novel properties of milk products. It was then demonstrated in 1999 that individual α_S -casein possessed molecular chaperone activity [1.104]. Since then, β - and k -casein have both been shown to also act as molecular chaperones [1.105, 1.106, 1.107]. The presence of high numbers of phosphate groups in the casein proteins appears to be important for chaperone action against amorously aggregating target proteins under both reduction and heat stress, with studies showing that removal of these in α_S - and β -casein reduced their ability to prevent the aggregation of target proteins [1.108, 1.109].

1.5.1 Structural features of Caseins

Structurally, the caseins are classified as ‘intrinsically or natively disordered’ proteins under physiological conditions [1.110, 1.111, 1.105, 1.106]. This disordered structure, which is present to some extent even in globular proteins, is different to random coil conformation. In natively disordered proteins, conformations of these regions are still relatively fixed with respect to the ϕ and ψ angles of the peptide bonds, as opposed to true ‘random coil’ polypeptide chains, which exhibit greater and more rapid fluctuation in bond angles [1.99]. The lack of well-defined structure in the casein proteins is believed to facilitate proteolysis and therefore ready absorption of amino acids and small peptides in the gut [1.97], but is another likely factor in the unwillingness of the caseins to crystallise to provide a 3D crystal structure [1.112]. Physical characterisations of caseins in solution and predicted 3D models have shown that the caseins have relatively little tertiary structure, but possess some secondary structure, similar to the classic ‘molten globule’ states described in [1.113]. The greatest degree of secondary structure exists in α_{S2} - and k-casein, mainly in the form of β -sheets and β -turns rather than α -helix [1.114-1.116].

The formation of higher proportions of secondary and tertiary structural elements in the caseins is likely to be inhibited by high numbers of proline residues which distort protein folding into α -helices and β -sheets [1.97]. Each of the casein proteins has a high degree of hydrophobicity as a result of containing approximately 35-45% non-polar amino acids (e.g. Val, Leu, Phe, Tyr, Pro). However, this does not preclude them from being quite soluble in aqueous solvents due to the presence of high numbers of phosphate and sulfur-containing amino acids, and in the case of k-caseins, carbohydrates [1.97]. The flexible and relatively unfolded structure likely favors the exposure of the hydrophobic regions that tends to occur in patches along the sequence of the caseins, interspersed with hydrophilic regions. It is this structural feature that is credited with making the caseins good emulsifying agents, a property exploited in the food industry. The clustered exposed hydrophobicity is also thought to be a major feature of the molecular chaperone action of the caseins [1.102] as discussed in the following.

1.5.2 Alpha-Casein as a Molecular chaperone

Investigations into the chaperone action of α_S -casein have revealed that it prevented the stress-induced aggregation of natural target proteins such as the whey proteins β -lactoglobulin and bovine serum albumin, but also of unrelated proteins such as alcohol dehydrogenase and carbonic anhydrase. The stabilization of partially unfolded ‘target’ proteins takes place through direct interactions resulting in the formation of soluble, high molecular weight complexes similar to those induced by small heat-shock proteins (sHsps) and another unrelated chaperone, clusterin. In addition, it has been shown that α_S -casein is able to protect target proteins from aggregation in fibrillar aggregates, and that its chaperone activity is dependent on the target protein present. Under the stress conditions applied, the mode of protein aggregation (i.e. amorphous versus fibrillar), the speed of aggregation, and the presence of competing ions.

Previous work showed that α_S -casein, acting as a molecular chaperone under these conditions, was able to interact with partially unfolded target proteins and prevent their incorporation into insoluble aggregates which would then have formed precipitates [1.104]. As shown in Figure 1.11, the putative mode of action of α_S -casein is based on a similar model proposed for sHsps where a natively folded protein (N) unfolds via a number of intermediately folded states (I1, I2 etc.) or ‘molten globule’ states on its way to the unfolded state (U).

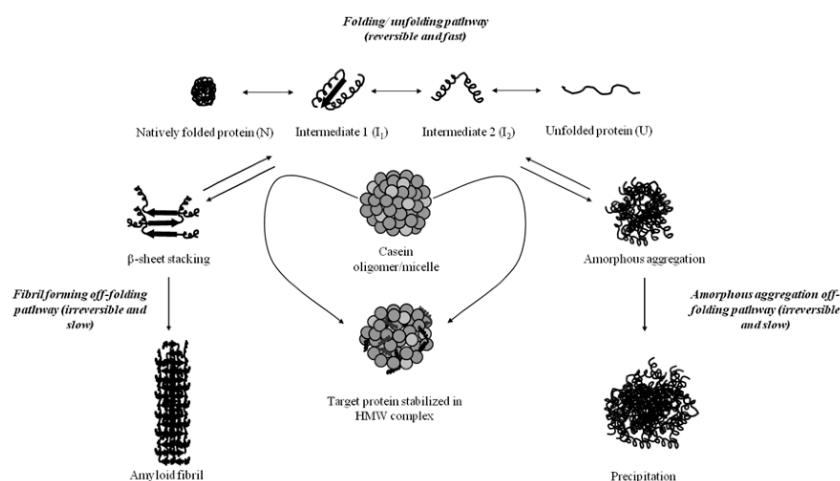


Figure 1.11 Putative mechanism of action of α_S -casein: showing its interaction with target proteins on the folding and off-folding pathways. See text for explanation. Reprinted with permission from [1.117].

This folding and unfolding is fast and reversible and involves the exposure of hydrophobic regions normally buried in the interior of the protein.

Under conditions of cellular stress, when intermediately folded states are present for longer periods, self-association is promoted by the prolonged exposure of hydrophobic surfaces. When self-association occurs, the intermediately folded states enter the off folding pathways which are slow and irreversible and may lead to either amorphous aggregation as shown on the right hand side of the figure 1.11 or to fibril formation as shown on the left. Amorphous aggregates result from disordered aggregation and lead to the formation of insoluble protein precipitates. Conversely, the ordered amyloid pathway leads to highly ordered β -sheet stacking giving cross β -sheet fibrils. Casein micelles or oligomeric forms of α S-or β -casein are able to interact with partially folded proteins and stabilize them against aggregation and precipitation by forming a soluble high molecular weight (HMW) complex [1.117].

Understanding the mechanism/s by which α S-casein exerts the role of molecular chaperone is of great interest to the dairy industry as it may provide an alternative method for long life milk treatment [1.94]. Processing treatments in dairy foods have the potential to induce partial or complete protein denaturation. The presence of proteins in denatured configuration may either present a problem or offer opportunities for novel foods to be developed [1.118]. This is where the action of molecular chaperones may play an important role. Thus, a better understanding of the aggregation processes in milk and how these can be modified opens up potential avenues for new milk based products with novel textures and other organoleptic properties to be developed. Moreover, investigation on its interaction mechanism could help to better understand the structural basis of the substrate binding in sHsps, which is able to exert a stabilizing function through direct interaction (see chapter 4, 4.2).

Chapter II

“Molecular chaperones involved in human diseases”

2.1 Molecular Chaperones and protein misfolding diseases

Proteins are central to all biological processes. To become functionally active, newly synthesized protein chains must fold into unique three-dimensional conformations, based on the information encoded in their amino acid sequences. Although in vitro many proteins can fold to their native state spontaneously without the aid of additional components, in vivo molecular chaperones are essential for protein folding to occur with high efficiency. As described in chapter 1 the main role of these components is to prevent protein misfolding and aggregation, off-pathway reactions that would otherwise limit the folding yield under cellular conditions.

In recent years, the process of protein folding has been recognized of considerable medical relevance. Indeed, a number of human diseases are now known to result, directly or indirectly, from aberrant folding reactions. Classic examples include Alzheimer’s disease, cystic fibrosis and hypertrophic cardiomyopathy, to mention only a few (see Table 2.1).

Table 2.1 Examples of human diseases caused by protein misfolding

Diseases	Genes involved	Risk factor	Proteins involved	Pathology	Affected brain areas	Symptoms
Alzheimer’s	APP and presenilin 1, 2	ApoE4	A β and Tau	A β -plaque and Tau tangle	Hippocampus and frontal cortex	Memory loss, personality change, worried, and depressed
Parkinson’s	α -synuclein, Parkin, CHL-1, and LRRK2	Tau linkage	α -ynuclein and tau	Lewy body and tangle	Substantia nigra, striatum, and PFC	Impairment of sensorimotor coordination and cognition
Huntington	Huntingtin (HTT)	Number of CAG repeats in HTT allele	Huntingtin	Inclusion odies in cytoplasm and nucleus	Striatum	Uncontrolledovements, clumsiness, and balance impairment
Prion	PRNP	Homozygosity at prion codon 129	PrPSc	Prion plaque	Whole CNS	Memory loss, personality change, and movement disorder
Amyotrophic Lateral sclerosis	SOD	—	SOD1	Bunina body	Motor neuron of CNS	Disturbances of muscularactivity
Multiple sclerosis	HLA, IL2RA, and IL7RA	Kinesin KIF1B, Vit D	—	Demyelinating lesion	White matter of the brain and spinal cord	Physical and cognitive disability
Tauopathies	Tau	Tau-linkage	Tau	Tau tangle	Whole CNS	Memory loss
Lewy bodies Dementia	PARK11	E4 allele of ApoE	α -Synuclein and ubiquitin	Lewy bodies	Hippocampus, amygdale, and frontal cortex	Impair, alertness/attention movement, posture, muscle stiffness, emoryloss, hallucinations, confusion

Panchanan Maiti et al., Molecular Chaperone Dysfunction in Neurodegenerative Diseases and Effects of Curcumin BioMed Research International Volume 2014, Article ID 495091, 14 pages <http://dx.doi.org/10.1155/2014/495091>

Human misfolding diseases arise when proteins adopt non-native conformations that endow them with a tendency to aggregate and form intra- and/or extra-cellular deposits. Hence, misfolding diseases result from the failure of proteins to reach their active state or from the accumulation of aberrantly folded proteins.

There are various mechanisms by which the accumulation of misfolded protein chains may cause cellular dysfunction, and often a combination of mechanisms appears to be responsible for the disease. Misfolded polypeptides not only lose their normal function, but may also form toxic species, including oligomers or larger aggregates (e.g. amyloid precursor protein (APP) in Alzheimer's and other neurodegenerative diseases). Moreover, they may be prevented from reaching their proper cellular localization due to retention and/or degradation (e.g. CFTR in cystic fibrosis), or may exert a dominant negative effect by preventing the function of interacting partners (e.g. myosin in hypertrophic cardiomyopathy).

In aggregation diseases, specific peptides or misfolded proteins, often as a result of mutations, can give rise to amyloid-like deposits, i.e. highly ordered fibrillar aggregates (Fig. 2.1).

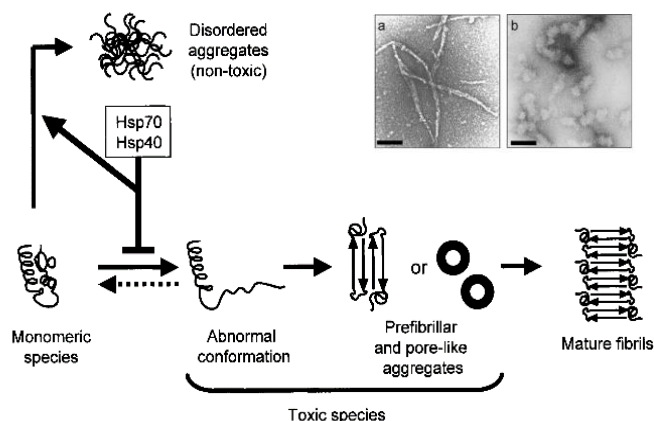


Figure 2.1 A scheme depicting common features of misfolding and aggregation in neurodegenerative misfolding diseases. The toxic aggregation pathway begins when a monomeric disease protein undergoes a structural transition from a native fold into a misfolded abnormal conformation. Aggregation proceeds *via* a multi-step process that involves intermediate species, which are thought to be less stable, but more toxic, than the final mature fibrils. These species may recruit or interact aberrantly with essential cellular components, including machinery of the quality control system. Sequestration of these cellular components may inhibit their cellular function, thus contributing to toxicity. Aggregation intermediates may also form doughnut-shaped assemblies that interact with membranes to form pores, disrupting cellular homeostasis. The end products of the aggregation process accumulate in disease-associated deposits, such as amyloid fibrils with cross- β structure. Molecular chaperones Hsp70 and Hsp40 may prevent the conversion of native protein species into toxic, amyloidogenic intermediates and instead facilitate the deposition of disease proteins in non-toxic, disordered aggregates. On the right top (panels a and b): Suppression of huntingtin fibril formation by molecular chaperones.

In AD, extracellular A β peptide deposition is thought to be intimately associated with the initiation of disease, whereas in certain forms of PD it is the intracellular formation of aggregates of the protein alpha-synuclein [2.1]. HD is caused by a mutant version of the protein huntingtin, which results in an expansion of its polyglutamine (polyQ) domain and renders the protein aggregation-prone [2.2]. The same type of mutation gives rise to a collection of other neurodegenerative polyQ diseases, including SCAs and Kennedy's disease.

Nuclear inclusions of mutant huntingtin, or other polyQ-containing disease proteins, in brain tissue are a key feature of these dominantly inherited disorders. The central event in CJD is the extracellular deposition of aggregates of abnormally folded prion protein, PrP^{Sc}, in the brain and nervous system of affected individuals. In each of these cases, it is thought that either the aggregates of the disease protein themselves or, more likely, the process of their formation confers cellular toxicity, thus supporting the notion that misfolded disease proteins act through a gain-of-function mechanism that eventually leads to cell death.

The disease proteins involved in aggregation disorders have no obvious sequence similarities, but the amyloid fibrils into which they can convert are very similar in morphology. Amyloid fibrils often consist of two to six 'protofilaments' which share a common core structure based on the presence of highly ordered β -sheets, a so-called cross- β structure [2.3]. The fibrillar deposits may be organized into larger aggregates or amyloid plaques, which reside outside the cell in the case of AD and CJD. In PD and HD, structurally similar amyloid-like deposits are found inside the cell. It is clear that there are a variety of steps involved in the aggregation process that converts soluble monomers into insoluble fibrillar aggregates (see Fig. 2.1) [2.3-2.5]. It has been proposed that the aggregation process begins when a polypeptide chain undergoes a structural transition from a native fold into a misfolded β -sheet conformation. While for the disease proteins this transition can occur under physiological conditions (e.g. due to destabilizing mutations), similar changes may be affected in non-disease proteins by more extreme conditions of pH or temperature [2.6]. Under appropriate circumstances, misfolded monomers may oligomerize into pre-fibrillar assemblies that give rise to mature fibrillar structures. Within cells, these aggregates become actively concentrated and sequestered in specialized aggresomes at the microtubule organizing center [2.7-2.10].

Recently, a more direct involvement of molecular chaperones in human diseases of protein folding has become increasingly evident [2.11-2.14].

The mechanisms by which molecular chaperones influence the development of these diseases is beginning to be understood. Mutations that compromise the activity of chaperones lead to several rare syndromes (see paragraph 2.1.3). The more frequent amyloid-related neurodegenerative diseases are caused by a gain of toxic function of misfolded proteins. Toxicity in these disorders may result from an imbalance between normal chaperone capacity and production of dangerous protein species. Valuable therapeutic strategies could be aimed to increase the expression of chaperones capable to suppress the neurotoxicity of these molecules.

Molecular chaperones, such as Hsp60, Hsp70 and TCP-1 Ring Complex (TRiC)/chaperonin containing TCP-1 (CCT), have been implicated as potent modulators of misfolding disease [2.11]. These chaperones suppress toxicity of disease proteins and modify early events in the aggregation process in a cooperative and sequential manner reminiscent of their functions in de novo protein folding. Further understanding of the role of molecular chaperones in misfolding disease is likely to provide important insight into basic pathomechanistic principles that could potentially be exploited for therapeutic purposes.

2.1.1 Mechanisms of toxicity in aggregation diseases

The exact mechanism by which protein misfolding and aggregation is linked to disease is still unclear, but there is increasing evidence that the main toxic agents are soluble precursors (monomers or oligomers) of the disease proteins, rather than the mature insoluble fibrils into which they develop (see Fig. 2.1-2.2 and [2.15-2.23]). For instance, recent experiments with a species of the A β peptide in an AD model have shown that A β oligomers, and not the mature amyloid fibrils, are neurotoxic [2.19].

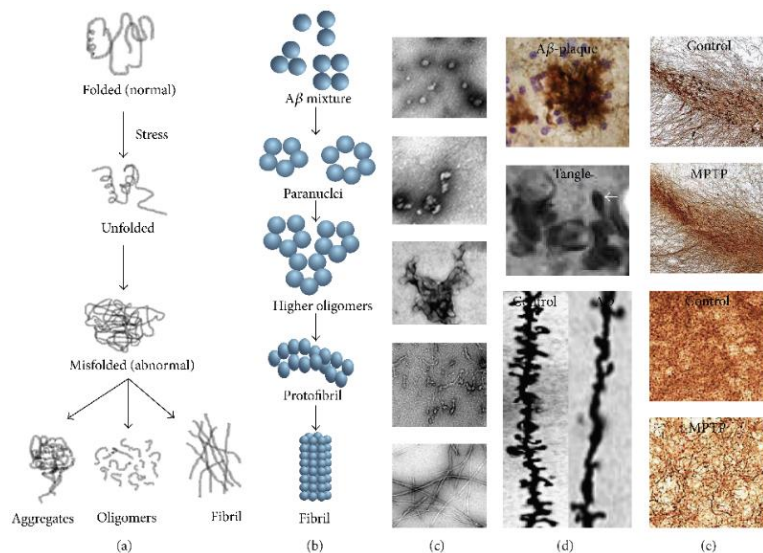


Figure 2.2 Protein misfolding and aggregation in different neurodegenerative diseases. (a) Schematic diagram showing steps of formation of different abnormal protein species after the cellular stress response; (b) schematic diagram of sequential formation of different amyloid species; (c) electron micrographs of different species of amyloid beta protein; (d) amyloid beta plaques (upper) stained with 4G8 antibody from brain tissue of AD mouse model, neurofibrillary tangle (middle), and synaptic (dendritic spine, Golgi-Cox stain) loss in mouse model of Alzheimer's disease (lower); (e) tyrosine hydroxylase (the indicator of dopaminergic neuron) positive (small arrow) neuronal loss in the substantia nigra-pars compacta and tyrosine hydroxylase positive fiber loss in the striatum of MPTP-model of Parkinson's disease.

Additionally, expression of polyQ-expanded huntingtin causes toxicity in a yeast model of HD, before insoluble aggregates can be detected [2.23].

Taken together, these studies suggest that oligomeric precursors of the mature fibrils present in a wide variety of misfolding diseases may be the principal agent of toxicity. However, the possibility that mature fibrils may also contribute to neuronal toxicity should not be ruled out [2.7, 2.24]. There are currently three main non-exclusive hypotheses to explain the mechanism of toxicity caused by misfolded disease proteins:

- The first, termed 'the channel hypothesis', suggests that ring-shaped oligomers, exposing hydrophobic surfaces, form early in the aggregation process and cause toxicity by forming pores in cellular membranes. The formation of such pores has been described under experimental conditions

for several aggregation disease proteins, including A β -peptide, PrPSc, alpha-synuclein, and polyQ-peptides [2.25-2.28].

- A second disease mechanism stresses aberrant interactions of misfolded proteins with other proteins, rendering them non-functional. For example, polyQ expanded huntingtin can cause the co-aggregation of several transcription factors that contain polyQ sequences in the normal range [2.18].
- Finally, the association of aggregating disease proteins with the quality control machinery may itself contribute to cellular toxicity. Misfolded proteins may sequester components of the chaperone and degradation systems, reducing their activity in the cell.

2.1.2 Role of molecular chaperones in Alzheimer's disease

The principal misfolded proteins in Alzheimer's disease (AD) are A β and tau [2.29]. The first one is formed from amyloid precursor protein (APP) and deposited as amyloid plaques, mostly in extracellular spaces. Tau is the microtubule stabilizing protein and when it is hyperphosphorylated accumulates intracellularly (and sometimes extracellularly) in neurofibrillary tangles [2.30-2.33].

Cell free experiments demonstrate that several HSPs (see Table 2.2), alone or in synergistic action, are able to significantly slow down or eventually suppress protein aggregation involved in severe amyloid diseases. In vivo studies, using various animal and cellular models reveal that treatment with specific chaperones or their overexpression can ameliorate pathological behavior dysfunction characterizing AD pathology [5.11, 5.16-5.19].

Table 2.2: Different heat shock proteins, their localization, functions, and involvement in different neurodegenerative diseases.

HSPs	MW (kDa)	Localization	Co-localization	Function	Involved in diseases
Hsp10	10	Mitochondria, cytosol, ER, and nucleus	A β	Protein folding	AD, MS, and tauopathies
Hsp27	20-30	Cytosol,	Tau, A β , HTT, and α -synuclein	Protein degradation	AD, HD, and PD
Hsp40	40	Cytosol, ER, and nucleus	HTT and α -synuclein	Protein folding	HD and PD
Hsp60	60	Mitochondria	A β	Prevent protein aggregation	AD
Hsp70	70	Cytosol, ER, nucleus, and mitochondria	A β , HTT, α -synuclein, and PrPc	Protein folding/unfolding	AD, HD, PD, Prion, and MS
Hsp90	90	Cytosol and ER	A β , HTT, α -synuclein, and PrPc	Protein degradation and transcription factor	AD, PD, and HD
Hsp104/110	104-110	Cytosol and ER	α -synuclein and PrPc	Thermal tolerance	PD and prion

Panchanan Maiti et al., Molecular Chaperone Dysfunction in Neurodegenerative Diseases and Effects of Curcumin BioMed Research International Volume 2014, Article ID 495091, 14 pages <http://dx.doi.org/10.1155/2014/495091>

HSPs especially HSP70 can bind with APP and interfere with the APP secretory pathway to reduce the production of both A β 40 and A β 42 [2.34]. Dickey et al. reported that HSP70 and HSP90 interact with tau and A β oligomers and degrade them through proteasome system [2.30] (Figure 2.3). Similarly, overexpression of HSP70 decreases the amount of insoluble tau, reduces tau phosphorylation, increases tau stability, promotes tau binding to microtubules, and decreases the in vitro and in vivo toxicity associated with tau protein (Figure 2.3). In contrast, downregulation of HSPs by RNA-mediated interference (RNAi) has the opposite effect [2.35]. Heat shock cognate 70 (HSC70) together with HSP70 or HSP90 can directly bind to tau, independent of its phosphorylation status, thus facilitating microtubule polymerization and limiting tau aggregation [2.36]. In addition, HSP90 and its dependent cochaperones and client proteins may be essential for refolding denatured or misfolded tau and A β [2.36]. Both HSP70 and HSP90 can promote

tau solubility and tau binding to microtubules as well as reduce insoluble tau and tau phosphorylation [2.35].

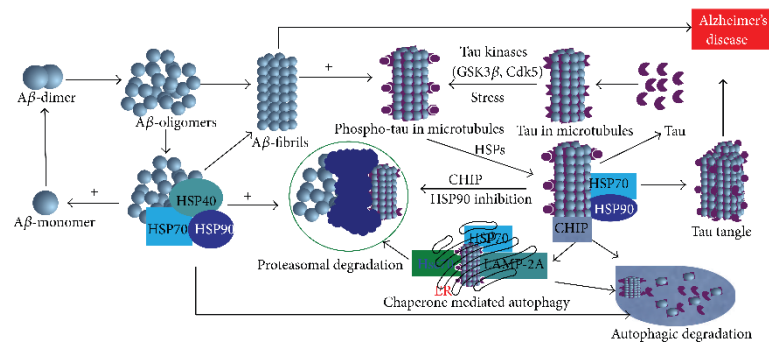


Figure 2.3 Role of molecular chaperones in Alzheimer's disease. HSP90, HSP70, and other client proteins are directly involved in degradation of Aβ oligomers and phosphorylated tau containing microtubule and help them to degrade either proteasome pathway or through autophagy pathway. Failure to dephosphorylate by HSPs leads to formation of tau tangle, a hallmark of AD.

Overexpression of inducible HSP70 reduced soluble and insoluble tau levels in 30-month-old mice [2.37]. Levels of HSP90 are inversely associated with granular tau oligomers and neurofibrillary tangles in AD [2.38] and in a mutant tau-model [2.36] (Figure 2.3).

Current research on the development of therapeutic approaches of intervention in amyloid diseases bases on at least four broad approaches:

- I) Block the production of the amyloidogenic peptide or protein;
- II) Block its "misfolding" or transformation from a nonpathogenic monomer or low-oligomer to toxic oligomers and polymers;
- III) Block the toxic effects of amyloid;
- IV) Modulate an auxiliary cellular pathway that affects beneficially one or more of the foregoing approaches [5.20-5.22].

2.1.3 Mutations in molecular chaperones as the cause of human diseases

The identification of mutations responsible for a wide variety of inherited human diseases has been greatly accelerated in recent years, due to the availability of detailed genetic mapping tools developed in the large-scale genome sequencing projects. Analysis of the open reading frames (ORFs) that contain mutations has revealed alterations in genes encoded for molecular chaperones that may be responsible for some complex human diseases. These diseases are likely to be caused by the loss of function of one or more chaperone substrate proteins. Some examples are described in the following.

- **Hsp60**

The hereditary spastic paraplegia SPG13 is caused by a missense mutation of a conserved Valine (V72I) residue in the mitochondrial chaperonin Hsp60 [2.39]. The disease is characterized by weakness and poor coordination of lower limbs, resulting from severe degeneration of the distal ends of long axons in the spinal cord [2.40]. The relatively mild phenotype associated with the mutation is rather surprising, as Hsp60 is crucial for mitochondrial biogenesis and the missense mutation renders Hsp60 partially or completely nonfunctional. It is possible that compensatory mechanisms are in place to allow mitochondrial biogenesis without functional Hsp60 proteins.

- **hMKKS**

Mutations in the cytosolic chaperonin hMKKS have been implicated in McKusickKaufman Syndrome (MKKS), characterized by malformations of the genital tract, polydactyly and congenital heart disease; and Bradet-Biedel type 6 Syndrome (BBS6), characterized by obesity, retinal dystrophy, renal malformations, learning and behavioral abnormalities and endocrinological dysfunction [2.41, 2.42]. hMKKS is 40% similar to human TRiC protein, and is known to be expressed during development and in adults, but not much is known about its biochemical or structural properties.

- **TRiC/CCT**

Mutations in human Group II CCT subunits 4 and 5 cause rare debilitating diseases. Mutation in the epsilon subunit of the cytosolic chaperonin-containing t-complex peptide-1 (Cct5) gene causes autosomal recessive mutilating sensory neuropathy with spastic paraplegia. For instance, the His147Arg mutation in human CCT5 causes mutilating peripheral sensory neuropathy [6.19].

- **The α -crystallins**

α -Crystallins are small HSPs, mutations in which have been linked with two diseases: R116C mutation in α A-crystallin is linked to a form of hereditary cataract [2.43]; and R120G substitution in α B-Crystallin results in a form of desmin-related myopathy (DRM) [2.44]. Although the precise mechanism by which mutant α A-Crystallin causes cataract is not known, it is predicted that the mutant chaperone fails to properly fold other major lens proteins. In the case of DRM, it is known that α B-Crystallin specifically interacts with desmin in muscle cells, possibly mediating its folding and/or assembly into intermediate filaments [2.45].

- **Tubulin-specific chaperones**

The tubulin-specific chaperone E (cofactor E, TBCE) is an essential chaperone required for efficient folding of α -tubulin and its dimerization with β -tubulin. Mutations in TBCE lead to a reduction in the amount of available α -tubulin to be incorporated into microtubules, causing severe cytoskeletal defects such as aberrant polarity of microtubule network. Several severe diseases have been linked with mutation in this gene, including HRD (hypoparathyroidism, mental retardation and facial dysmorphism), Sanjad–Sakati syndrome, and autosomal recessive Kenny–Caffrey syndrome (AR-KCS) [2.46].

- **Sacsin**

Sacsin was originally reported to consist of a single gigantic exon spanning 12.8 kb with an 11.5-kb ORF, with mutations linked to autosomal recessive spastic ataxia of Charlevoix–Saguenay (SACS) [2.47]. Recently, eight exons upstream from the original one have been found, and the new ORF has elongated to 13.7 kb. Sequence similarity revealed an ubiquitin domain and a DnaJ molecular chaperone homology

domain preceding a HEPN (higher eukaryotes and prokaryotes nucleotide binding) domain. The mutations R4325X and N4549D that cause SACS are present in the DnaJ domain and the HEPN domain, respectively [2.48]. The DnaJ heat shock domain is essential for interactions with chaperone Hsp70-like proteins and the HEPN domain is implicated in nucleotide binding [2.48]. This raises possibilities of Sacsin functioning either directly or indirectly in chaperone mediated protein folding.

2.2 Molecular Chaperones and Oncogenesis

As described before molecular chaperones constitute a major arm of the proteostasis network; they play a central role in the maintenance of protein homeostasis through an intricate system of cooperative mechanisms that balance protein biosynthesis, folding, translocation, assembly/disassembly, and clearance [2.49, 2.50].

Increased protein chaperone capacity has been linked to the etiology of many diseases including cancer [2.51]. Considerable evidence now exists implicating molecular chaperones in the development of cancer. They have been shown to play a fundamental role in the molecular mechanisms that lead to the emergence and progression of the tumor phenotype. Accordingly, levels of heat-shock factor 1 (HSF1), a transcriptional regulator of protein homeostasis that activates the transcription of HSPs has been shown to be elevated in many cancer cell lines and tumors [2.52]. Indeed, the expression of several HSPs is increased in many tumors, such that HSPs are prognostic biomarkers in cancer and their overexpression is linked to poor survival and response to therapy [2.53]. The sensitivity of a wide variety of tumors to inhibitors of HSPs exemplifies the importance of molecular chaperones in maintaining survival of cancer cells [2.54].

Detailed information on the involvement into oncogenesis for the two proteins (Hsp60 and TRiC/CCT) that are the subject of this thesis work, are reported in the two following paragraphs.

2.2.1 Hsp60: Contribution to oncogenesis

Hsp60 in eukaryotes is considered typically a mitochondrial chaperone (also called Cpn60) but in the last few years it has become clear that it also occurs in the cytosol, the cell surface, the extracellular space and in the peripheral blood [4.4 2.55].

Studies with prokaryotic models have shown that Hsp60 plays a role in assisting nascent polypeptides to reach a native conformation, and that it interacts with Hsp10 (which also resides in the mitochondria and is also named Cpn10). In addition to its role in polypeptide folding in association with Hsp10, other functions and interacting molecules have been identified for Hsp60 in the last several years. Some of these newly identified functions are associated with carcinogenesis,

specifically with tumor cell survival and proliferation. Thus, assessing the levels of Hsp60 in tumor cells and in sera of cancer patients is becoming an attractive area of investigation aiming at the development of means for practical applications in clinical oncology. Since Hsp60 participates in extracellular molecular interactions and cell signalling and also in key intracellular pathways of some types of tumor cells, the idea of using Hsp60 in anti-cancer therapy (chaperon-therapy) is being investigated. The Hsp could be used either as an anticancer agent alone or in combination with tumor antigens, or as target for anti-chaperone compounds

Intracellular Hsp60

In eukaryotes, Hsp60 typically resides in the organelles mitochondria (chaperonin 60 or Cpn60) and chloroplasts (in plants), and interacts with Hsp10 (or Cpn10) while chaperoning nascent polypeptides as they progress to achieve a functional conformation or native status. Hsp60 also interacts with mitochondrial Hsp70 (mortalin), and with surviving and p53 as it participates in the process of apoptosis. The levels of mitochondrial Hsp60 are regulated via complex mechanisms, one of which involves a DNA-dependent protein kinase, a molecule that plays a protective role against drug-induced apoptosis. In addition to its recognized role in protein folding, Hsp60 has been implicated in intracellular protein trafficking, and in peptide-hormone signalling in an experimental model of Lyme neuropathy. Hsp60 can bind and interfere with the functions of various endogenous and exogenous proteins. For instance, Hsp60 binds epolactaene, a microbial metabolite that if not bound to the chaperone arrests cell cycle and induces the outgrowth of neurites in human neuroblastoma cells.

Lately evidence show that Hsp60 is also found in the cytosol not only after mitochondrial release but also independently of such release, and the evidence also indicate that both, the mitochondrial and the cytosolic forms of Hsp60 can function in pro-survival or pro-apoptotic pathways, depending on the cellular situation [2.55-2.60].

Surface Hsp60

Hsp60 can also be found on the surface of normal and tumor cells. Increased amounts of Hsp60 on the cell's surface was considered to serve as a danger signal for the immune system leading to the activation and maturation of dendritic cells and the generation of an antitumor T-cell response.

Quite interestingly from the oncological viewpoint, surface Hsp60 has been found associated with alpha-3-beta-1 integrin, a protein involved in the adhesion of metastatic breast cancer cells to lymph nodes and osteoblasts, with the association being inhibited by mizoribine, an Hsp60-binding drug. It has also been shown that surface Hsp60 plays a critical part in the metastatization of pancreatic carcinoma, and that presence of Hsp60 on the surface of oral tumor cells determines cell lysis induced by gamma-deltaT lymphocytes [2.61-2.63].

Extracellular Hsp60

In addition to its intracellular and pericellular locations, Hsp60 also occurs in the extracellular space and in circulation, a fact that has become firmly established only in the last few years, although the mechanisms involved in its secretion, exosomal and/or other are not yet understood. Extracellular Hsp60 can interact with a number of cell-surface receptors such as CD14, CD40 and Toll-like-receptors (TLRs) can cause pro- and anti-inflammatory effects, and can bind to peptides (e.g., tumor-derived peptide antigens) and present them to immune system cells. When acting as a pro-inflammatory agent, Hsp60 induces secretion of cytokines from professional antigen presenting cells and causes activation of T cells. Hsp60 can also stimulate the maturation of dendritic cells via the TLR-2 and -4 signal-transduction pathways, synergizing the pro-inflammatory action of IFN-gamma. On the other hand, as anti-inflammatory agent, extracellular Hsp60 can be a ligand for gamma-delta T lymphocytes in oral tumors, determining anti-tumoral immunosuppression. After stimulation by Hsp60, gamma-deltaT cells showed downregulation of Fas expression and nitric oxide production, leading to a loss of mitochondrial membrane potential and caspase-9 activation, followed by induction of lymphocyte-cell death. Extracellular Hsp60 can also enter into the blood stream and be found in plasma of healthy subjects [2.64-2.70].

Controversial role of Hsp60

Most heat shock proteins (HSPs) have pro-survival functions. However, the role of HSP60 is somewhat controversial with both pro-survival and pro-apoptotic functions reported. In numerous apoptotic systems HSP60 protein accumulates in the cytosol. In BMD188-induced cell death, HSP60 accumulates in the cytosol with significant mitochondrial release. In contrast, in apoptosis induced by multiple other inducers, the cytosolic HSP60 accumulates without an apparent mitochondrial release. The short interfering RNA-mediated knockdown experiments revealed that in BMD188-induced apoptosis, HSP60 has a pro-death function and that the pro-death role of HSP60 seems to involve caspase-3 maturation and activation in the cytosol. In contrast, HSP60 appears to play a pro-survival role in other apoptotic systems where there is no apparent mitochondrial release as its knockdown promotes cell death. In these latter apoptotic systems HSP60 does not associate with active caspase-3. In both cases, HSP60 does not appreciably interact with Bax. Taken together, our results suggest the following:

- 1) Cytosolic accumulation of HSP60 represents a common phenomenon during apoptosis induction;
- 2) Cytosolic HSP60 accumulation during apoptosis occurs either with or without apparent mitochondrial release;
- 3) The cytosolically accumulated HSP60 possesses either pro-survival or pro-death functions, which involves differential interactions with caspase-3.

Key questions still unanswered pertain to the differences in structure-function features that might exist between the mitochondrial HSP60 and the largely unexplored cytosolic Hsp60. Studies on human Hsp60 structure and oligomeric state *in vitro* could help to validate its role in physiological or pathological cases.

2.2.2 TRiC/CCT: Contribution to oncogenesis

The contribution of TRiC to cancer has not received as much attention as members of HSPs [2.71], but, evidence is now emerging implicating TRiC in the pathogenesis of numerous cancers. In the last years, many proteins associated with tumorigenesis have been identified as bona fide TRiC clients; these include signal transducer and activator transcription (STAT3), cyclins B and E, P53 and Von

Hippel-Lindau [2.72]. A recent study suggested that TRiC subunits (in particular CCT2 and CCT1) are essential for survival and proliferation of breast cancer [2.73]. CCT1 was shown to be transcriptionally modulated by the driver oncogene, phosphatidylinositol 3-kinases (PI3K). Whether these observations reflect the protein folding function of TRiC complex or a non-chaperoning role of individual subunits is not clear; however, individual subunits of TRiC have been shown to have protein-folding capacity [2.74]. While higher expression levels of TRiC have been associated with tumorigenesis, a recent analysis of cancer cell lines appeared to show less correlation between TRiC concentrations and its specific activity. The disparity between TRiC concentrations and TRiC activity has been attributed to the dynamic partitioning of substrates between TRiC, its co-chaperones, and HSPs that seems to be influenced by concentrations of HSP70 within the cell [2.75].

TRiC has been estimated to directly assist the folding of as many as 10% of cytosolic proteins [2.76, 2.77] and it provides the unique ability to fold certain proteins that cannot be folded by simpler chaperone systems. This strict requirement of TRiC is also essential for folding proteins involved in oncogenesis. This suggests that TRiC plays a potential role in cancer cell development by direct modulation of the folding and activity for client proteins related to oncogenesis, such as tumor suppressor Von Hippel-Lindau (VHL) [2.78, 2.79] and p53 as well as the pro-oncogenic protein STAT3 [2.80, 2.81].

The main contributions of the Type II Chaperonin, TRiC/CCT, to Oncogenesis are:

- Chaperonin TRiC works as an Assembly Station for the Tumor Suppressor, VHL (Von Hippel-Lindau);
- TRiC contributes to STAT Protein Folding and Function;
- Interaction of TRiC with p53 Promotes the Protein Folding and Activity of p53;
- TRiC Modulates Cell Cycle Regulatory Proteins;
- Contribution of LOX-1, a newly identified TRiC Substrate, to Inflammation and Oncogenesis.

It is clear that chaperones are critical mediators of oncogenesis. TRiC activity is linked to oncogenesis through its clients-oncoproteins and tumor suppressor proteins that have well-established roles in cancer. TRiC may play an important role in oncogenesis by modulating cancer cell growth, apoptosis, and genome instability. Major advances have been made in clarifying how TRiC folds its substrates, but additional work is necessary to elucidate the mechanisms of TRiC substrate recognition, which could be exploited to develop strategies for identifying new cancer therapies. In addition, because TRiC is required for the proper folding of ~10% of the proteome, a systematic approach to the identification of TRiC substrates that contribute to the many different types of cancer will be challenging. Thus, development of new methodologies and further experimental studies are warranted to increase our understanding of the role TRiC in cancer development and progression.

Chapter III

“Materials and methods”

3.1 Materials

3.1.1 Chaperonins (Group I and II)

The recombinant mitochondrial (mt) and naïve (p-mt) Hsp60 were obtained from ATGen (Seongnam, South Korea) in stock solutions at 16.0 mM (1 mg/ml) (buffer 20 mM Tris-HCl, pH 8.0, and 10% w/w glycerol). Lyophilized GroEL from SIGMA (St. Louis, MO, USA) was dissolved in the same buffer. The experiments on the three proteins were conducted at varying protein concentration in the range 0.04–0.4mg/ml. The final buffer for all the three proteins was 20 mM Tris-HCl (pH 8) containing 30mM NaCl and 3% glycerol (w/w). The samples were filtered through a series 0.22 µm membrane and 1 MDa Vivaspin filters with Polyethersulfone membrane (Sartorius, Germany). Higher protein concentrations were obtained with Vivaspin concentrators with Polyethersulfone membrane and 10 kDa molecular weight cut-offs (Sartorius, Germany). Protein concentration for each experiment was determined by the area under a peak from the corresponding High Performance Liquid Chromatography (HPLC) chromatogram. Bovine serum albumin, used for HPLC calibration, (BSA) was purchased from Sigma and dissolved in buffer 50 mM sodium phosphate buffer.

The recombinant proteins Pf-CD1, Pf-CD1 Ile138His, and Pf-CD1 Ile138Arg, were all derived from the *Pyrococcus furiosus* chaperonin Group II Pf-Cpn (Supplementary material A.1) [3.1]. CD1 refers to a C-terminal deletion of the last 22 residues of Pf. It had been reported that the removed segment is disordered, promotes protein solubility and has only minimal effect on protein function and stability. Pf-CD1 Ile138His (designated Pf-H for short) represents the wild-type humanized version of the archaeal protein since it contains His at the site corresponding to that of the human mutation. Pf-CD1 Ile138Arg (designated Pf-R) represents the pathogenic human mutant since it features Arg at the mutation site.

The wild-type archaeal CCT subunit orthologous gene was amplified from *P. furiosus* genomic DNA, then modified in *Escherichia coli* to produce the three constructs as previously reported [3.1]. Sequences are given in the Supplementary material. The pET33b(1) vector (Novagen, Madison, WI, USA) was used for recombinant expression in *E. coli* BL21 (DE3) and inoculated into 15 mL of LB medium plus 50 µg/µL kanamycin at 37 °C, and this 15 mL culture was transferred into 1 L of ZYM Auto-Induction medium with kanamycin selection 10 h later. Cells were grown in 4 L baffled flasks at 200 rpm at 25 °C for 3 days. The cell pellets were re-suspended in re-suspension buffer (25 mM Tris-HCl, 200 mM NaCl and pH 7.5), 30 % w/v prior to cell disruption using a continuous flow Cell Disrupter (TS Series Benchtop, Constant Systems Ltd. GA, USA) and centrifuged at 11,500 xg for 20 min to collect cellular debris. The supernatant extract was heated to 80 °C (Pf-CD1 and Pf-H) or 70 °C (Pf-R) for 30 min and centrifuged at 11,500 xg for 30 min to remove non-heat tolerant proteins. The supernatant was further purified to homogeneity by anion exchange chromatography (Bio-Rad MiniMacro Prep High Q Column, Hercules, CA, USA), using a 200 mM to 1 M NaCl gradient for 30 min at 3 mL/min. Pure fractions were concentrated using 30 kDa spin filters (Amicon Milipore, Darmstadt, Germany) spun at 3,500 xg for 20 min. Protein homogeneity was assessed by running concentrated fractions on 12% SDS-PAGE gel and protein concentration was determined by Bradford assay.

3.1.2 Abeta amyloid

The lyophilized synthetic peptide A β 1-40 (Anaspec) was solubilized in NaOH 5 mM (Sigma-Aldrich), pH 10, sonicated and lyophilized according to Fezoui et al. protocol [3.2]. The lyophilized peptide was then dissolved in 20 mM Tris pH 7.7, 3% glycerol, 30 mM NaCl, and then filtered with two filters in series (Millex-Lg filters with a diameter of 0.20 µm and Whatman filters with a diameter of 0.02 µm) in order to eliminate large aggregates. The sample preparation was operated in asepsis using a cold room at 4 °C. A β concentration was determined by tyrosine absorption at 276 nm using an extinction coefficient of 1390 cm⁻¹M⁻¹.

All other chemicals used in the experiments were purchased from Sigma unless specified otherwise

3.2 Methods & Characterization

3.2.1 Differential Scanning Calorimetry, DSC

DSC experiments were conducted on a Nano-DSC (TA Instruments, New Castle, DE, USA) equipped with 0.3 mL capillary platinum cells. The sample cell was filled with 0.3 mL of protein solution and the reference cell with the same volume of buffer (we used different buffer in function of the study, see results). Samples and buffers were filtered and degassed in vacuum before loading into the DSC cell. Baselines were obtained by performing blank buffer-buffer scans. The total enthalpy change needed for the complete unfolding, ΔH_{cal} , was calculated by integration of the excess heat capacity of the unfolding transition, $\Delta C_{P,trs}$, over temperature in the significant temperature interval:

$$\Delta H_{cal} = \int_{T_1}^{T_2} \Delta C_{P,trs} dT$$

Here T_1 and T_2 represent absolute temperature values before and after the unfolding process, respectively. Nano-Analyze TA and MicroCal Origin Pro 8.0 Software were used for baseline subtraction and ΔH_{cal} calculation.

Thermograms on mitochondrial Hsp60, naïve Hsp60 and GroEL were obtained within the temperature range 25 ÷ 90 °C at various scan rate (10 ÷ 90 °C/h). The protein concentration was 0.08 ÷ 0.4 mg/ml. Thermograms on chaperonins Pf-CD1, Pf-H and Pf-R were obtained within the temperature range 25 ÷ 120 °C at a scan rate of 60 °C/h. The protein concentration was 0.1 ÷ 0.4 mg/ml. Thermograms on α -casein and insulin were carried out within the temperature range 7 ÷ 85 °C, at a scan rate of 20 °C/h.

When discussing results in the following chapters (IV-VII) T_m will indicate the apparent melting temperature, i.e., the temperature at which excess unfolding heat capacity is maximal. The calorimetric enthalpy ΔH_{cal} , which is determined

independently of any model will be compared with the van't Hoff enthalpy (ΔH_{vh}) derived by the differential scanning calorimetry data according to the *Privalov* and *Khechinashvili* procedure, as follows:

$$\Delta H_{vh} = 4RT_M^2 (\Delta C_{P,max}/\Delta H_{cal})$$

Where R is the gas constant.

3.2.2 Isothermal Titration Calorimetry, ITC

Two models of ITC calorimeters (Nano ITC Low Volume and Nano ITC Standard Volume) by TA Instruments were used in the course of the thesis' work. The oligomeric equilibrium of chaperonins GroEL, mitochondrial Hsp60 and its precursor native form was studied by using the Nano ITC Low Volume with a reaction cell volume of 166 μ L. The experimental procedure was similar to that described in a recent work on the oligomeric equilibrium of the co-chaperonin GroES [3.3 - 3.4]. Briefly, the protein solution (20 mM Tris-HCl (pH 8) buffer containing 30mM NaCl and 3% w/w glycerol) was loaded into the titration syringe at a concentration of 0.4mg/ml, and the reaction cell was filled with buffer solution. Prior to use, both protein solutions and buffer were filtered and degassed in vacuum. The experiments were carried out at 25 °C. Each titration consisted of 34÷25 successive injections of 1.5÷2 μ L of the protein solution into the reaction cell. The time interval between consecutive injections was 5 min and stirring at 300 rpm was applied to ensure complete mixing. The heat values were obtained by integrating each thermal power peak. Data analysis and modeling were carried out using Nano-Analyze Data Analysis TA® and MicroCal Origin Pro 7.0 Software.

The same Nano ITC Low volume was used in investigating the binding reaction between the group I chaperonin mt-Hsp60 and amyloid peptide A β 1-40 at different stages of its fibrillization process. The experiments were carried out in buffer 20 mM Tris-HCl (pH 8), 30mM NaCl, 5mM DTT, and 3% w/w of glycerol at 25°C. Titration experiments consisted in successive 2 μ L injections (25 steps) of A- β solutions (50 μ M) into mt-Hsp60 (2 μ M), with a time interval between injections

of 300 sec. Stirring at 280 rpm should ensure good mixing. All samples were degassed before the experiment.

Binding isotherms were corrected by subtracting both the ligand and protein (receptor) dilution isotherms. These are determined by titrating A- β solutions into buffer or titrating buffer into mt-Hsp60 solutions. The heat of binding corrected for dilution effects is [3.5]:

$$Q_{\text{corr}} = Q_{\text{meas}} - Q_{\text{dil,ligand}} - Q_{\text{dil,macromolecule}} - Q_{\text{blank}}$$

Data analysis and modeling were carried out by using Nano-Analyze Data Analysis TA® and MicroCal Origin 7.0 software.

For all the experiments, the dependence of the heat of reaction on the mole of titrant added conforms to a simple model of one-set binding. The model assumes that there is a single independent binding site on each subunit forming 1:1 ligand/protein complex. In this case, the analytical solution for the normalized heat associated with each injection is:

$$Q_i = \frac{V_0 \Delta H}{v_{\text{inj}} L_0} \left([PL]_i - [PL]_{i-1} \left(1 - \frac{v_{\text{inj}}}{V_0} \right) \right) + q_d$$

Where V_0 is the reaction volume, ΔH is the enthalpy of binding, $[PL]_i$ is the concentration of protein-ligand complex in the reaction volume after each injection i , v_{inj} is the injected volume, L_0 is the ligand concentration in the syringe, and q_d is the background injection heat effect. The concentration of protein-ligand complex after each injection i , $[PL]_i$, is calculated by solving and applying the following equations:

$$[P]_{t,i} \frac{K[L]_i}{1 + K[L]_i} + [L]_i - [L]_{t,i} = 0$$

$$[PL]_i = [P]_{t,i} \frac{K[L]_i}{1 + K[L]_i}$$

Where K is the equilibrium binding constant, and $[P]_i$ and $[L]_i$ are equilibrium concentrations on protein and ligand, respectively. The total concentrations of protein and ligand in the calorimetric cell after each injection i are given by:

$$[P]_{t,i} = P_0 \left(1 - \frac{v_{inj}}{V_0}\right)^i$$

$$[L]_{t,i} = L_0 \left(1 - \left(1 - \frac{v_{inj}}{V_0}\right)^i\right)$$

Data fit to the model provides the equilibrium constant K and the change of enthalpy ΔH as fitting parameters. The corresponding changes of free energy, ΔG , and entropy, ΔS , are then determined by:

$$\Delta G = -RT \ln K$$

$$\Delta G = \Delta H - T\Delta S$$

Where R is the gas constant and T the absolute temperature.

The oligomeric equilibrium for Group II chaperonins Pf-CD1, Pf-H and Pf-R was studied by using a Nano ITC Standard Volume (TA Instruments) with a reaction cell volume of 1 mL. Prior to use, protein solutions and buffer were filtered and degassed in vacuum. The experiments were carried out at 25 °C. The protein solution (20mM phosphate, pH 7.5, containing 100 mM NaCl) was loaded into the titration syringe at a concentration of 0.3 mg/mL. Each titration consisted of 18-19 successive injections of 5 μ L protein solution into the reaction cell (980 μ L) filled with buffer only. The time interval between consecutive injections was 5 min and stirring at 300 rpm was applied to ensure complete mixing. A new hexadecamer-monomer equilibrium model was developed to analyze ITC curves.

The Nano ITC Standard Volume was also used for experiments on ATP binding to Group II chaperonins Pf-CD1, Pf-H and Pf-R. The measurements were carried out at 37 °C in 20 mM Tris-HCl, 20 mM MgCl₂ and 10 mM KCl (pH 7.6). Prior to use, all solutions were degassed under vacuum to eliminate air bubbles. ATP concentration was determined by the absorbance at 259 nm using an extinction coefficient of 15,400 M⁻¹ cm⁻¹. Titration experiments were performed by successive 5 µL injections of freshly prepared 200 µM ATP solution into the reaction cell (volume 1 ml) filled with the protein solution at 7.5 µM concentration. The volume of the reaction cell is, spaced at 5 min intervals (stirring speed was 280 rpm). The time interval between consecutive injections was 600 s and stirring rate was 300 rpm. Binding isotherms were corrected by subtracting the ligand dilution isotherms, determined by titrating ATP solution into buffer. For all three proteins, the model of one-set binding well described the dependence of the heat of reaction on the mole of titrant added.

3.2.3 Circular Dichroism, CD

CD measurements were performed on a JASCO J-815 (Easton, MD, USA) spectropolarimeter equipped with a Peltier unit for the temperature control. Far-UV CD spectra (260-190 nm) on chaperonins in solution were recorded at 20 °C with 0.1 mm quartz cuvettes, using a data pitch of 0.5 nm, a bandwidth of 3 nm, a scan rate of 50 nm/min, a response time of 4 s. Each spectrum measurement was obtained by averaging over eight scans and subtracting the blank solvent.

Secondary structure composition and assignments from CD spectra in terms of percent of alpha-helix, beta-sheet, turn and random coil content, were obtained by CDPro analysis [3.6].

3.2.4 High Performance Liquid Chromatography, HPLC

Size-exclusion chromatography was employed to investigate the effect of mt-Hsp60 on the fibrillization of the amyloid peptide β_{1-40} . Chromatographic separations were performed with a modular Prominence Shimadzu HPLC device equipped with a mobile phase degasser (DGU-20As), a quaternary pump (LC-2010 AT) a photodiode array detector (SPD-M20A). A 20 μ L sample loop was used for analytical measurements and a 500 μ L sample loop was employed to design collection of A β . For both analytical and preparative measurements, samples were separated with a Superdex 200 increase (GE Healthcare), at room temperature and eluted with a flow of 1 ml min⁻¹ in the sample buffer (20 mM Tris - HCl pH 7.7 with 3% glycerol and 30 mM NaCl) degassed by an in-line degasser filter (DGU 20A5). The chromatographic profiles were reported at 280 nm. Analytical measurements were used to determine the Hsp60 concentration [3.7]. The column was calibrated using two specific calibration kits for both low and high molecular weights globular proteins (low code n 28-4038-41; High code n 28-4038-42 - GE Healthcare Life Science). The protein used are: Aprotinin MW 6500 Da, Ribonuclease A MW 13700 Da, Stoke Radius (SR) 1.64 nm; Carbonic anhydrase MW 29.000; Ovalbumin 44000 Da, SR 3.05 nm; Conalbumin MW 75000 Da; Aldolase MW 158000 Da, SR 4.81 nm, Ferritin 440000 Da, SR 6.1 nm; Tyroglobulin 669000 Da SR 8.5 nm.

Size-exclusion chromatography was employed to investigate the relative distribution size-distribution of oligomers for Group II chaperonins. We used a Tosoh TSKgel SuperSW3000 column, 4 μ m particle size, 4.6 mm ID \times 30 cm (Montgomeryville, PA, USA) connected to an Agilent 1200 (Palo Alto, CA, USA) equipped with an isocratic pump and photodiode UV detector. In each run, 7 μ g of sample were eluted over 25 min using 20 mM sodium phosphate containing 100 mM sodium chloride (pH 7.3) as running buffer. The flow rate was 0.25 mL/min at a pressure of 68 bar. Absorbance was monitored at 280 nm. After the UV module, the flowpath included a Minidawn Treos (Wyatt Technologies, Santa Barbara, CA, USA) multiangle light scattering instrument followed by a REx refractive index detector (Wyatt Tecnologies). A dn/dc value of 0.185 was used to determine the

concentrations for molecular weight calculations. Data analysis was carried out with Astra Software version 5.3.4 (Wyatt Technologies).

3.2.5 Light Scattering, LS

The light scattered intensity and its time autocorrelation function were measured by using a Brookhaven BI-9000 correlator and a 50 mW He–Ne laser tuned at $\lambda=632.8$ nm. The samples were filtered through 0.2 μm Millex-LG filters into a dust-free quartz cell and placed in the cell compartment of a Brookhaven Instruments BI200-SM goniometer. The temperature was controlled within 0.1°C using a thermostatic recirculating bath. Measurements were taken at 90° scattering angle. Static light scattering data were corrected for the background scattering of the solvent and normalized by using toluene as a calibration liquid. In Dynamic light scattering experiments, the correlator was operated in the multi-channel mode. The electric field autocorrelation function, $g^{(1)}(q,t)$, obtained from the intensity autocorrelation function, was analyzed by using CONTIN to determine the distribution of relaxation times according to:

$$g^{(1)}(q, t) = \int A(\Gamma) \exp(-\Gamma t) d\Gamma$$

Where $A(\Gamma)$ denotes the contribution amplitude of the mode with characteristic time Γ^{-1} . The latter is related to the translational diffusion coefficient by $\Gamma = q^2 D_T$. The hydrodynamic radius R_H is obtained by the Stokes–Einstein relationship:

$$D_T = \frac{k_B T}{6\pi\eta R_H}$$

Where k_B is the Boltzmann constant, T is the absolute temperature, and η is the solvent viscosity

3.2.6 Fluorescence Spectroscopy, FS

ThT fluorescence emission was monitored by using a JASCO FP-6500 spectrometer. The excitation and emission wavelengths were 450 and 485 nm, respectively. The slit width was 3 nm. ThT final concentration was 12 μ M. The sample was placed at 37 °C in the thermostated cell compartment (10 mm). When required, a magnetic stirrer at 200 rpm (mod. 300, Rank Brothers Ltd., Cambridge) was used.

3.2.7 Atomic Force Microscope measurements, AFM

AFM measurements were performed by using a Nanowizard III (JPK Instruments, Germany) mounted on an Axio Observer D1 (Carl Zeiss, Germany) or on an Eclips Ti (Nikon, Japan) inverted optical microscope. Aliquots of protein solutions were deposited onto freshly cleaved mica surfaces (Agar Scientific, Assing, Italy) and incubated for up to 20 min before rinsing with deionized water and drying under a low pressure nitrogen flow. Imaging of the protein was carried out in intermittent contact mode in air by using NCHR silicon cantilever (Nanoworld, Switzerland) with nominal spring constant ranging from 21 to 78 N/m and typical resonance frequency ranging from 250 to 390 kHz.

Chapter IV

(Dis)assembly and Structural Stability of chaperonins group I (GroEL/Hsp60)

4.1 Aim and introduction

Heat shock protein (Hsp60) is a molecular chaperone that assists protein folding in mitochondria. It is synthesized in the cell cytoplasm as a higher molecular weight precursor form (named p-mtHsp60) containing an N-terminal targeting sequence, which is cleaved after import into the mitochondrial matrix [4.1, 4.2]. The protein deprived of the N-terminal sequence is generally named mt-Hsp60. It has been established, and demonstrated by various techniques, Hsp60 can accumulate in the cytosol, in various pathological conditions (i.e., cancer and chronic inflammatory diseases). The accumulation of cytosolic Hsp60 may occur with or without concomitant mitochondrial release, so that the two types of 60 kDa chaperonin proteins, (mtHsp60 and its precursor naïve form, p-mtHsp60) could coexist in the cytosol [4.3]. The precursor naïve Hsp60 is able to assemble in both heptamers and tetradecamers over a wide range of concentration [4.4]. Key questions still unanswered pertain to the differences in structure-function features that might exist between the well-studied prokaryotic homolog GroEL and the largely unexplored eukaryotic Hsp60 proteins. Moreover, studies on human Hsp60 structure and oligomeric state *in vitro* could help to validate its role in physiological or pathological cases. In order to pursue this goal, High-sensitivity Nano differential scanning calorimetry (Nano-DSC), Nano Isothermal Titration calorimetry (Nano-ITC), Circular Dichroism (CD), and High Performance Liquid Chromatography (HPLC) were applied for the first time to study the (dis)assembly, structural and thermal stability of chaperonins group I Hsp60 either in its precursor or mitochondrial form.

4.2 Results & Discussion

Thermal stability of GroEL and Hsp60s

Owing to the ready availability and the marked stability of the bacterial chaperonin system, most of our understanding of chaperonin structure and function comes from investigation of the GroE chaperonin proteins (GroEL and GroES) from *Escherichia coli*. Numerous previous studies have revealed that there are some significant differences between the bacterial and the mitochondrial chaperonins with respect to their oligomeric state, the effect of nucleotides on their interaction with co-chaperonins and their ability to function with co-chaperonins from different sources [4.5, 4.6].

The purpose of the DSC experiments was to compare (for the first time by DSC and CD performed under the same conditions) the thermal unfolding of GroEL, mtHsp60 and its precursor naïve form, p-mtHsp60. Results in Fig. 4.1 show that for all protein systems the oligomer denaturation is a two-stage process, as also evidenced by the ratio between calorimetric enthalpy and van't Hoff that is, as expected by the curve shapes, larger than 1.1 (see Table 4.1). Accordingly, data fit with a two-state unfolding model well reproduces the experimental curve. The relative thermodynamic parameters are also reported in Tab. 4.1.

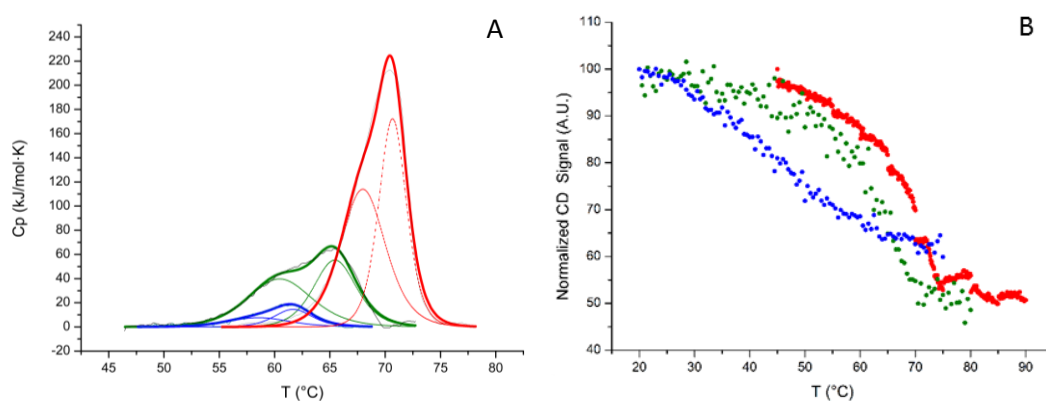


Figure 4.1 Human Hsp60s (mitochondrial and precursor form, respectively blue and green) **compared to bacterial homolog GroEL** (red), at the same condition, scan rate 30°C/hr, protein concentration (0,4mg/ml): a) DSC data. The profile of three proteins contained two distinct endotherms, and was fitted in terms of two coupled transitions. This fitting had the lowest chi square of different models tested independently (data not shown). b) CD data: Characterization of unfolding by following the change in ellipticity at a single wavelength (225 nm) as a function of temperature.

Table 4.1 Parameters of GroEL, mt and p-mtHsp60 heat denaturation

Protein	Sample concentration	ΔH^{Cal} (kJ/mol)	ΔH^{vh} (kJ/mol)	R ^a
GroEL	7 μ M	1205	938	1,28
P-mtHsp60	7 μ M	593	490	1,21
mt-Hsp60	7 μ M	124	80	1,5

ΔH^{Cal} and ΔH^{vh} per subunit

$$^aR = \Delta H^{Cal} / \Delta H^{vh}$$

The three proteins have different thermal and structure stability, in fact they unfold with different melting temperatures (T_m) and different calorimetric enthalpy changes (ΔH_{Cal}). GroEL shows up more stability in respect to mtHsp60 and p-mtHsp60. Indeed, the calorimetric enthalpy of GroEL transition (1205 kJ/mol) is twice larger than that of the precursor form (593 kJ/mol) and about 10-fold the mitochondrial one (124 kJ/mol). The proteins display different cooperativity, too. The sharpness of the transition peak can be measured as the Full Width at Half Maximum (FWHM), which is an index of the cooperative nature (two-state or multistate process) of the transition from native to denatured state. GroEL transition shows the highest cooperativity, as its unfolding transition occurs within a narrow temperature range (FWHM of GroEL denaturation is about 4.69, versus 9 and 6 for p-mt and mtHsp60 respectively). Results from CD measurements as a function of temperature at the same conditions, are in agreement with DSC data (Fig. 4.4). Indeed, as highlighted by the shape and inflection point of the sigmoidal curve, GroEL seems to unfold extremely cooperatively while both p-mt-Hsp60 and mt-Hsp60 unfold gradually (particularly mt-Hsp60). Thus, it appears that the evolution of GroEL has generated such extreme cooperativity in unfolding in order to maximize its functional lifetime under harsh conditions. In turn, mt-Hsp60 is less stable than p-mt-Hsp60, with a lower cooperativity in the thermal denaturation transition. We think that the main biological indication from these results is that a major versatility and flexibility of eukaryotic (particularly mtHsp60) than prokaryotic proteins is closely related to the evolutionary history of a complex.

Thermal investigation and analysis on (dis)assembly and unfolding of GroEL and Hsp60s

As a large mess of information in the literature concerns the unfolding of GroEL, initial experiments were performed to establish whether DSC measurements on structure and thermal stability (in the absence of Mg-ATP) of GroEL could validate basic findings achieved through other techniques, such as light and X-ray scattering [4.7-4.9], urea gradient gel electrophoresis [4.10], etc.

We found that for GroEL (as for both mt-Hsp60 and p-mt Hsp60, see table 4.1) the ratio between calorimetric enthalpy and van't Hoff per subunit is larger than 1.1 (the characteristic value expected for a two state thermal denaturing transition [4.11]). Observing that $\Delta H^{vh} < \Delta H^{cal}$ indicates that most likely there is an unfolding intermediate. The asymmetry observed in the DSC thermograms is evident for all proteins, and DSC unfolding peaks are skewed at temperatures below the transition midpoint (T_m), where the transition is less sharp and deviates more from the two-state fit (Fig. 4.1). Accordingly, best fitting with a two-state unfolding model well reproduces the experimental curves for all three proteins (Fig. 4.1).

The existence of partially unfolded species before and around the transition midpoint but not after it [4.14-4.16] is in agreement with previous data obtained for GroEL by transverse urea gradient gel electrophoresis. In fact, the denaturation of GroEL from the urea-unfolded state in the absence of Mg-ATP [4.10, 4.17] is associated to a two-stage variation in the hydrodynamic volume, which firstly decreases in the region of 2 M urea and then increases noticeably at larger urea concentration. Moreover, it was previously shown by ultracentrifugation, circular dichroism, light scattering, intrinsic tyrosine fluorescence and fluorescence of the hydrophobic probe, 1,1'-bis(4-anilino)naphthalene-5,5'-disulfonic acid (bisANS) [4.18] that urea induces dissociation of the oligomer GroEL [4.16] at moderate concentration and complete dissociation of GroEL into monomers at concentration larger than 2.6 M.

To ascertain the hypothesis of unfolding couple to oligomers dissociation, we made DSC measurements on GroEL samples at different protein concentration (at the same scan rate Fig. 4.2). We observed that the melting temperature and the calorimetric enthalpy increases with protein concentration as expected for a transition coupled to dissociation [4.12].

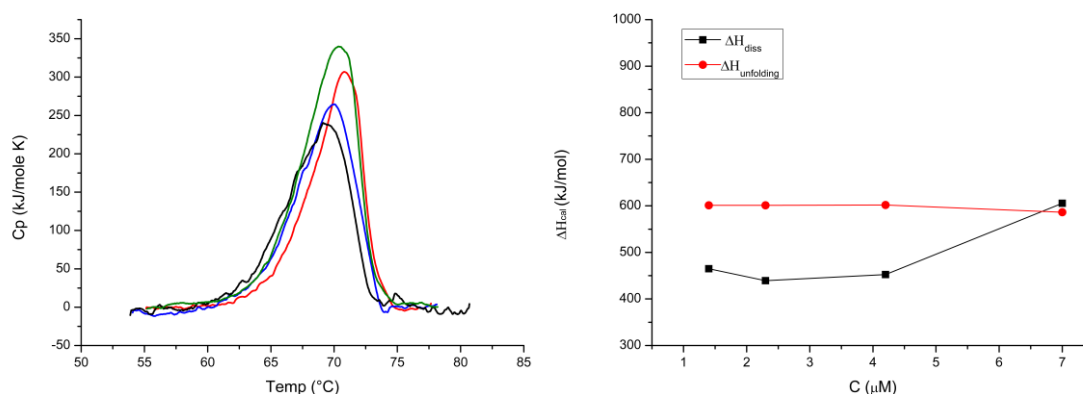


Figure 4.2 Thermal unfolding of GroEL at different protein concentrations. Left panel: DSC profiles for 1.4 μ M (black), 2.3 μ M (blue), 4.2 μ M (red), 7 μ M (green) protein concentration. Right panel: enthalpy contributions of oligomers dissociation (ΔH_{diss}) and monomers unfolding ($\Delta H_{\text{unfolding}}$), obtained by data fitting in terms of two coupled transitions, as a function of GroEL concentration.

DSC thermograms at various protein concentrations were fitted in terms of two coupled transitions. The contributions of each transition to the total enthalpy are shown in the right panel of Fig. 4.2 as a function of protein concentration. It is evident that the enthalpy of dissociation of oligomeric GroEL into subunits (partially unfolded under dissociation) increases with protein concentration, while the enthalpy of unfolding remains constant (this is in agreement with light scattering too, where there is a drastic decrease in intensities of light, data not shown). Thus, our DSC results are consistent with the hypothesis of a dissociation (thermally induced) of the oligomeric protein into monomers that precedes the unfolding.

Complementary CD measurements were done to follow the change in the secondary structure due to unfolding at the same scan rate used for DSC (30°C/hr). The dependence of GroEL ellipticity (measured at 225nm) in the region of absorption of peptide bonds as a function of temperature is shown in Fig. 4.3 (left panel). Data show a slow decrease in the amplitude of circular dichroism and a sharp change in the range from 60 to 75 with a midpoint in the region of 67–70 °C. CD spectra at different temperatures are shown in the right panel of the same figure.

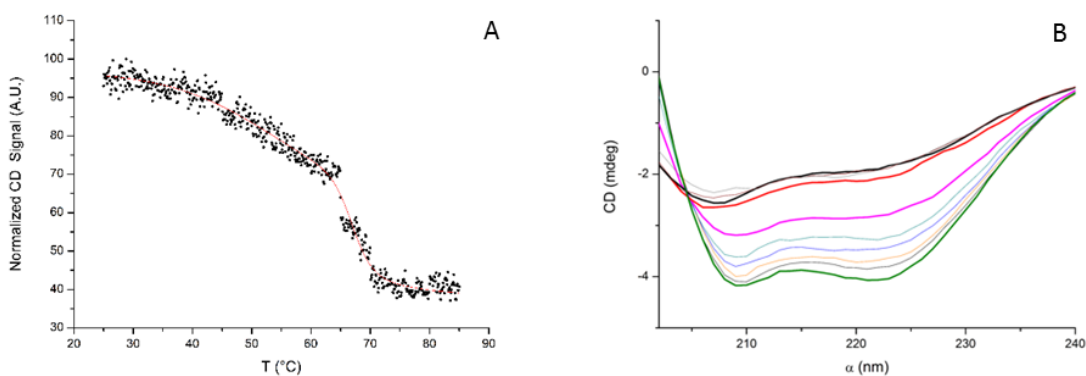


Figure 4.3 CD results for GroEL unfolding. Panel A: dependence of GroEL ellipticity (measured at 225 nm) on temperature (at 30°C/h scan rate). Panel B: CD spectra in the absorption area of peptide bonds at different temperature, green curve (25°C), cyan (60°C), magenta (65°C), red (70°C), black (75°C). Samples contained 2.3 μ M GroEL in 20 mM Tris-HCl (pH 8), 30mM NaCl, and 3% glycerol (w/w). Signals of the buffer blank at different temperature were subtracted from the corresponding samples.

Consistently with DSC results, the initial slow decrease of CD signal at 225 nm and any deviation from the native state spectrum (green spectrum in Fig. 4.3 b) suggest partial unfolding of the protein. In fact, an additional loss of helical CD takes place from 25 to 60°C (cyan spectrum) that could be attributed to a partial loss of secondary structure associated to the oligomers dissociation. The sharp decrease between 67°C and 75°C is conceivably due to the unfolding of protein subunits, since by 75-76 the protein has lost most of its detectable secondary structure (Fig. 4.3 b). It is worth to note that the major variations of secondary structures are observed in the temperature interval where the monomers thermal unfolding falls. Results by means HPLC separations pointed out later in the text, furtherly confirm our data interpretation.

Results for the unfolding of p-mtHsp60 at different concentration as detected by DSC and CD measurements are reported in Fig. 4.4 and Fig. 4.5. Similarly to what observed for GroEL unfolding, DSC thermograms are skewed towards the low temperature side of the transition and are well described by two coupled transition model. Deviations from the native state CD spectrum (black spectrum in Fig. 4.4 b) indicate partial unfolding of the protein, and additional loss of helical CD from 45 to 55°C (cyan spectrum). At temperature above 55°C the protein has lost most

of its detectable secondary structure, in agreement with DSC results. Measurements at different protein concentration show that both the melting temperature and calorimetric enthalpy increase with protein concentration as expected for a transition coupled to dissociation. Thus, our results demonstrate that the unfolding of bacterial and human Hsp60 is coupled with the dissociation of the oligomeric protein. At the best of our knowledge, this result is new and original.

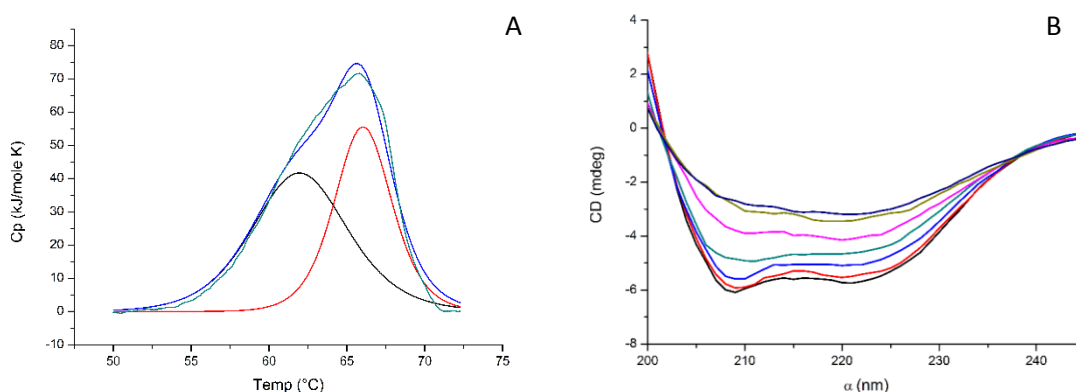


Figure 4.4 Thermal unfolding of p-mtHsp60 followed by DSC and CD. A) p-mtHsp60 (7 μ M) shows a profile with two distinct endotherms. B) CD spectra in the absorption area of peptide bonds at different temperature: black curve (25°C), red (35°C), blue (45°C), dark cyan (55°C), magenta (65°C), dark yellow (75°C), navy (85°C). Samples contained 7 μ M p-mtHsp60 in 20 mM Tris-HCl (pH 8), 30mM NaCl, and 3% glycerol (w/w).

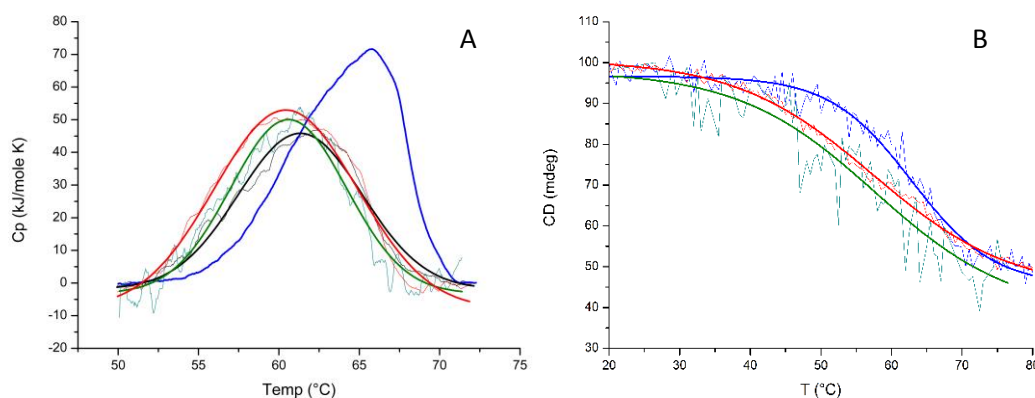


Figure 4.5 A) Thermal unfolding of p-mtHsp60 at different protein concentrations: dark cyan (1.4 μ M), black (2.3 μ M), red (4.2 μ M), blue (7 μ M). B) Dependence of p-mtHsp60 ellipticity measured at 225 nm at different concentrations as a function of temperature (30°C/hr). The interpolated sigmoidal curves are drawn as eye guides.

Due to the very low intensity of signal detected by the nano-DSC it was not possible to investigate the same range of concentrations in the case of mt-Hsp60. However, CD and DSC results (Fig. 4.1b and Fig. 4.6) indicate that the thermal unfolding can be similar to that observed for GroEL and p-mt-Hsp60. Results from SEC-HPLC presented in the following (see figures 4.7-4.9) confirm the presence of different oligomeric species in equilibrium. In comparison with p-mt-Hsp60, mt-Hsp60 in the native state is less rich in tetradecamers, and this can account for the lower total enthalpy of denaturation.

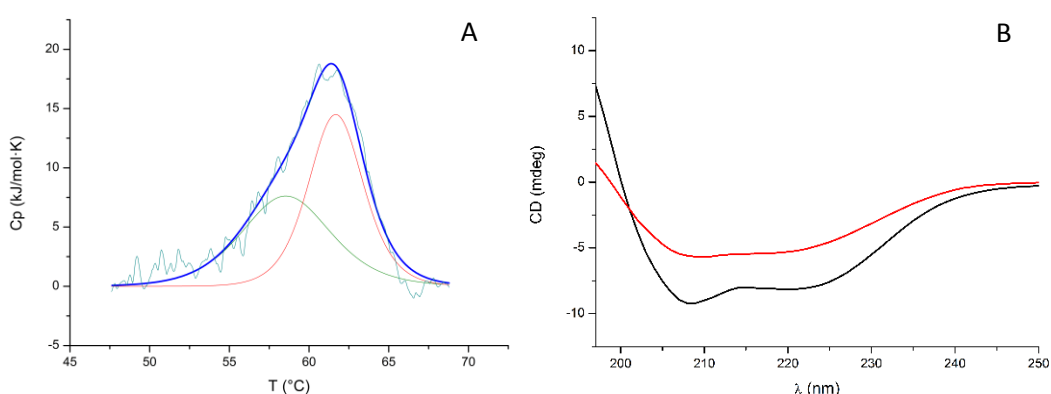


Figure 4.6 Thermal unfolding of mtHsp60 followed by DSC and CD. A) mt-Hsp60 (7 μM) had a profile with two distinct endotherms that was fitted with two coupled transitions model. B) CD spectra in the absorption area of peptide bonds of mtHsp60 at 25°C (black curve) and 70°C (red curve).

HPLC investigation on (dis)assembly of GroEL and Hsp60s

A variety of conditions destabilize GroEL tetradecamers, favoring dissociation to monomers, such as moderate urea concentration [4.26], high hydrostatic pressure [4.27], presence of nucleotides and adsorption onto ion-exchange resins [4.28], and replacement of Lysine 3 at the N-terminus [4.29]. The GroEL N-terminal region is located in the subunit interface and is involved in links that stabilize the protein's quaternary structure. Moreover, mutations in the region encompassing the first 4 amino acids of the mtHsp60 N-terminal region destabilize the protein oligomeric state causing its disassembly at low protein concentrations [4.30].

We made chromatographic separations at HPLC to probe qualitatively and quantitatively the dissociation of the proteins (GroEL and Hsp60) thermally induced, using a superdex increase 200 10/30 GL size exclusion columns (see material and methods).

As highlighted before, in our DSC and CD results there be a partially unfolding of GroEL, that leads first to dissociation (thermally induced) of the protein tetradecameric structure to heptamers and monomers, and it would be consistent with HPLC separations. In fact, for GroEL, we saw in the region of the dissociation thermally induced (light green curve), a dissociation in heptamers and monomers (see retention time from 8 to 13 in the panel on the right of Fig.4.7).

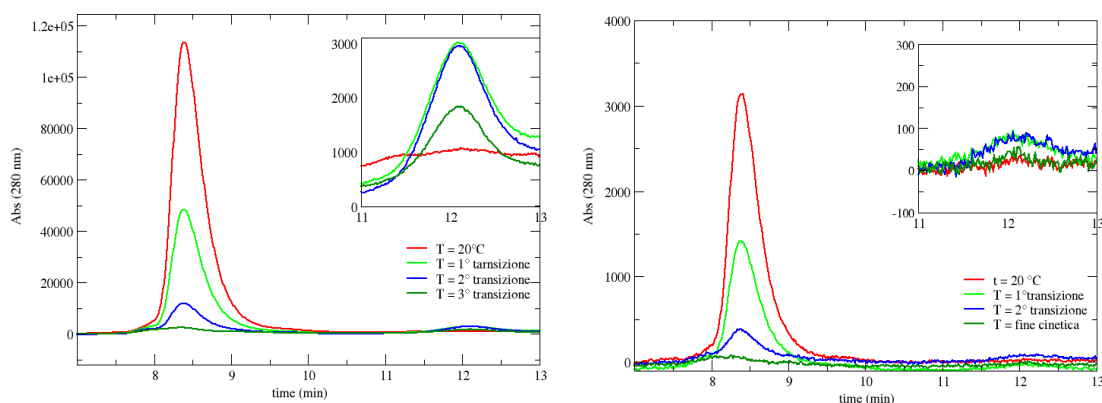


Figure 4.7 GroEL (3,5 μ M) chromatographic separations at HPLC. Sample scanned 30°C/hr till different temperatures: Native protein (red curve), T=25°C; on the peak of the deconvolution of dissociation (light green), T=69°C; after the melting point (blue), T =72°C, and at the end of the transition, T=74°C (dark green).

For p-mtHsp60, in the region of the dissociation thermally induced, we saw a clear dissociation of tetradecamers in heptamers (Fig. 4.8), from 30% to 50%. While in the case of mt-Hsp60 just at room temperature 25°C is evident the dynamic equilibrium between tetradecamers heptamers and monomers (Fig. 4.9).

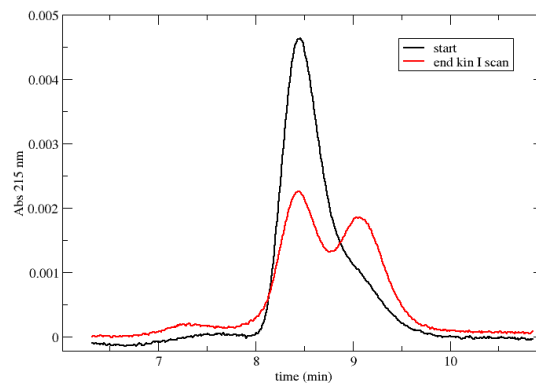


Figure 4.8 P-mtHsp60 (1 μ M) chromatographic separations at HPLC. Sample scanned 30°C/hr: Native protein (black curve), T=25°C; on the peak of the deconvolution of dissociation (light green), T=62°C.

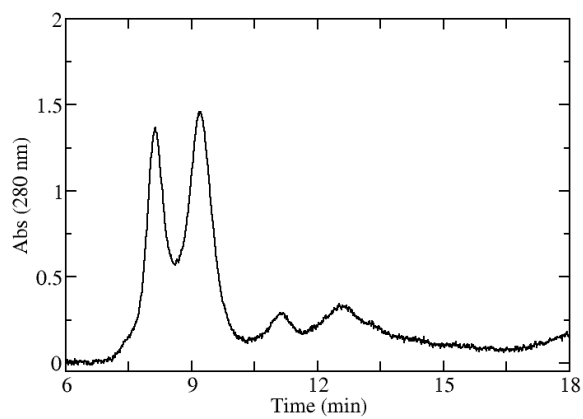


Figure 4.9 Mt-Hsp60 chromatographic separations at HPLC at 25°C.

The Tetradecamer-Heptamer-Monomer Dissociation/Unfolded Model (THMDU model)

To gain major information on the processes responsible for the DSC signal recorded for the three proteins upon a temperature scan, we developed an *ad hoc* model. It assumes a first dissociation of tetradecamers into heptamers followed by dissociation of heptamers into monomers simultaneous with monomer unfolding. The Tetradecamer-Heptamer-Monomer Dissociation/Unfolded Model (Eqn 1) was adapted and used for the analysis of the DSC curves. All the equations and thermodynamic parameters are given in terms of moles of protein monomer. At any given total protein concentration, P_t , the molar fractions of the polypeptide chains forming the native Tetradecamer (F_T), the heptamer fraction (F_H) the unfolded monomer (F_M) and the equilibrium constants K_{d1} and K_{d2} are combined in the following expression:

Chemical balance



$$K_{d1} = \frac{[H]^2}{[T]} \quad K_{d2} = \frac{[M]^7}{[H]}$$

$$F_M = \frac{[M]}{P_t} \quad F_H = \frac{7[H]}{P_t} \quad F_T = \frac{14[T]}{P_t}$$

As $1 = F_M + F_H + F_T$, and considering the mass balance $P_t = M + 7H + 14T$

We obtained:

$$P_t = M + 7 \frac{[M]^7}{K_{d2}} + 14 \frac{[H]^2}{K_{d1}} = M + 7 \frac{[M]^7}{K_{d2}} + 14 \frac{[M]^{14}}{K_{d1} K_{d2}^2}$$

$$7 \frac{[M]^7}{K_{d2}} + 14 \frac{[M]^{14}}{K_{d1}K_{d2}^2} + M - P_t = 0$$

$$14 \frac{P_t^{14}}{K_{d1}K_{d2}^2} \frac{P_t^{14}}{P_t^{14}} + 7 \frac{[M]^7 P_t^7}{K_{d2} P_t^7} + M \frac{P_t}{P_t} - P_t = 0$$

$$14 \frac{[P_t]^{14}}{K_{d1}K_{d2}^2} F_M^{14} + 7 \frac{P_t^7}{K_{d2}} F_M^7 + P_t F_M - P_t = 0$$

Solving this equation leads to F_M . The enthalpy of the system will be:

$$\Delta H_{\text{ext}} = F_{\text{monomer}} * \Delta H_2 + F_{\text{heptamer}} * \Delta H_1;$$

Where ΔH_1 is the unfolding enthalpy change. The derivative of this expression with respect to temperature at a constant pressure gives the heat capacity of the protein, C_p :

$$C_p = (dH_{\text{ext}} - dH_{\text{exp}}) / (T_t - T_p) - F_{\text{monomer}} * dC_p d - F_{\text{heptamer}} * dC_p u + C_{p0}$$

The Fig. 4.10 shows the fit and the fraction of the different populations as a function of temperature for GroEL at different protein concentrations. The corresponding thermodynamic parameters are reported in Table-4.2.

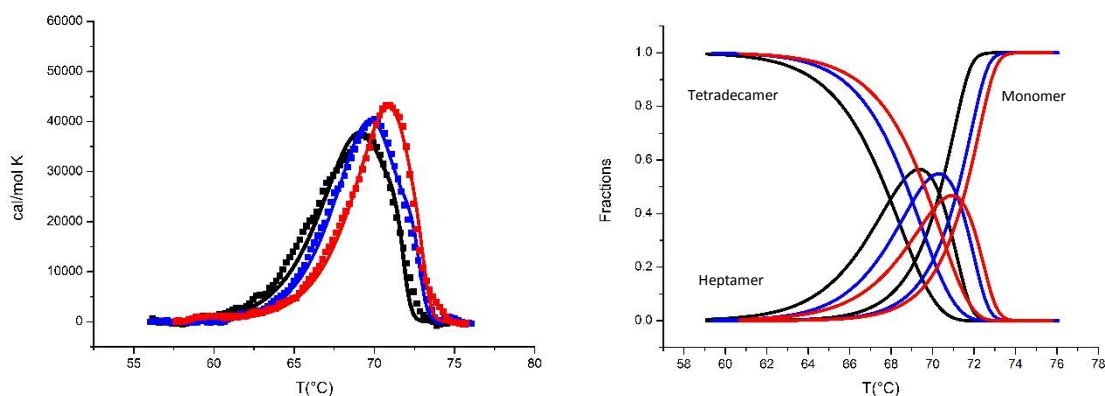


Figure 4.10 On the left: DSC thermograms for GroEL (at different concentrations, black 1.4 μM , blue 2.3 μM , red 4.2 μM). Symbols represent the experimental data. The continuous lines are the fit with Tetradecamer-Heptamer-Monomer Dissociation/Unfolded Model. On the right: Fraction of the different populations in function of the temperature as obtained by the model.

Table 4.2-Thermodynamic parameters obtained by fitting DSC thermograms of GroEL with THMDU model

GroEL Concentration (μM)	1.4	2.3	4.2
$T_{1/2}$ (Tetradec. conversion) ($^{\circ}\text{C}$)	67.67	68.7	69.5
ΔH1 (cal/mol)	62920	63977	98389
ΔH2 (cal/mol)	162160	163512	168458
ΔCp1 (cal/mol K)	-2560	-3270	-1204
ΔCp2 (cal/mol K)	349	370	769

We found a negative ΔCp for the ring dissociation. ΔCp could be negative when transient interactions are involved (as it occurs for tetradecamer-heptamer transition in GroEL) and the proportion of hydrophobic-to-hydrophilic (or apolar-to-polar)

surface ratio is more shifted to the hydrophilic component. Most of polar amino-acids presented in the GroEL monomer (on 548 a.a. 286 are apolar and 262 are polar) are in the equatorial domain (see Fig. 4.11) that is in the interaction surface for both heptamers. The equatorial domains are located at the interface of the *cis* and *trans* rings (residues 6-133, 409-523). In the residues 409-523, 58 amino acids are polar and 57 are apolar, while in the residues 6-133, 65 are apolar and 63 are polar.

The Figure 4.11 shows the GroEL tetradecamer complex obtained by Pymol. Each atom is represented as a sphere of Van der Waals radius; in light cyan are shown the apolar amino acids, while in dark cyan the polar ones. Most of polar amino acids are located in the equatorial domain. The panel on the right side shows the surface of the interface from one of the heptamers. There is a predominance of polar residues, similar to the polar/apolar distribution on the lateral surface (permanently exposed to solvent) and the interface with the chaperonin GroES (transiently exposed to solvent). The predominance in polar residues provides the structural and energetic basis for establishing transient and/or dynamical interactions between the two heptamers. In addition, polar residues contribute to a negative heptamer dissociation heat capacity (as observed from DSC results).

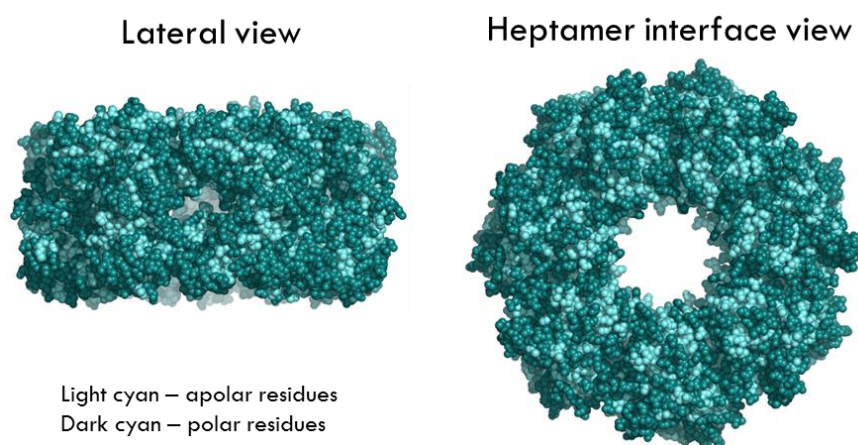


Figure 4.11 GroEL tetradecamer complex obtained by Pymol. Apolar residues are shown in light cyan, polar residues in dark cyan.

Results of DSC data fitting with THMDU model for p-mtHsp60 and mtHsp60 are reported, respectively in Figs. 4.12, 4.13 and Tables-4.3, 4.4. As it occurs for tetradecamer-heptamer transition in GroEL, a negative ΔC_p of ring dissociation was obtained for both p-mtHsp60 and mtHsp60 (Table 4.3 and 4.4), implying that transient interactions are involved for the human homologue.

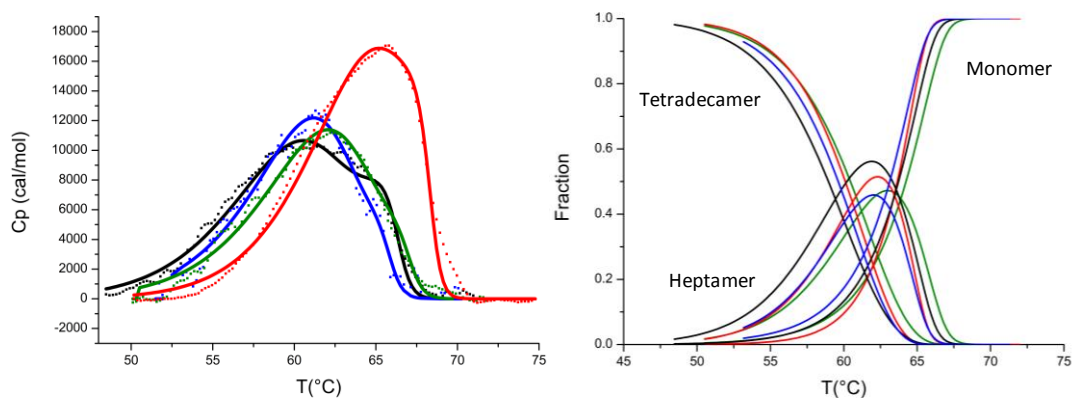


Figure 4.12 On the left: DSC thermograms for p-mt Hsp60 (at different concentrations, black 1.4 μM , blue 2.3 μM , red 4.2 μM). Symbols represent the experimental data. The continuous lines are the fit with Tetradecamer-Heptamer-Monomer Dissociation/Unfolded Model. On the right: Fraction of the different populations in function of the temperature as obtained by the model.

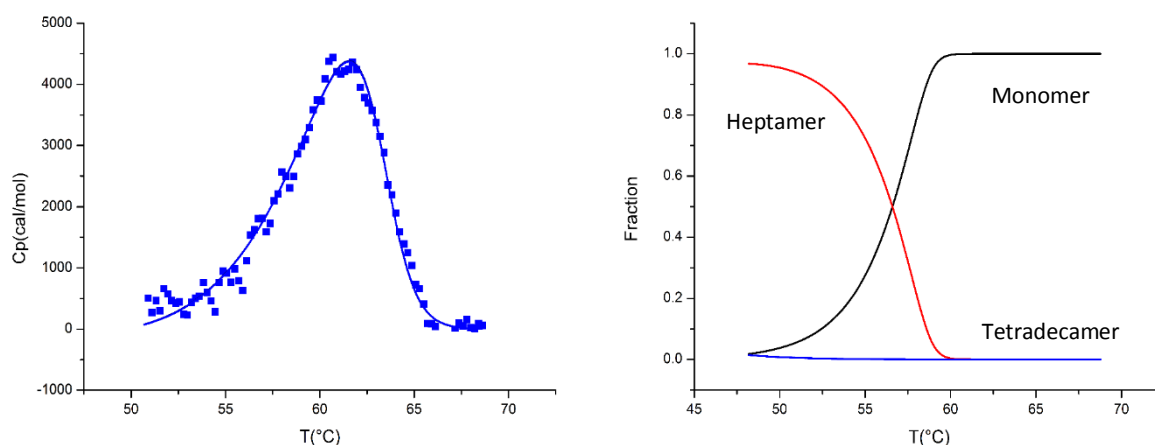


Figure 4.13 On the left: DSC thermogram for mt-Hsp60 at 7 μM . Symbols represent the experimental data. The continuous lines is the fit with Tetradecamer-Heptamer-Monomer Dissociation/Unfolded Model. On the right: Fraction of the different populations in function of the temperature as obtained by the model.

Table 4.3-Thermodynamic parameters obtained by Fit with THMDU model for p-mtHsp60

p-mtHsp60 Concentration (μM)	1	2	4	7
$T_{1/2}$ (Tetradec. conversion) ($^{\circ}\text{C}$)	59.3	60	59.5	62.7
ΔH1 (cal/mol)	1500	1500	3428	11580
ΔH2 (cal/mol)	147663	122537	118220	122534
ΔCp1(cal/mol K)	-1254	-1154	-1601	-1492
ΔCp2 (cal/mol K)	2503	1597	942	847

Table 4.4-Thermodynamic parameters obtained by Fit with THMDU model for mtHsp60

mtHsp60 Concentration (μM)	7
$T_{1/2}$ (Tetradec. conversion) ($^{\circ}\text{C}$)	59
ΔH1 (cal/mol)	518
ΔH2 (cal/mol)	117593
ΔCp1(cal/mol K)	-921
ΔCp2 (cal/mol K)	2572

The fit quality for all three proteins (GroEL and p-mt and mtHsp60) at the same concentration is illustrated in Fig. 4.14. The relative thermodynamic parameters are compared in table 4.5.

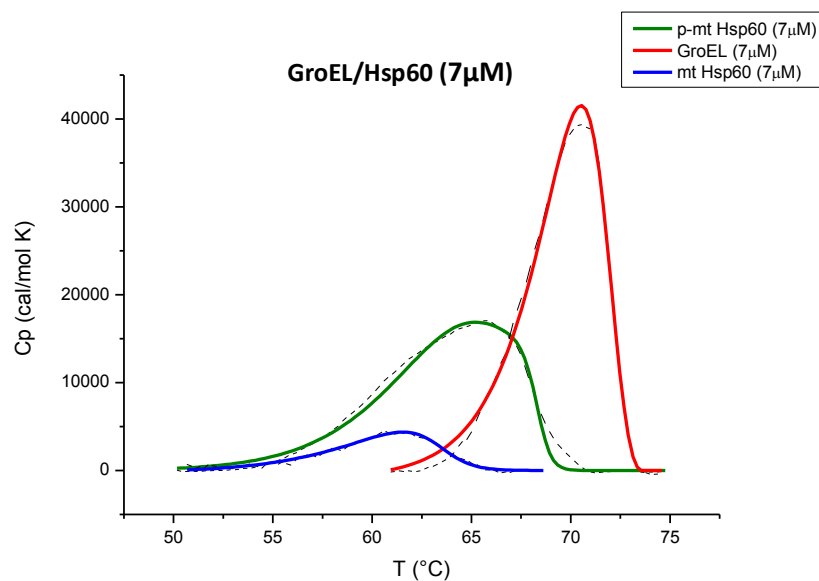


Figure 4.14 Experimental DSC thermograms and best fit with Tetradecamer-Heptamer-Monomer Dissociation/Unfolded Model for GroEL (red curve), p-mt Hsp60 (green curve) and mt Hsp60 (blue curve).

Table 4.5- Comparison of the Thermodynamic parameters obtained by Fit with THMDU model for the three proteins

Protein (7 μ M)	GroEL (Bacterial Hsp60)	p-mt Hsp60	mt Hsp60
$T_{1/2}$ (Tetradec. conversion) ($^{\circ}$ C)	69.3	62.7	59
$\Delta H1$ (cal/mol)	81929.2	11580	518
$\Delta H2$ (cal/mol)	159517	122534	117593
$\Delta Cp1$ (cal/mol K)	-1122	-1492	-921
$\Delta Cp2$ (cal/mol K)	1913	847	2572

Further investigation of (dis)assembly and unfolding of GroEL and Hsp60s: dealing with irreversibility

By literature and by our own results, we know that partial unfolding of GroEL leads first to the dissociation of the oligomeric protein. Considering this point, we tried to study separately the oligomer dissociation and monomer unfolding by combined DSC and by HPLC measurements. We stop the DSC experiment to 66°C, in the region of the thermally induced oligomers dissociation (and partially unfolding) and then rescan again from 25 to 85°C (Fig. 4.15). We obtained a transition peak very similar to the second peak (assigned to unfolding) obtained from deconvolution of the original DSC signal for a fresh protein sample.

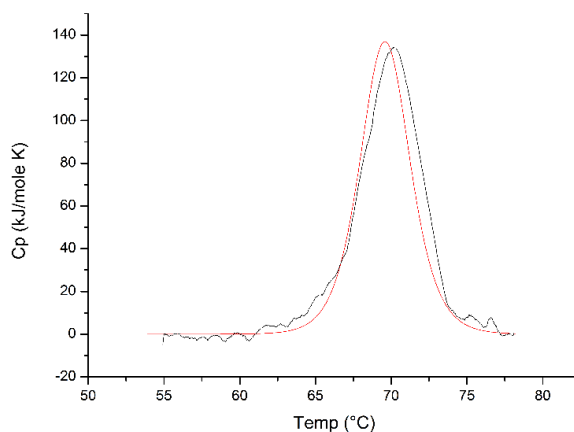
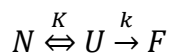


Figure 4.15 DSC thermogram for a sample of GroEL firstly brought to 66°C at 30°C/hr scan rate and then re-cooled at room temperature (black curve). The red curve represents the second peak (assigned to unfolding) obtained from deconvolution of the original DSC signal for a fresh protein sample.

We evaluated this transition by comparing ΔH^{Cal} with ΔH^{vh} to assess whether the transition occurs as a two-state or multistate process. Our system undergoes cooperative two-state unfolding with $\Delta H^{Cal} / \Delta H^{vh} \approx 1$, so the transition occurs in a two-state mode. A closer inspection of the peak assigned to unfolding was then performed for taking into account partial irreversibility of the unfolding process. Irreversible protein denaturation is thought to involve, at least, two steps: (a) reversible unfolding of the native protein (N); (b) irreversible alteration of the unfolded protein (U) to yield a final state (F) that is unable to fold back to the native

one. There are several processes responsible for the irreversible step (aggregation, autolysis, chemical alteration of residues, etc.) [4.19, 4.20].

The two-step nature of irreversible denaturation is depicted in the following simplified scheme, which is usually known as the Lumry and Eyring model [4.21]:



Where K and k are the unfolding equilibrium constant and the rate constant, respectively. We will assume that chemical equilibrium between N and U is always established and that the unfolding enthalpy, ΔH_U , is constant. Then, the temperature dependence of K , can be expressed as,

$$1) \quad K = \frac{[U]}{[N]} = \frac{x_U}{x_N} = \exp \left\{ -\frac{\Delta H_U}{R} \left[\frac{1}{T} - \frac{1}{T_{1/2}} \right] \right\}$$

Where x_U and x_N stand for the molar fractions of unfolded and native states and $T_{1/2}$ (or T_m) is the temperature at which $K=1$. The apparent excess enthalpy, $\langle \Delta H \rangle$, is given by,

$$2) \quad \langle \Delta H \rangle = x_U \Delta H_U + x_F \Delta H$$

Where ΔH_U and ΔH are, respectively, the enthalpies of the states U and F (taking N as the reference state). Note that the enthalpy of the final state (ΔH) is equal to the calorimetric enthalpy of the DSC transition, because eventually all protein molecules will be found in the final state. We made the reasonable assumption that the processes responsible for the irreversible step have much lower enthalpy than the cooperative unfolding (see Fig. 4.16). Many authors have previously supported the applicability of the equilibrium thermodynamics analysis to irreversible DSC transitions [4.22-4.24]. Accordingly, we will assume that the enthalpy of the $U \rightarrow F$ transition is zero and that, therefore, $\Delta H_U = \Delta H$. Eq. 2 can be written as,

$$3) \quad \langle \Delta H \rangle = \Delta H(x_U + x_F) = \Delta H(1 - x_N)$$

and the apparent, excess heat capacity, C_p^{ex} is given by,

$$4) C_p^{\text{ex}} = -\Delta H \frac{dx_N}{dT}$$

as ΔH has been assumed to be constant. Finally, dx_N/dT is substituted in Eq. 4 to yield:

$$5) C_p^{\text{ex}} = \frac{K\Delta H}{(K+1)^2} \left(\frac{k}{v} + \frac{\Delta H}{RT^2} \right) \exp \left\{ -\frac{1}{v} \int_{T_0}^T \frac{kK}{K+1} dT \right\}$$

Where v is the constant scanning rate ($v = dT/dt$). It is interesting that the equation corresponding to a two-state reversible unfolding:

$$C_p^{\text{ex}} = \frac{K\Delta H^2}{RT^2(K+1)^2}$$

Can be derived from Eq. 5) either by setting $k = 0$ at any temperature (the irreversible process does not take place) or by setting $1/v = 0$ (infinite scanning rate). In spite of that, it is clear that direct application of equilibrium thermodynamics to the irreversible transition would not lead to large errors [4.19]. We obtained (with $av = 30^\circ\text{C/hr}$) an unfolding enthalpy (ΔH_U) of 660 kJ/mol and an unfolding temperature of 70.2 °C. So, the second stage is associated with further unfolding of GroEL and it occurs in a two-state mode (two-state folding/unfolding model). Actually, the irreversible step in the thermal denaturation of GroEL subunits takes place (with negligible thermal effect) at temperatures somewhat above than those corresponding to the DSC transition; therefore, we were able to study the irreversible step separately and we found an energy of activation of ≈ 32 kJ/mol, that correspond to the irreversible step itself (Fig. 4.16, b).

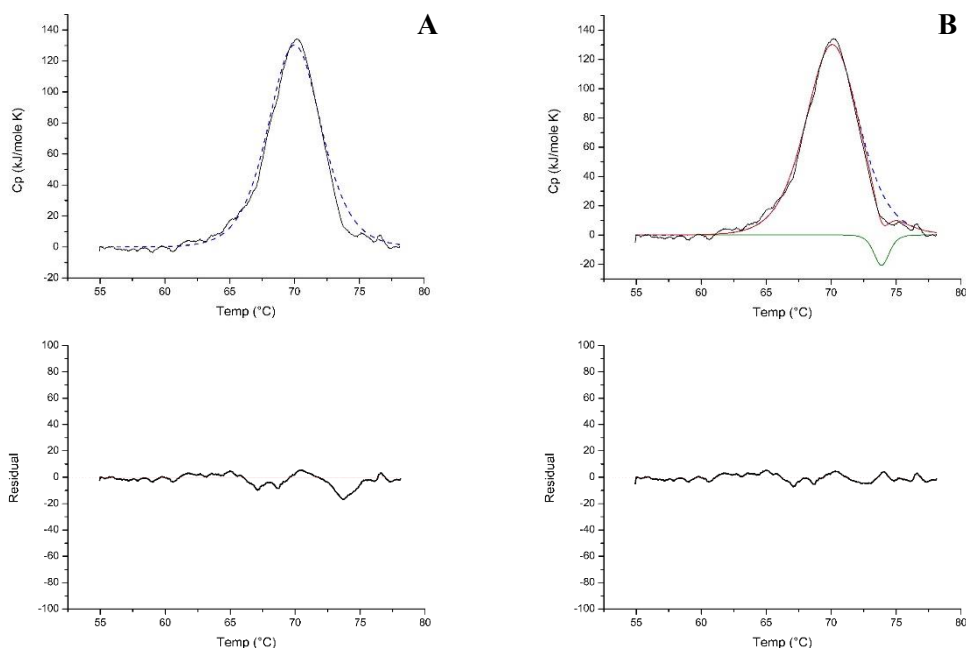


Figure 4.16 Thermal unfolding of GroEL subunits after thermally induced dissociation of oligomers: on the top and residuals of the Fit on the bottom. A) The blue dashed curve is a fit of these data to a simple two-state unfolding model. B) The red curve curve is a fit of these data to a simple two-state unfolding model, containing the irreversible step (green transition) in the thermal denaturation.

Values for the free energy $\Delta G_{\text{trs}}(T)$ were determined by analyzing the experimental data in terms of a two-state transition model. The DSC values for $\Delta G_{\text{trs}}(T)$ are extrapolated to room temperature of 298.15 K, and we used Gibbs–Helmholtz equation:

$$\Delta G(T) = \Delta H_m \left(1 - \frac{T}{T_m} \right) - \Delta C_p (T_m - T + T \ln \left(\frac{T}{T_m} \right))$$

The change in heat capacity ΔC_p for the unfolding was $2.62 \pm 0.13 \text{ kcal mol}^{-1} \text{ K}^{-1}$. We found a ΔG_{trs} of 50 kJ/mol, in accordance with value obtaining by chemical denaturation [4.25].

We made the same experiment for Hsp60 (precursor form, Fig. 4.17), obtaining (with a $v = 30^\circ\text{C}/\text{hr}$) an unfolding enthalpy (ΔH_U) of 490 kJ/mol, an unfolding temperature of 65°C and an energy of activation of the irreversible step of ≈ 52 kJ/mol. We found a ΔG_{trs} of 40 kJ/mol (400kJ/mol dH_m ; dC_p about 3kJ/Kmol), in accordance with value obtaining by chemical denaturation [4.25].

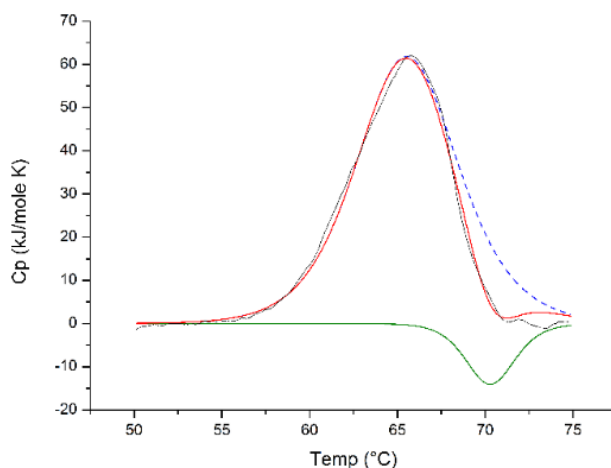


Figure 4.17 Thermal unfolding of Hsp60 subunits after dissociation thermally induced (black curve). The blue dashed curve is a fit of these data to a simple two-state unfolding model; while the red curve curve is a fit of these data to a simple two-state unfolding model, containing the irreversible step (green transition) in the thermal denaturation.

Investigation by ITC

We made ITC dilution measurements to probe the dissociation of the protein [4.31]. The first set of injections into the cell results in a complete protein dissociation and thus give the largest heat changes (Fig. 4.18 and Fig. 4.19). The following injections will reveal a gradual decrease in the heat-changes as the protein concentration in the cell approaches the midpoint (concentration of the Tetradecameric/heptameric rings/monomer equilibrium), toward the end of the titration, injections will not

result in dissociation and there will only be heat changes associated with sample dilution.

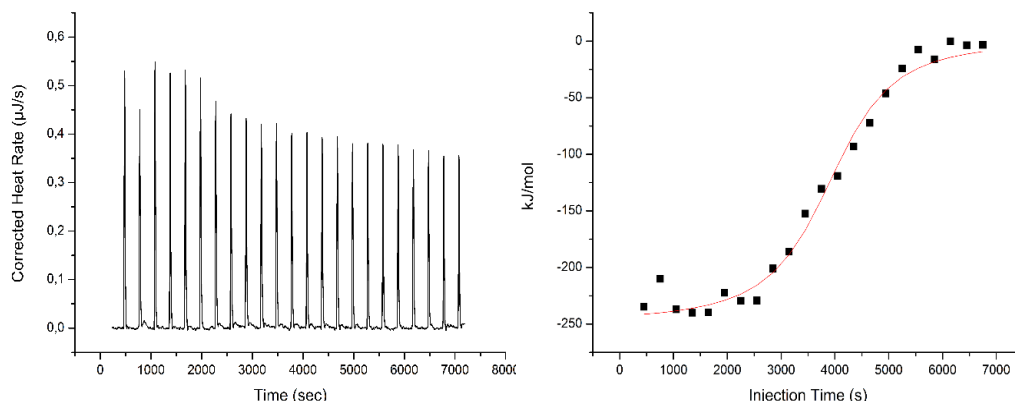


Figure 4.18 GroEL ITC profiles: Calorimetric dilution experiments for exothermic dissociation of tetradecamers at pH 8.0. A) Thermogram of thermal power ($\mu\text{J}/\text{sec}$) as a function of time (sec) for an ITC-dilution experiment (GroEL was loaded into the titration syringe at a concentration of $0.4\text{mg}/\text{ml}$). B) The right panel shows the integrated injection heat values, obtained by integrating each peak and subtracting dilution heat. Continuous lines (red) correspond to interpolations of the experimental data to sigmoid functions and are drawn as a guide for the eye.

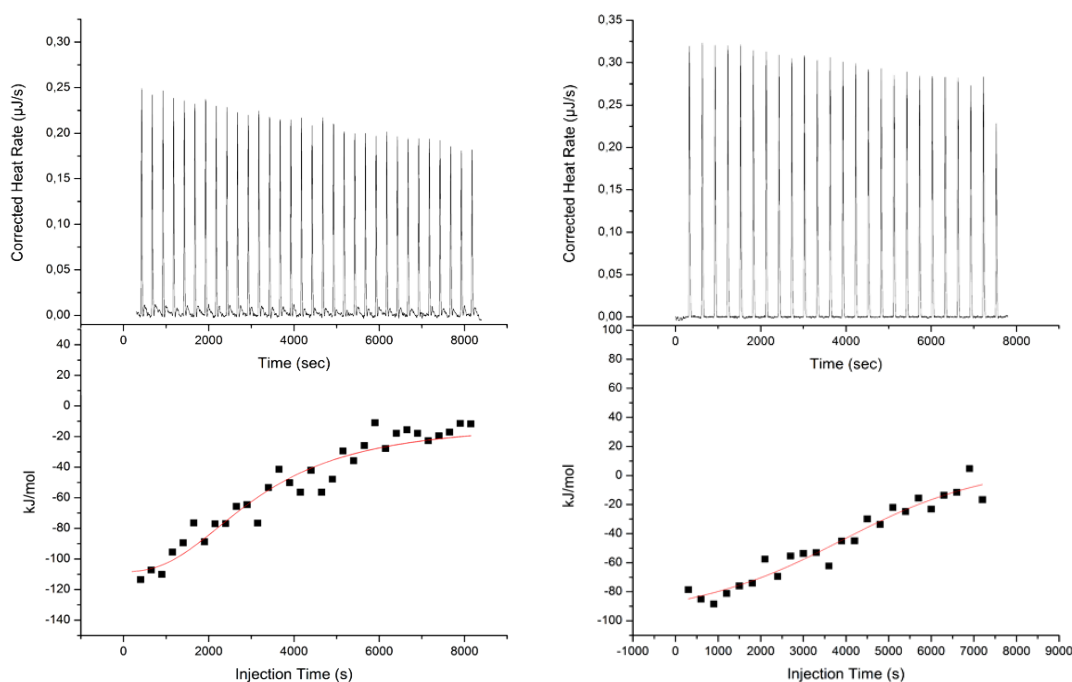


Figure 4.19 Hsp60 ITC profiles: Calorimetric dilution experiments for exothermic dissociation of tetradecamers of p-mtHsp60 and mtHsp60, respectively on the left and on the right. The top panel shows thermograms of thermal power ($\mu\text{J}/\text{sec}$) as a function of time (sec) for an ITC-dilution experiment (Hsp60 was loaded into the titration syringe at a concentration of $0.4\text{mg}/\text{ml}$). While the low panel shows the integrated injection heat values, obtained by integrating each peak and subtracting dilution heat.

We made ITC Titrations measurements to probe the disassembly and the dynamic oligomeric equilibrium in function of protein concentration. We tried to investigate this dynamic equilibrium between Monomers, Heptamers and tetradecamers. The Bayesian information criterion (BIC) suggest as to prefer the model with the lowest BIC (Table 4.6). That in our study means the Tetradecamer-Heptamer-Monomer Dissociation (THMD), Model 3. ITC results support the hypothesis that chaperonin group I can exist in a dynamic equilibrium between Monomers, Heptamers and Tetradecamers. Moreover, the three proteins, as expected, show different stability in the dynamic equilibrium, as highlighted by the different dH_{diss} (250kJ/mol GroEL, 120 kJ/mol p-mtHsp60 and 80kJ/mol mtHsp60), in accordance with HPLC and DSC conclusions.

Table 4.6 BIC of different models for GroEL

Model	Description	BIC
1	Heptamer-Monomer Dissociation (HMD)	24
2	Tetradecamer-Monomer Dissociation (TMD)	34
3	Tetradecamer-Heptamer- Monomer Dissociation (THMD)	20

4.3 Conclusions

We investigated the (dis)assembly and thermal stability of mtHsp60, p-mtHsp60 and GroEL in vitro, by means of DSC, ITC, HPLC and CD. Altogether, our findings suggest that the evolution of GroEL has generated such extreme cooperativity in unfolding in order to maximize its functional lifetime under harsh conditions. In turn, mtHsp60 is less stable than GroEL and p-mtHsp60, with a lower cooperativity in the thermal denaturation transition and a lower ΔH_{diss} . We think that the main biological meaning is due to a more versatility and flexibility of eukaryotic (particularly mtHsp60) proteins than prokaryotic, suggesting that subunit flexibility should be closely related to the evolutionary history of a complex. Moreover our results suggests that GroEL and Hsp60s exist in a dynamic equilibrium between monomeric/heptameric/tetradecameric rings, and that the unfolding is coupled to the dissociation of the oligomeric protein. We believe that these studies in vitro of cooperativity, structural and thermal stability, on bacterial and human Hsp60 (across two proteins where these differences have functional relevance) could help to validate their role in physiological or pathological cases, and moreover for the development of biomolecular nanocarriers, opening new possibilities for targeted drug delivery.

The major part of the results discussed in this chapter are contained and were presented in the following works:

“(DIS)Assembly and Structural Stability of mtHsp60 and its Precursor Naïve Form”, by **Dario Spigolon**, Silvia Vilasi, Maria Rosalia Mangione, PierLuigi San Biagio, Donatella Bulone, presented during the Biophysical Society (Biophysical Society 59th Annual Meeting, Baltimore, Maryland, February 7-11, 2015) and published in *Biophysical Journal* Volume 108, Issue 2, Supplement 1, p502a, 27 January 2015 DOI: <http://dx.doi.org/10.1016/j.bpj.2014.11.2751>

Biophysical Journal

Volume 108, Issue 2, Supplement 1, p502a, 27 January 2015

(DIS)Assembly and Structural Stability of mtHsp60 and its Precursor Naïve Form

Dario Spigolon, Silvia Vilasi, Maria Rosalia Mangione, PierLuigi San Biagio, Donatella Bulone

[Open Archive](#)

DOI: <http://dx.doi.org/10.1016/j.bpj.2014.11.2751>

Chapter V

Hsp60, amateur chaperone in amyloid-beta fibrillogenesis

5.1 Aim and introduction

As was explained in chapter I, molecular chaperones are a very special protein class that plays essential roles in many cellular processes like folding, targeting and transport of proteins. In chapter II was highlighted that recent evidence indicates that chaperones can act as potentially strong suppressor agents in Alzheimer's disease (AD). Indeed, *in vitro* experiments demonstrate that several chaperones are able to significantly slow down or suppress aggregation of A β peptide and *in vivo* studies reveal that treatment with specific chaperones or their overexpression can ameliorate pathological behavior dysfunction of AD.

We investigated, by a biophysical approach, the effect of the human chaperonin Hsp60 (at a protein concentration, as seen in paragraph 4.1, where most of the oligomeric equilibrium is shifted versus tetradecameric and heptameric state) on A β fibrillogenesis. The binding between mt-Hsp60 and A β was evaluated, by ITC, at different A β structures, both in monomeric and in monomer/oligomer equilibrium forms as well as during fibrillogenesis.

We found that Hsp60 exerts a powerful inhibiting action on A β aggregation. Despite the homology of Hsp60 to GroEL, a folding chaperone (chapter I, paragraph 1.1.4), we observe that Hsp60 inhibits A β through a different more complex mechanism. The action is specifically tooled on the early oligomeric species behaving as aggregation seeds for on pathway amyloid fibrillogenesis. This amateur mechanism has the surprising appearance of memory effect, by which if the A β peptide species, prone for amyloid aggregation, had been once in contact with Hsp60, they cannot fibrillate anymore (see Fig. 5.1).

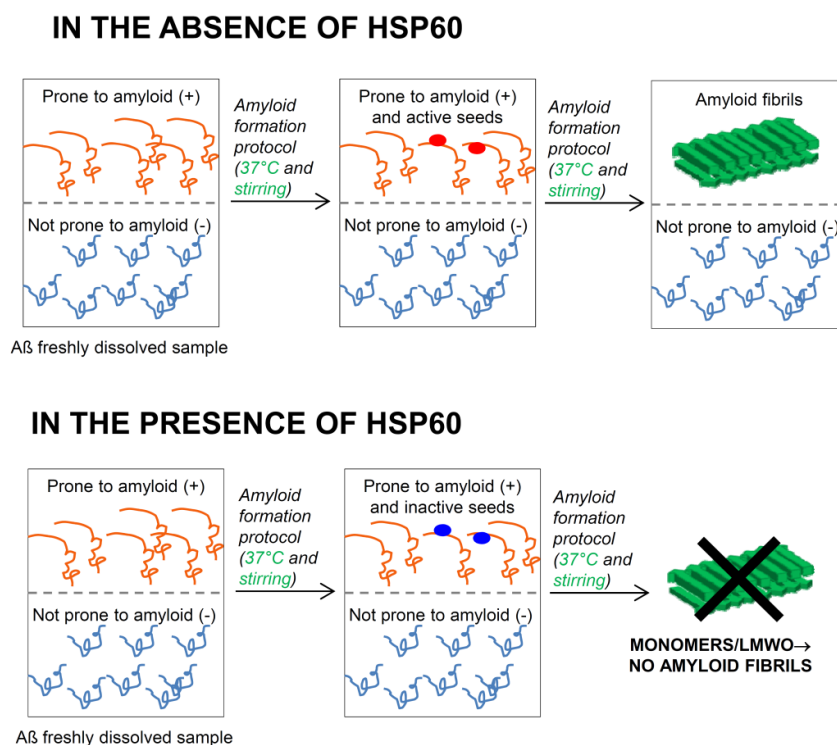


Figure 5.1 Simplified scheme of A β ₁₋₄₀ amyloid aggregation in the absence and in the presence of Hsp60. The initial sample is heterogeneously formed by generically described on-pathway (orange) and off pathway species (dark blue) with different amyloid molecular fates. Under amyloid formation protocol (37°C and stirring) seeds (red full circles) able to catalyze the reaction form allowing the on pathway species aggregating toward amyloid fibrils. The remaining off-pathway species are those not able to form fibrils. In the presence of Hsp60, the active seeds become inactive (blue full circles) and, in this condition, neither off-pathway species can form fibrils anymore.

5.2 Results & Discussion

Molecular chaperones act at all the above mentioned levels we listed in paragraph 2.1.2 (“Role of molecular chaperones in Alzheimer’s disease”) and, considering their functional complexity, it is hard to imagine other molecules, synthetic or natural, able to exert the same action with the same effectiveness. All these considerations strongly suggest that the pharmacological activation and induction of specific chaperones can be an effective therapeutic approach [5.1-5.4]. Indeed, these strategies are rapidly emerging as promising treatments for cancer intervention [5.4, 5.5], but, in the neurodegeneration field and particularly in AD, a

careful evaluation of potential pitfalls is necessary. In fact, A β oligomers are characterized by a very broad structural polymorphism with different epitope exposure, antibody-binding properties and peculiar toxicity features [5.6, 5.7]. To be considered for a promising therapeutic approach, chaperones should be able to block monomer aggregation or to favor the formation of nontoxic A β oligomeric variants. In the working mechanism of molecular chaperones, folding/holding/disaggregating (see chapter I), could be involved the coexistence of several and more complex mechanisms related to the specific nature of the molecular interactions between chaperone and protein aggregates. Increasing evidence highlights an intriguing feature of the activity of a natural molecular chaperone against misfolding events and associated reactions, suggesting that chaperones activity is not limited to sequestrate single unfolded monomers, but they can selectively interact with specific aggregated species [5.8, 5.9]. Moreover, in the chaperone mechanism of action, a crucial role is assumed by the presence of intrinsic disorder regions (IDRs) along the protein sequence [5.10]. IDRs are able to modulate specificity and affinity in protein binding. Therefore, it becomes fundamental to study the specific mechanisms of interaction of these chaperones with pathogenic amyloid-forming proteins. In this study, we analyze the effect of a human chaperonin Hsp60, homologous to the bacterial GroEL, on the aggregation process of A β 1-40 peptide involved in AD. As studied in the previous paragraph 4, differently from GroEL, (that is found mainly as a tetradecameric conformation organized in two heptameric rings) Hsp60 seems to exist in a deeper dynamic heptamer/tetradecamer equilibrium [4.1, 5.11, 5.12] where monomers are found, as well, under certain conditions for mitochondrial Hsp60 [5.13, 5.14] (see SEC-HPLC results in chapter 4). The major flexibility and richer functional conformational ensemble have evolutionary occurred at the cost of protein stability and unfolding cooperativity as seen in the previous chapter [4.1, 5.15]. Hsp60, in its naïve and mitochondrial form assumes a crucial role in several carcinogenic and inflammatory processes [5.16, 5.17]. Strong interactions between Hsp60 and amyloid precursor protein (APP) [5.18], as well as hamster prion protein PrPc [5.19], have been recently revealed. Moreover, it has been found by NMR measurements that GroEL suppresses A β 1–40 amyloid formation by interacting with its two hydrophobic segments Leu17-Ala21 and Ala30-Val36, key residues in

fibril formation [5.20]. Furthermore, GroEL inhibits the formation of toxic alpha-synuclein aggregates and it is capable of inhibiting the fibrillization of other amyloidogenic proteins such as β 2 microglobulin [5.21].

In this chapter we show for the first time that human Hsp60, even in the absence of its cochaperonin Hsp10 and ATP, binds A β 1-40 peptide and inhibits the fibrillogenesis of A β 1-40 peptide leaving the peptide in an unordered conformation. We suggest a possible mechanism underlying this inhibitory action that could constitute a basic building block in the research field of therapies based on human molecular chaperones for AD and other neurodegenerative diseases.

ITC Measures: Binding A β /mtHsp60

ITC measurements were performed to investigate the chaperone effect and mechanism on A β aggregation process. The binding between mt-Hsp60 and A β was evaluated at different A β structures, both in monomeric and in monomer/oligomer equilibrium forms as well as during fibrillogenesis.

The observed binding isotherms were fitted to the “one set of sites” model (see material and methods). In this model, the putative chaperonin has several identical substrate binding sites, which are independent of each other and have a uniform binding constant, K_a , and enthalpy change, ΔH . The best fitting parameter values are listed in Table 5.1. The binding curves are shown in Fig. 5.2.

Table 5.1 Binding parameter for a β and mtHsp60

Titrant in mtHsp60 (50 μ M)	n	k_d (M)	ΔH_d (kJ/mol)	K_a (M^{-1})	ΔS_d (kJ/mol K)
a β monomer/mtHsp60	3.9	$3.30 \cdot 10^{-8}$	-13.23	$3 \cdot 10^7$	98.84
a β oligomer/mtHsp60	4.1	$3.04 \cdot 10^{-6}$	-27.82	$3.3 \cdot 10^5$	12.29
a β fibers/mtHsp60	n.a	n.a	n.a	n.a	n.a

The theoretical curves (solid red lines) show a good match with the experimental data (squares) at different A β structures, both in monomeric and in monomer/oligomer equilibrium forms as well as during fibrillogenesis. No binding occurs between a β fibers and mtHsp60, while mtHsp60 shows up more affinity in the binding with a β monomer, as highlighted by the lowest K_d ($3.30 \cdot 10^{-8}$ M), than a β oligomer ($3.04 \cdot 10^{-6}$ M).

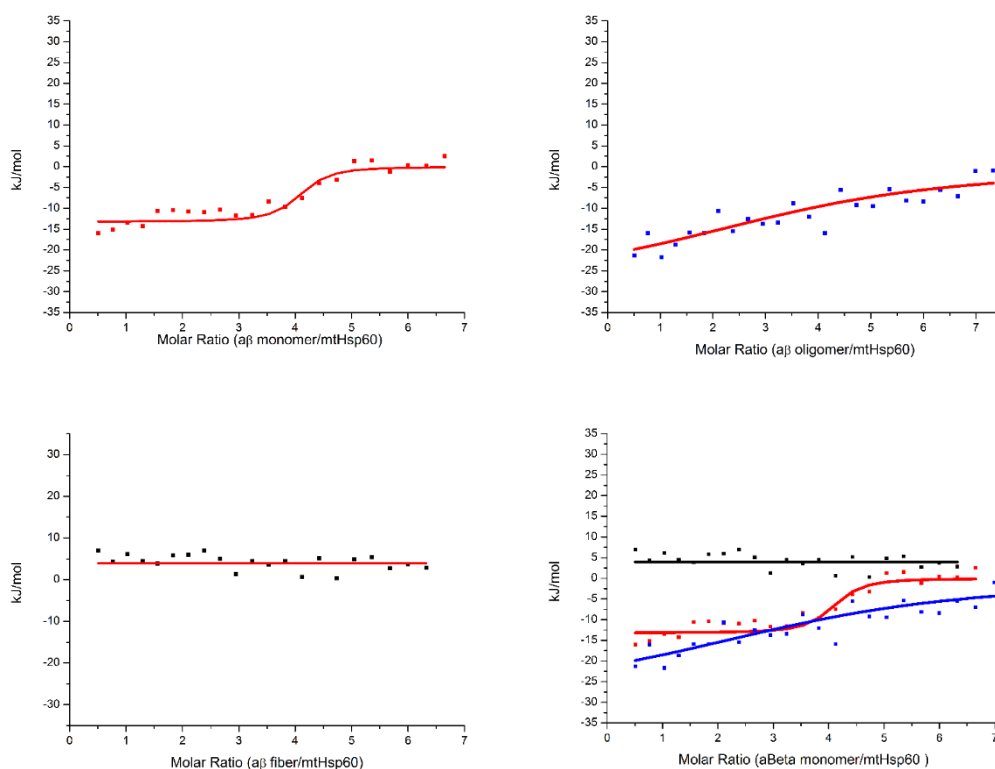


Figure 5.2 ITC Binding curves: Hsp60/A β at different structures; red spot are the monomer, blue ones are the oligomers and black ones are the fibers.

Effect of mtHsp60 on A β 1-40 amyloid aggregation process

In order to investigate the direct effect of Hsp60 on A β 1-40 amyloid aggregation process, different experimental techniques were used to investigate the evolution of the structural organization of aggregates formed in the presence and in the absence of Hsp60 under pro-aggregating conditions, i.e. stirring and 37 °C [5.22, 5.23].

ThT fluorescence assay, a widely accepted method to reveal β -sheet formation preliminary to the fibrillation process, was applied. Figure 5.3 shows a quick and sharp increase in ThT emission intensity for A β sample that indicates the

appearance of cross- β -structure. On the contrary, no significant change of ThT fluorescence can be observed for A β ₁₋₄₀ sample treated with Hsp60 up to 24 hours, suggesting that the amyloid fibrillation is inhibited by chaperone presence. Coherently, at the end of the kinetics, the secondary structural conversion that accompanies amyloid formation for A β peptide is not observed in the presence of the chaperonin (Fig. 5.3B) and no fibrils are observed by AFM (Fig. 5.4). Figure 5.3B shows the dichroic spectra of A β ₁₋₄₀ samples in presence or in absence of the chaperonin, recorded at the initial time and after 24 hrs from the beginning of the process. The CD spectra show a typical evolution of A β ₁₋₄₀ peptide from random coil to β -sheet structure. On the other hand, the sample incubated with Hsp60 retains a typical random coil profile until the end of kinetics. Therefore, CD experiments agree with ThT assays confirm that Hsp60 exercises an inhibitory role on the onset of A β ₁₋₄₀ beta structure formation that typically accompanies the peptide assembly toward more ordered structures. Other details on the structural organization of these samples were obtained by AFM imaging. Figure 5.4 shows images acquired at initial and final state for both samples, incubated with or without Hsp60. Noteworthy, the fibrillation is evident for sample of A β ₁₋₄₀ alone, whereas the peptide treated with Hsp60 does not show fibers, neither significant differences between the initial and the final step of the kinetics.

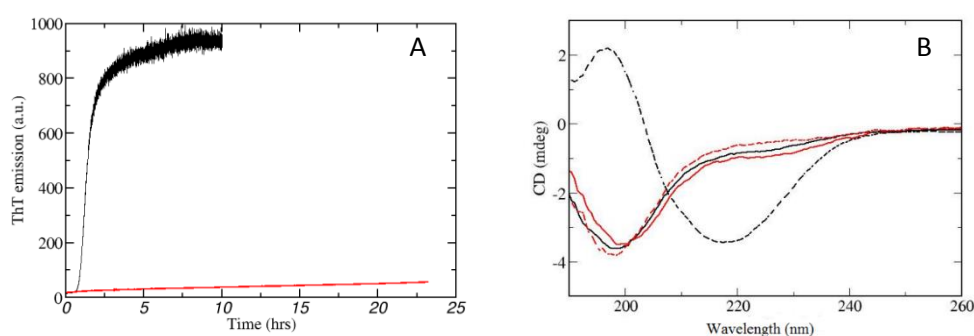


Figure 5.3 On the left (panel A): Influence of Hsp60 on A β aggregation kinetics. Kinetics of 50 μ M A β (black line) and 50 μ M A β + 2 μ M Hsp60 (red line) monitored by ThT fluorescence assay. Condition: T = 37°C stirring 200 rpm ThT 12 μ M. **On the right (panel B): Influence of Hsp60 on A β aggregation secondary structure variations during fibrillogenesis.** CD spectra recorded at 20 °C for 50 μ M A β ₁₋₄₀ at initial time (black line) and after 24 hrs at 37°C and 200 rpm (black dotted line), compared with spectra for sample with 2 μ M Hsp60 at the at initial time (red line) and after 24 hrs at 37°C and 200 rpm (red dotted line). The CD contribute of Hsp60 was subtracted to a better comparison.

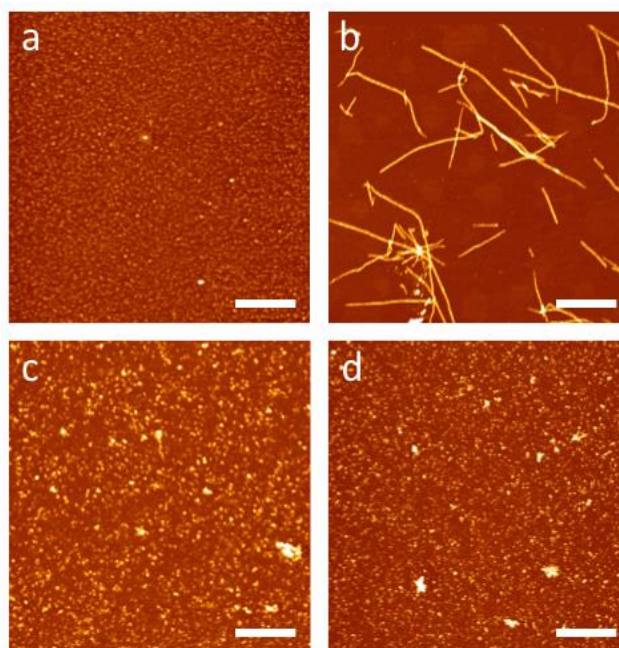


Figure 5.4 Morphology of A β species formed in the presence of Hsp60 under amyloid aggregation conditions. AFM images acquired for: 50 μ M A β at the at initial time (a) and after 24 hrs incubation at 37 °C and 200 rpm (b) compared with 50 μ M A β 1-40 incubated with 2 μ M Hsp60 at the initial time (c) and after 24 hrs of incubation at 37 °C and 200 rpm (d). Scale bars: 1 μ m, Z-range: (a, b, c) 7 nm; (d) 9.6 nm.

Molecular mechanism of HSP60

Different hypotheses about possible molecular mechanisms of Hsp60 could be formulated to explain the phenomena observed. One of these, considering the absence of ATP, would attribute to Hsp60 a “holding” role. Hsp60 could act as a non-catalytic inhibitor of polypeptide aggregation, by sequestering single unfolded conformations of monomers [5.10]. SEC experiments helped us getting light on this hypothesis.

Hydrodynamic size and oligomeric organization of A β 1-40 samples incubated for 24 hrs with or without HSP60 were analyzed by SEC using a Superdex 200 increase column. The chromatographic profiles, registered at 280 nm, are shown in figure 5.5 and compared with the A β chromatographic profile registered at the initial state of the aggregation kinetics. The early part of the chromatogram (7-10 min) accounts for Hsp60 in tetradecameric and heptameric structures. Hsp60 monomers and its

fragments fall in the region of the chromatogram between 10 and 14 min (as seen in chapter 4.1). Finally, A β 1-40 peptide peak is observed in the region between 16 and 18 minutes. The A β chromatographic area is notably lower for the sample incubated at 37°C for 24 hrs (blue curve in the last part of the chromatogram where A β 1-40 elutes). The missing sample is the component of the A β peptide sample predestined for forming amyloid on pathway large prefibrillar structures and mature fibers, evidenced by AFM experiments.

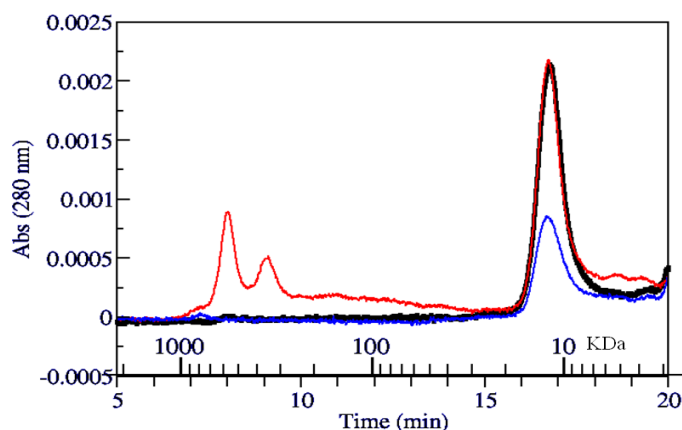


Figure 5.5 Investigation on the influence of Hsp60 on oligomeric distribution of A β after incubation under amyloid aggregation conditions. Analytical chromatographic profiles recorded at 280 nm for 50 μ M A β ₁₋₄₀ freshly dissolved (black line) and after 24 hrs of incubation at 37°C and 200 rpm with or without 2 μ M Hsp60, red line and blue line respectively. The column was calibrated using globular protein standards.

After incubation at 37 °C under stirring, A β sample, as a consequence of fibril formation, presents a significant reduction in the low size oligomeric peak (70% of the initial sample) (see scheme reported in Fig. 5.1).

The residual part of this peak, not involved in amyloid aggregation, is formed by off-pathway species that, when incubated again under amyloid formation conditions, result only able to form very low amounts of amyloid fibrils. In the presence of Hsp60 under the same conditions, no large difference in the chromatographic profile is noticeable in the A β sample other than peaks corresponding to chaperone oligomers. In particular, the low size oligomeric peak seems to be almost unvaried, with respect to the freshly dissolved A β sample. This means that also the fraction of A β molecules that in the absence of Hsp60 would be involved in amyloid fibrils formation, in the presence of the chaperonin is

unaffected both in hydrodynamic size and amount with respect to the freshly dissolved sample. The A β molecules normally involved in the aggregation pathway leading to fibers are no longer recruited in presence of Hsp60. Moreover, this evidence strongly excludes the possibility that the molecular chaperone sequesters the total A β sample, or a substantial part of it, by exerting a global holding action on A β molecules.

These results lead naturally to the hypothesis that Hsp60, following its professional activity but in the absence of ATP, induces a conformational change in A β peptide that irreversibly impair any further aggregation. Differently from GroEL, whose chaperone molecular actions are widely studied and known to involve cochaperonin GroES and ATP in an allosteric communication between the two heptameric rings [5.24, 5.25], functional mechanisms of the mitochondrial human homologue Hsp60 are very poorly investigated.

Differences in the key residues involved in the double rings formations reflect the existence of a dynamic equilibrium in solution between monomers, heptamers and tetradecamers conformations [4.1, 5.11, 5.14, and 5.26]. Indeed a single ring seems to be sufficient for folding assistance *in vivo* [5.26], even though potential mechanisms involving the interaction with co-chaperonins should be further clarified. For sure, similarly to GroEL, the apical domain of Hsp60 contains hydrophobic residues that could be the most involved in the misfolded proteins recruitment [5.27]. However, our data exclude any active influence of Hsp60 influence on A β folding, either monomers or low size oligomers present in the sample after the preparation protocol but before incubation with the chaperone. In fact, no variation in amyloid aggregation behavior is detectable in A β sample isolated after incubation with the chaperone under not destabilizing conditions (4 °C without stirring) [results shown in the article “Hsp60, amateur chaperone in amyloid-beta fibrillogenesis”, Mangione MR, Vilasi S, Marino C, Librizzi F, Canale C, Spigolon Dario, Bucchieri F, Fucarino A, Passantino R, Cappello F, Bulone D, San Biagio PL, published in *Biochimica et Biophysica Acta (BBA)* 2016 Jul 26. pii: S0304-4165(16)30266-5].

The only acceptable conclusion is that Hsp60 might act selectively on the specific A β amyloid species activated by simultaneous stirring and temperature increase, or by preventing their formation, or, as more probable, by inhibiting their activity by

a folding or a holding action (see scheme reported in Fig.5.1). These seeds although very low in number, have the proper molecular determinants to constitute productive steps in the fibrillation pathway and to determine the behavior and amyloid aggregation in the highest fraction of the whole A β population [5.28].

It is well known in fact that a given protein can self assemble into various aggregated forms, depending on the peculiarities of its environment. The presence of active seeds, paves the way, among the heterogeneous routes leading to the various aggregated forms, of the amyloid on pathway fibrillization [5.28]. In the presence of Hsp60, the recruitment or inactivation of these catalytic seeds close the route of on pathway amyloid fibrillogenesis.

Actually, as recently shown, a strong inhibition of aggregation can be observed, even at extremely low doses of inhibitors, for systems such the A β peptide, where secondary nucleation mechanisms play a key role. In fact, in these cases, the whole aggregation process can be prevented by the sequestration of small amounts of aggregates, before that these seeds can trigger the autocatalytic proliferation of aggregates brought about by secondary nucleation, as will be investigated in the chapter 7 [5.8, 5.9, 5.29, 5.30]. This shows an intriguing feature recently proposed for the activity of a natural molecular chaperone against misfolding events and associated reactions, indicating that the roles of chaperones are not limited to the sequestration of single monomeric unfolded conformations, but can involve multiple interactions with aggregated species [5.8, 5.9]. Our hypothesis is that the chaperone selectively exerts a selective action against the A β aggregated species that specifically form during on pathway aggregation under environmental stress conditions, probably by means of interactions involving peculiar hydrophobicity and exposure to the solvent properties of these A β aggregates conformations. These prion-like A β conformations could represent novel targets for interrupting the spread of A β deposition in AD patients [5.31].

5.3 Conclusions

Our results confirm the extraordinary potentiality of molecular chaperones in interfering with the crucial molecular steps leading to amyloid aggregation in neurodegeneration and demonstrate that Hsp60 is able to target the A β species

responsible for induction of amyloid protein assembly. Although, the specific mechanisms by which the presence of the chaperone neutralize these types of A β protein aggregates, preventing their formation or inhibiting them, remain to be elucidated. Due to the high grade of flexibility of the protein structure, chaperones can interact with a very wide spectrum of biological molecules and protein conformations and with a high versatility of mechanisms of action [5.10], exploiting as in the case of Hsp60 and A β oligomers, amateur, non-classical mechanisms [5.32]. In the absence of active seeds, and in the only presence of off-pathway species, also the highly prone to aggregate A β peptide becomes unable to form new seeds and subsequently to fibrillate.

In the last few years, chaperones appear to be an emerging and hopeful therapeutic strategy for the neurodegeneration field. In this respect, we believe that the investigation on the biophysical features of the interactions between specific chaperones and the specific protein structures involved in disease is a crucial basic step towards the development of effective chaperones-based approaches.

The major part of the results discussed in this chapter are contained in the paper: “Hsp60, amateur chaperone in amyloid-beta fibrillogenesis”, by Mangione MR, Vilasi S, Marino C, Librizzi F, Canale C, **Spigolon Dario**, Bucchieri F, Fucarino A, Passantino R, Cappello F, Bulone D, San Biagio PL, published in *Biochimica et Biophysica Acta (BBA)* 2016 Jul 26. pii: S0304-4165(16)30266-5. doi: 10.1016/j.bbagen.2016.07.019.





Biochimica et Biophysica Acta (BBA) -
General Subjects

Volume 1860, Issue 11, Part A, November 2016, Pages 2474–2483



Hsp60, amateur chaperone in amyloid-beta fibrillogenesis

Maria Rosalia Mangione^{a, 1}, Silvia Vilasi^a, ¹, , Claudia Marino^{a, b, c}, Fabio Librizzi^a, Claudio Canale^d, Dario Spigolon^{a, e}, Fabio Bucchieri^{c, f, g}, Alberto Fucarino^{c, g}, Rosa Passantino^a, Francesco Cappello^{a, c, g}, Donatella Bulone^a, Pier Luigi San Biagio^a

Chapter VI

Diseases caused by defective molecular chaperones: Quantitative analysis of the impact of a pathogenic mutation on the CCT5 chaperonin subunit using a proxy archaeal ortholog (Dis)assembly and Structural Stability

6.1 Aim and introduction

Defects in protein folding and other abnormalities, many associated with chaperonopathies, are typical of a wide variety of human diseases, including chronic inflammatory and autoimmune conditions, cancer, and amyloid diseases such as Huntington's, Parkinson's, and Alzheimer's diseases [6.14, 6.15]. However, the elucidation of the structure-function relationship of pathogenic chaperones remains challenging due to the complexity of the chaperoning multi-molecular machines typical of humans and even of simpler eukaryotes. Recently, a protein model has been proposed for investigating the functionality of a Group II chaperonin: the eukaryotic CCT (chaperonin containing TCP1), also called TRiC (TCP1-ring complex) [6.1-6.3]. CCT is an obligate chaperone for at least 10% of eukaryotic proteomes [6.4]. Several chaperonopathies linked to CCT loci are clinically well characterized and, for those due to non-lethal genetic mutations, there is considerable information on their mode of inheritance [6.5]. The Group II chaperonins such as CCT, which are universally found in Archaea and eukaryotes, feature a built-in lid that opens and closes over a central chamber. In eukaryotes in general, the chaperonin CCT is hetero-oligomeric, consisting in humans of two stacked rings of eight non-identical but similar subunits per ring. CCT is required for folding and stabilization of various essential proteins such as actin, tubulin, and cell-cycle regulators in humans and other organisms [6.6-6.11]. In addition, CCT modulates and suppresses the aggregation of neurologically toxic proteins with polyglutamine motifs [6.12-6.15]. The CCT conformation induced by ATP hydrolysis is closely associated with the productive folding of the substrate [6.16].

The protein model recently developed was aimed to address the mechanism of a crippling hereditary sensory neuropathy which is the result of a point mutation (His147Arg) in CCT5, one of the eight subunits of the human CCT [6.18, 6.19]. The critical mutation identified in patients suffering from this progressive condition was introduced into the ortholog chaperonin encoded by a hyperthermophilic marine archaeon, *Pyrococcus furiosus*, which shares 44% sequence identity with the human CCT5 [6.17, 6.20]. In the disease model, each of the 8 archaeal subunits in the two identical octamers that build the chaperoning hexadecamer carries the mutation. Therefore, the impact of the mutation is multiplied eight-fold per ring compared to the human CCT octamer. This amplification has proved instrumental for detecting subtle effects of a mutation, such as those which are likely to occur in humans, namely mutations that cause pathology but are compatible with survival. Indeed, the authors (Min et al., 2014) observed a decreased stability and impaired chaperoning function in the hexadecamer formed by the mutant subunit. In this work, we use differential scanning calorimetry (DSC), isothermal titration calorimetry (ITC), high performance liquid chromatography (HPLC), static light scattering (SLS) and circular dichroism (CD) to obtain quantitative information on the loss of structural stability in the hexadecamer containing the pathogenic mutation.

6.2 Results & Discussion

Thermal Unfolding

DSC experiments were carried out to gain quantitative information on the thermodynamic parameters controlling the protein stability. Fig. 6.1 shows the thermal profiles for Pf-CD1, Pf-H and Pf-R obtained at 60 °C/h scan rate and 7 μ M concentration. For all three proteins, we observed a biphasic melting that could be reasonably attributed to dissociation of the molecular complex followed by monomers unfolding. The asymmetry observed in the DSC thermograms is evident for all three proteins (particularly for Pf-H and Pf-R), and all peaks are skewed at temperatures below the transition midpoint (T_m), where the transition is less sharp and deviates more from the two-state fit, as expected for a transition coupled to dissociation [6.21, 6.22]. Overall, the three proteins showed a considerable difference in structural stability, as demonstrated by the strong difference in calorimetric enthalpy (182 kcal/mol for Pf-R, versus 308 and 515 kcal/mol, for Pf-H and Pf-CD1, respectively, Table 6.1). In particular, the pathogenic mutant Pf-R is the least able to maintain the complex structure with increasing temperature, whereas Pf-CD1 is the most stable.

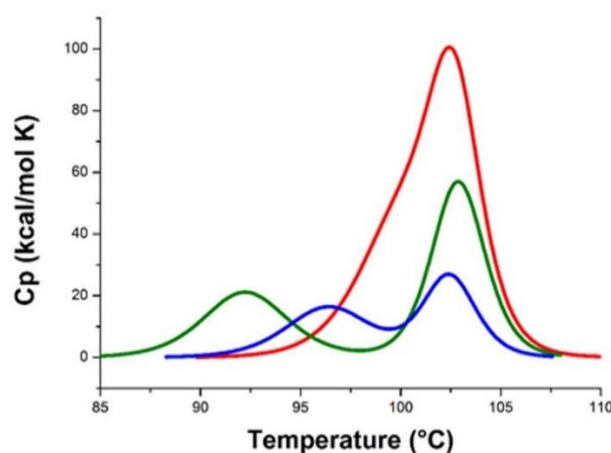


Figure 6.1 Differential scanning calorimetry thermograms for Pf-CD1 (red), Pf-H (green), and Pf-R (blue), at 7 μ M concentration. The scan rate was 60 °C/h. Calorimetric traces are given after subtraction of the instrumental base line. All the three proteins show biphasic melting that is interpreted in terms of hexadecamer disassembly followed by monomers denaturation (see text). For Pf-CD1, the two transitions are closer coupled.

Pf-CD1 showed more stability with respect to Pf-H and Pf-R and the highest ability to maintain the complex structure. Moreover, the asymmetry observed in the DSC thermograms is evident for all proteins (particularly for Pf-H and Pf-R), and all peaks are skewed at temperatures below the transition midpoint (T_m), where the transition is less sharp and deviates more from the two-state fit, as expected for a transition coupled to dissociation [6.21-6.24].

Table 6.1. Thermodynamic parameters for heat denaturation

Protein^a	T_m (°C)	ΔH_{cal}^b (kcal/mol)	ΔH_{vh} (kcal/mol)	R^c
Pf-CD1	102.6	515	214.2	2.4
Pf-H	103.2	308	197.2	1.56
Pf-R	102.7	182	160.3	1.14

^a7 μ M

^b ΔH_{cal} and ΔH_{vh} per subunit

^c $R = \Delta H_{cal} / \Delta H_{vh}$

To investigate the nature of the double peak in the thermogram, we did DSC experiments at varying protein concentration. Indeed, a decrease of the total molar calorimetric enthalpy should be observed if the unfolding is coupled to dissociation of oligomeric complexes. Results in Fig. 6.2 clearly illustrate that amplitude of the lower temperature peak decreases with decreasing protein concentration, while the higher temperature peak remains unchanged, thus validating the hypothesis of unfolding coupled to oligomers dissociation.

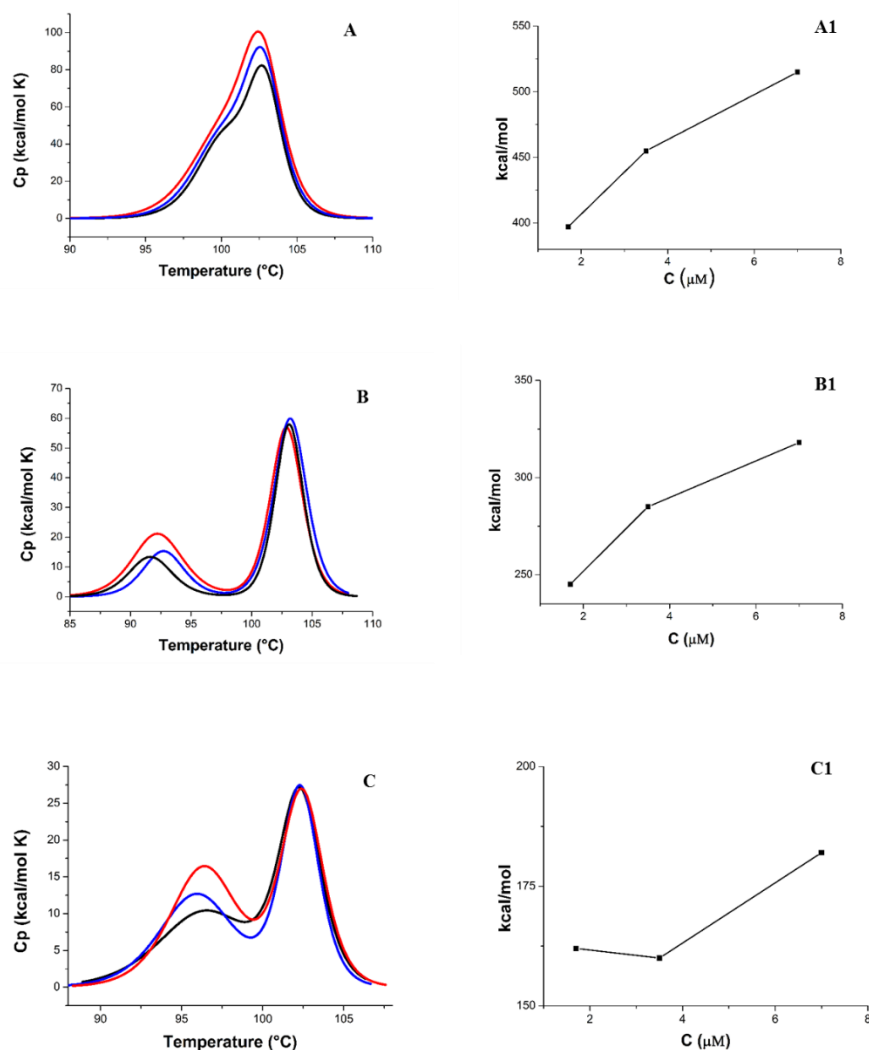


Figure 6.2 Differential scanning calorimetry at different protein concentrations. For each protein, the concentrations were 7 μM (red), 3.5 μM (blue), and 1.7 μM (black). Panels A, B, C are the thermograms for Pf-CD1, Pf-H, and Pf-R, respectively. Panels A1, B1 and C1 are the variations in total measured enthalpy as a function of concentration.

The presence of oligomers and the relative molecular weight distribution in native and unfolded proteins was investigated by HPLC measurements. Results in Fig. 6.3 evidence that all three proteins in the native state are mainly assembled in octamers and hexadecamers with some fraction of dimers and monomers. The total area of chromatogram for each protein after unfolding is strongly reduced, as probably due to formation of aggregates that do not enter in the column. The largest effect is found for Pf-R (72%). For Pf-H and Pf-CD1, the reduction is 50 and 26%,

respectively. In addition, the unfolded proteins display a different oligomeric size distribution as they appear enriched in dimers and monomers. This indicates that most of the thermal denatured transition is from the oligomeric dissociation. The largest change is observed for Pf-R, which becomes richer in monomer and dimer, compared with the other proteins. Thus, the mutation appears to impact the oligomer's thermodynamic stability and its ability for effective self-organization *in vitro*.

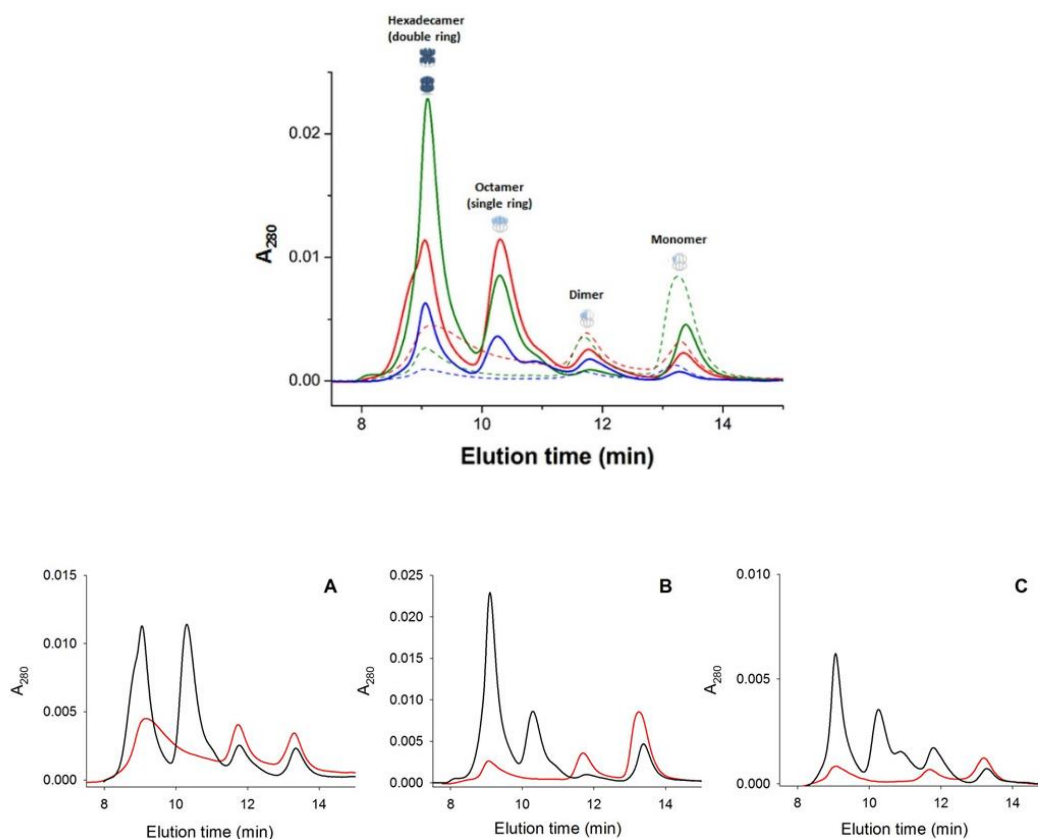


Figure 6.3 Analysis of oligomer components by size-exclusion chromatography. A₂₈₀ traces collected from samples of Pf-CD1, Pf-H and Pf-R, before (continuous lines) and after (dashed lines) thermal denaturation are shown all together in the top panel and divided by protein in the panels A, B, C. Non-denatured samples comprise four species (labels above peaks). After denaturation, some fraction of hexadecamer reforms while the octamer species is generally absent. After heating, Pf-R is richer in monomer and dimer, compared with the other proteins. For each protein, the total area of chromatogram is reduced after denaturation, as probably due to formation of aggregates that do not enter in the column. The largest effect is found for Pf-R (72%). For Pf-H and Pf-CD1, the reduction is 50 and 26%, respectively.

Results from Circular Dichroism measurements on native and thermally unfolded proteins, reported in Fig. 6.4, show that oligomeric dissociation is associated to a mild conformational change.

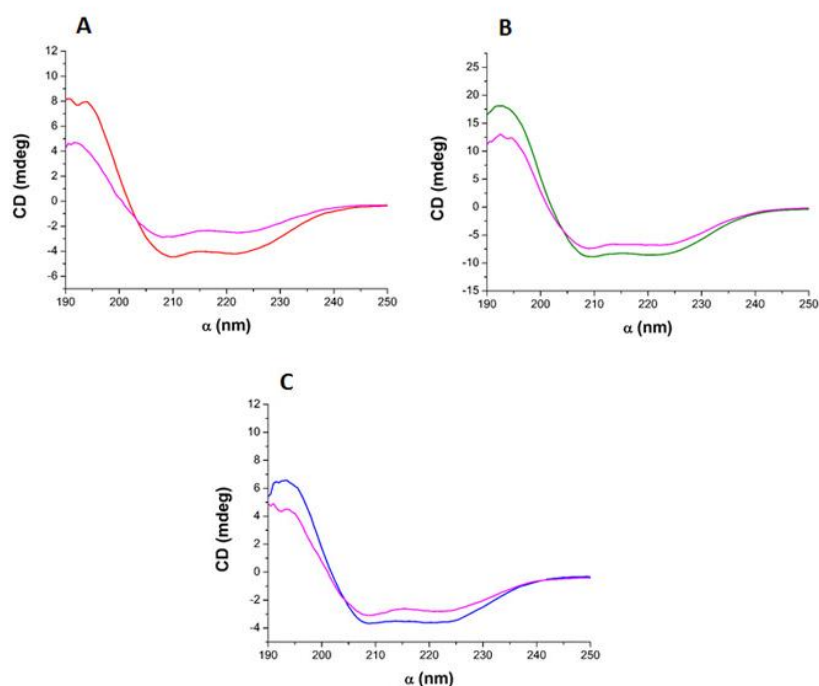


Figure 6.4 Circular dichroism. CD spectra for Pf-CD1 (panel A), Pf-H (panel B), and Pf-R (panel C) before (cred, green and blue lines) and after (magenta lines) thermal denaturation. All samples show a predominance of alpha helical structure (maxima near 190 nm and minima near 210 and 225nm), which is slightly reduced in unfolded samples. Secondary structure composition and assignments from CD spectra are given in Table 6.2.

Table 6.2 Secondary structure composition and assignments from CD spectra for native and unfolded protein

Protein	Alpha-Helix ^a	Beta-Sheet	Turn	Random Coil
Pf-CD1 native	50	12	12	26
Pf-CD1 unfolded	41	23	10	26
Pf-H native	49	21	10	20
Pf-H unfolded	40	24	10	26
Pf-R native	50	21	9	20
Pf-R unfolded	44	20	8	27

^aPercent of alpha-helix, beta-sheet, turn and random coil structure obtained by CDPro analysis of CD spectra [6.30].

Effect of mutation on the structural stability

The oligomeric equilibrium of the three chaperonins as a function of protein concentration was investigated by ITC measurements at room temperature. The protein solutions were loaded into the titration syringe at a concentration of 0.3 mg/mL. Each titration consisted of 18-19 successive injections of 5 μ L protein solution into the reaction cell (980 μ L) filled with buffer only. Results are shown in Fig. 6.5, panels A and B. ITC curves were analysed by using a hexadecamer-monomer equilibrium model.

The equilibrium constant and mass balance equations are in this case:



$$K_d = \frac{[M]^{16}}{[M_{16}]}$$

$$[M]_t = [M] + 16[M_{16}]$$

$$16 \frac{[M]^{16}}{K_d} + [M] - [M]_t = 0$$

Here K_d is the dissociation equilibrium constant, $[M]$ and $[M_{16}]$ are the equilibrium concentrations of the monomer and hexadecamer, respectively, and $[M]_t$ is the total monomer concentration. The total concentration of protein (in a monomer base) in the calorimetric cell after each injection i can be calculated as:

$$[M]_{t,i} = P_0 \left(1 - \left(1 - \frac{v_{inj}}{V_0} \right)^i \right)$$

The free monomer concentration after each injection i , $[M]_i$, can be calculated by using the previous equations, and the normalized heat associated with each injection, Q_i , is given by:

$$Q_i = \frac{V_0 \Delta H_d}{v_{inj} P_0} \left([M]_i - [M]_{i-1} \left(1 - \frac{v_{inj}}{V_0} \right) - F_0 P_0 \frac{v_{inj}}{V_0} \right) + q_d$$

Where ΔH_d is the enthalpy change due to dissociation, V_o is the reaction volume, v_{inj} the injected volume, P_o is the molar concentration in the syringe, and F_o is the fraction of monomers in the syringe.

The hexadecamer-monomer model reproduces reasonably well the experimental data, and there is no need for considering intermediate states. According to this model, the oligomeric equilibrium of the three chaperonins can be studied as a function of concentration, by revealing the fractions of monomers and oligomers in the cell after each injection. The heat released or absorbed in each injection will be proportional to the increment of monomer concentration. The presence of monomers at high protein concentration, especially for Pf-R, was confirmed by native 4-9% gradient native-PAGE analysis ([6.17]) and by HPLC (see Fig. 6.3). The oligomer's dissociation constants K_d , along with ΔH_d and other thermodynamic parameters calculated for the oligomeric equilibria of Pf-CD1, Pf-H and Pf-R are summarized in Table 6.3. The assembly of the hexadecameric complex is endothermic and entropically driven. Moreover, the negative Gibbs free energy indicates that, for all the three proteins, disassembly is a thermodynamically favorable reaction as long as the concentration is lower than the critical transition concentration (CTC).

The overall enthalpy change may include three different contributing factors: (i) Interaction enthalpy between subunits (ΔH_i); (ii) Conformational enthalpy of subunits (ΔH_c); and (iii) Solvation enthalpy of subunits (ΔH_s) [6.25]. ΔH_i corresponds to the enthalpy changes from non-covalent interactions such as hydrogen bonding, electrostatic forces, and van der Waals interactions. ΔH_s represents the enthalpy due to the uptake or release of the ordered water molecules from the contact interface (hydration-dehydration phenomena), and ΔH_c is related to the conformational enthalpy when an ordered secondary/tertiary/quaternary structure of the protein is formed. Considering the unfavorable positive enthalpy value of Pf-CD1 assembly and the large negative dissociation enthalpy, it may be concluded that $\Delta H_c + \Delta H_i$ values are exothermic. Consequently, oligomer dissociation with negative enthalpy implies that the aggregation process is endothermic and entropically driven [6.26]. The total endothermic enthalpy of monomer binding is attributed to a large unfavorable, positive solvation enthalpy due to the release of ordered water molecules from the monomer-oligomer

interface. Protein folding and ligand binding to proteins through hydrophobic interactions are often accompanied by the burial of nonpolar surfaces from water [6.27]. The positive entropy associated with Pf-proteins assembly follows the classical hydrophobic effect, which is an entropy-driven process. Partitioning of a nonpolar molecule from water to a nonpolar phase is accompanied by an increase in the entropy of the system. Since the Pf-protein interfaces are mostly hydrophobic, there may be a large number of ordered waters released upon assembly. Thus, both the favorable entropy and the unfavorable enthalpy can be explained by a release of ordered water molecules upon hexadecamer assembly, especially in the case of Pf-CD1, where the hydrophobicity is higher than for Pf-H and Pf-R.

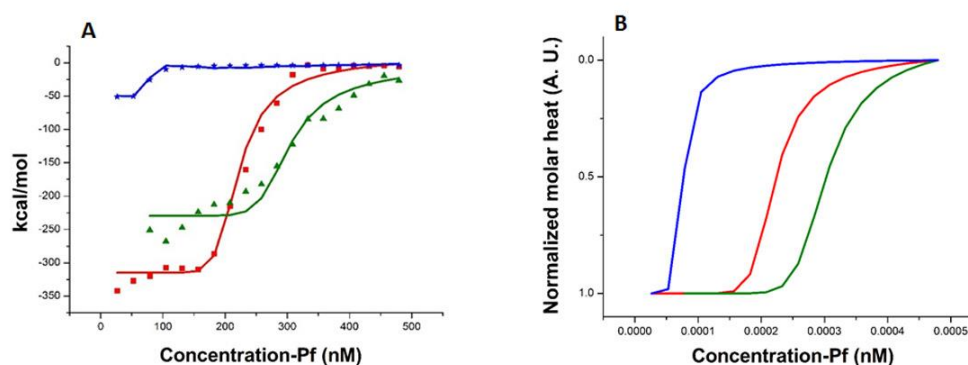


Figure 6.5 Isothermal titration calorimetry of the oligomer assembly process for Pf-CD 1 (red), Pf-H (green), and Pf-R (blue). Panel A shows the measured heat for 18 successive injections and best fit to a two-state curve according to a hexadecamer-monomer equilibrium. Panel B shows the corresponding normalized molar heat functions. Pf-R remains assembled in hexadecamers at lower concentration, but with a smaller energy of assembly.

Table 6.3. Thermodynamic parameters for the hexadecamer-monomer equilibria^a

Protein	k_d (μM)	ΔG_d (kcal/mol)	ΔS_d (kcal/mol K)	ΔH_d (kcal/mol)
Pf-CD1	0.31 ± 0.06	-8.8 ± 0.1	-1.14 ± 0.01	-350 ± 5
Pf-H	0.43 ± 0.05	-8.7 ± 0.24	-0.81 ± 0.02	-250 ± 7
Pf-R	0.1 ± 0.05	-9.5 ± 0.3	-0.13 ± 0.04	-49 ± 1.7

^aAll parameters are expressed per subunit.

Effect of mutation on protein function

ATP binding was investigated by ITC, Fig. 6.6, panels A, B, C. All three proteins bind ATP, but with different binding mechanisms. The binding isotherms best fit was in terms of a model considering several identical and independent binding sites (described in chapter III). In this model, the chaperonin has 16 identical nucleotide binding sites, which are independent of each other and have a uniform binding constant, K_a , and enthalpy change, ΔH . The best fitting parameter values are listed in Table 6.4. The theoretical curves showed a good match with the experimental data for ATP. The three proteins showed different ATP-binding mechanisms: in particular, Pf-R shows an exothermic binding enthalpy ΔH (-26.8 kcal/mol) compared to the endothermic ones of Pf-CD and Pf-H (4.3 and 6.5 kcal/mol, respectively).

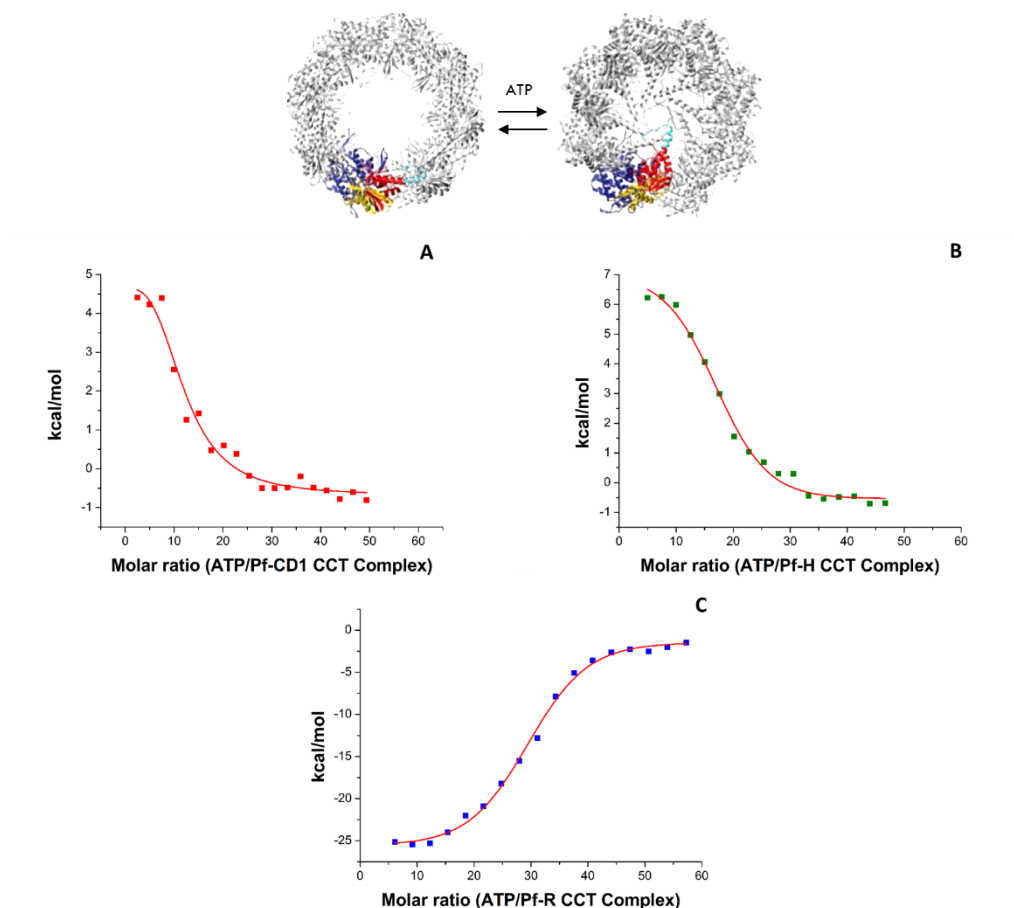


Figure 6.6 Isothermal titration calorimetry for ATP binding to the chaperonins: Pf-CD1 (A), Pf-H (B), Pf-R(C). The enthalpies of ATP binding are reported as a function of ATP stoichiometry. The best-fit curves are based on a model that assumes a single binding site per subunit. Note that a molar ratio of 16 corresponds to one ATP per subunit.

Table 6.4. ATP-binding parameters obtained by the “one set of sites” model^a

Protein	<i>n</i>	<i>k_d</i> (μM)	Δ <i>S</i> (cal/mol K)	Δ <i>H</i> (kcal/mol)
Pf-CD1	12 ± 3	0.21 ± 0.05	44.4 ± 9.5	4.3 ± 1.4
Pf-H	16 ± 1.2	0.2 ± 0.02	51.8 ± 5.8	6.5 ± 0.8
Pf-R	29 ± 0.6	0.38 ± 0.01	-57.2 ± 3.2	-26.8 ± 0.85

^aAll parameters are expressed per hexadecamer.

The effect of ATP binding on protein conformation were investigated by DSC experiments. Thermograms for the three proteins in the presence of ATP are shown in Fig. 6.7. The comparison between the thermodynamic parameters for unfolding in the absence (Tab. 6.1) and ATP presence (Tab. 6.5) indicates that for both Pf-H and Pf-R bounded to ATP the unfolding takes place at lower temperature, whereas little change is observed for Pf-CD1. The total enthalpy cost for unfolding in ATP presence is increased for Pf-H and decreased for both Pf-CD1 and Pf-H.

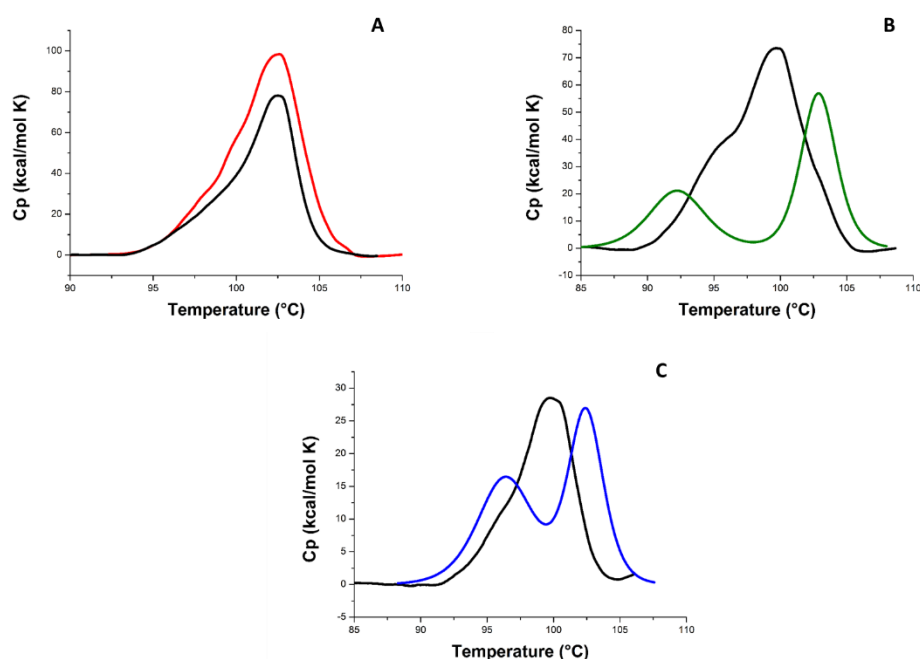


Figure 6.7 ATP effect on DSC thermograms for Pf-CD1 (A), Pf-H (B) and Pf-R (C). Colored profiles are relative to the proteins in absence of ATP. The black line in each panel is the thermogram recorded in the presence of 0.015 mM ATP.

Table 6.5. Thermodynamic parameters for heat denaturation in the presence of nucleotide

Protein ^a	<i>T_m</i> (°C)	ΔH_{cal} ^b (kcal/mol)	ΔH_{vh} (kcal/mol)	<i>R</i> ^c
Pf-CD1-Mg-ATP	102.5	365	239	1.52
Pf-H-Mg-ATP	99.6	518	156	3.3
Pf-R-Mg-ATP	99.7	157	200	0.8

^a7 μ M^b ΔH_{cal} and ΔH_{vh} per subunit^c $R = \Delta H_{cal} / \Delta H_{vh}$

CD spectra of the three proteins in their denatured state in the presence of ATP were recorded at 260 to 190 nm to observe the effect of nucleotide on the secondary structure. Percent of alpha-helix, beta-sheet, turn and random coil structure as obtained by CDPro analysis are reported in supplementary data A.2. The results showed that the three chaperonins undergo conformational changes upon ATP binding. Pf-CD1 and Pf-H became more structured upon ATP binding, while Pf-R lost structure and resembled to more closely the denatured state.

Overall, our results indicate that only the nucleotide endothermic binding to Pf-H, and to Pf-CD1, leads to conformational changes induced by Mg-ATP, showing the transition of the complex to the closed conformation, which is usually required for ATP hydrolysis to bring the lid helices into close proximity during the conformational cycling (conformational changes in CCT have also been observed by electron microscopy [6.28]. Opening of the lid occurs in conjunction with releasing ADP from the active site. The complex can exist in an asymmetrical conformation with one ring closed and one open, even during ATP cycling conditions, suggesting an inter-ring allosteric model mediated through a two-stroke mechanism [6.29]. However, the allosteric communication that occurs between the rings is not well understood.

6.3 Conclusions

In conclusion, the three chaperonin molecules tested have distinct thermodynamic profiles, showing different disassembly behavior and implying different cooperativity levels and different conformational trajectories. The pathogenic R mutant (Pf-R) is energetically the weakest at maintaining the oligomeric complex and displays a distinct oligomeric equilibrium characterized by the lowest enthalpy of dissociation (ΔH_d). Thus, the pathogenic mutation appears to reduce the protein's stability and its capacity for self-organization. The observed differences in ATP binding provide further evidence that the R mutation in Pf-R disrupts the chaperonin's functional cycle by failing to induce the normal conformational changes. Pf-R has an exothermic ΔH (-26.8 kcal/mol) compared to the endothermic values for Pf-CD1 and Pf-H (4.3 and 6.5 kcal/mol, respectively). This suggests that the pathology follows from a failure of ATP binding to induce the oligomer's closed conformation, which is required for ATP hydrolysis and the subsequent conformational cycling that underlies normal chaperonin function.

The major part of the results discussed in this chapter are contained in the following paper submitted:

“Diseases caused by defective molecular chaperones: Quantitative analysis of the impact of a pathogenic mutation on the CCT5 chaperonin subunit using a proxy archaeal ortholog”, by **Dario Spigolon**, Travis Gallagher, Adrian Velazquez-Campoy, Donatella Bulone, Jatin Narang, Pier Luigi San Biagio, Francesco Cappello, MD Alberto J Macario, MD, Everly Conway de Macario, Frank T Robb, recently submitted to Biochemical and Biophysical Research Communications.

Chapter VII

Caseins: α -Casein Inhibits Insulin Amyloid Formation by Preventing the Onset of Secondary Nucleation Processes

7.1 Aim and introduction

Our main goal was to study if an efficient inhibition of amyloid formation can be achieved by chaperone-like systems, α -Caseins, which are able to exert a stabilizing function through direct interaction, and to evaluate the mechanism of chaperone-like activity against aggregation. For α -Casein the stabilization of partially unfolded 'target' proteins takes place through direct interactions similar to those induced by small heat-shock proteins (sHsps) (see paragraph 1.5). Investigation on its interaction mechanism could help to better understand the structural basis of the substrate binding in sHsps.

As explained before, α -Casein is able to inhibit the aggregation of several proteins, including the amyloid β -peptide, by mechanisms that are not yet completely clear. We studied the chaperone-like systems effects on insulin¹, a system extensively used to investigate the properties of amyloids (many of which are common to all proteins and peptides, so that it seems appropriate to talk about an "amyloid state" for proteins, characterized by the formation of fibrillar β -sheet rich aggregates). Insulin fibrillization process is characterized by a prolonged lag-phase, in which nothing apparently happens, followed by a sudden, explosive, growth of aggregates [7.1- 7.7]. This phenomenology is the fingerprint of an extremely autocatalytic process, brought about by secondary nucleation mechanisms, such as branching, heterogeneous nucleation, fragmentation, i.e. all those processes which can exponentially increase the number of aggregation sites [7.8].

¹51 residue protein hormone with a molecular weight of ~5800 Da.

Furthermore, in some conditions, insulin is also able to form relatively small, amyloid-like, oligomers, whose formation does not show any relevant lag-phase and which have been suggested to be off-pathway with respect to standard insulin amyloid fibrillation [7.9, 7.10].

Therefore, we have here the possibility to investigate the hindering effects of α -cas on different aggregation pathways of the same protein giving useful information both on the basic mechanisms of amyloid formation and on the strategies for its inhibition.

We found that α -casein strongly delays amyloid formation, when the aggregation process is characterized by secondary nucleation. At difference, it has a vanishing inhibitory effect on the initial oligomer formation, which is observed at high concentration and does not involve any secondary nucleation pathway. These results indicate that an efficient inhibition of amyloid formation can be achieved by chaperone-like systems (see paragraph 1.5), by sequestering the early aggregates, before they can trigger the exponential proliferation brought about by secondary nucleation mechanisms.

7.2 Results & Discussion

We monitored the formation of amyloid aggregates by means of Thioflavin T (ThT) fluorescence [7.11, 7.12], following at the same time the conformational rearrangements of insulin molecules by their intrinsic tyrosine fluorescence². Fig. 7.1 reports the ThT (a) and the tyrosine (b) fluorescence signals as a function of time, during the fibrillation process ($T = 60^{\circ}\text{C}$, insulin concentration 1 mg/ml), at different α -cas concentrations.

²The area of the emission bands corresponding to tyrosine ($\lambda_{\text{max}} \approx 305$ nm) and to ThT ($\lambda_{\text{max}} \approx 485$ nm) were extracted from each spectrum and plotted as a function of time to follow tertiary structure conformational changes (tyrosines) and amyloid formation (ThT) on the same sample. In fact, UV excitation ($\lambda_{\text{ex}} = 270$ nm) allows to measure simultaneously both tyrosine and Thioflavin T emissions.

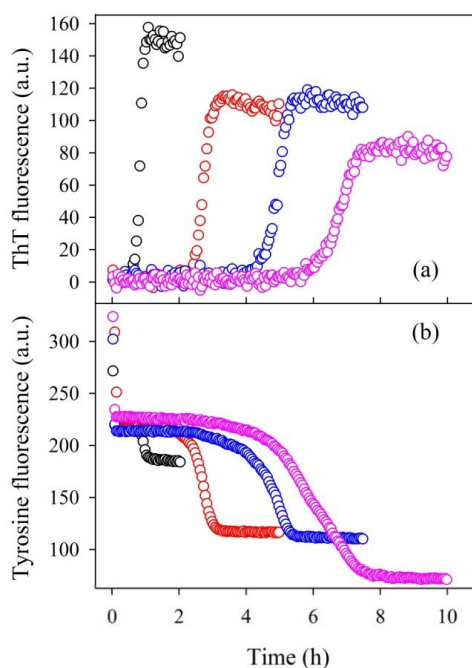


Figure 7.1 ThT (a) and tyrosine (b) fluorescence intensity as a function of time. The two fluorescence signals were measured contemporarily with an excitation wavelength of 270 nm. Insulin concentration 1 mg/ml; $T = 60\text{ }^{\circ}\text{C}$. Black: No casein; Red: casein 1:1000 (mol:mol); Blue: 1:300; Pink: 1:100.

In order to monitor at the same time the growth of amyloid aggregates and the accompanying conformational changes, we measured the two fluorescence signals during the same experiments, by exciting at the excitation wavelength of tyrosine (270 nm), which, as shown in Fig. 7.1a, is also able to produce ThT fluorescence (we remind that insulin has no tryptophans). This procedure lowers the resolution of the ThT fluorescence measurements, but allows the interesting comparison of the two signals[7.13]. ThT fluorescence data (Fig. 7.1a) clearly indicate that α -cas has a strong, dose-dependent, inhibiting effect on the kinetics of insulin fibril formation, even at extremely low concentration. In fact, a ~ 10 -fold lengthening in the initial lag-phase is produced by an α -cas dose of 1:100 (molar ratio; insulin and

α -cas have molecular weights of ~ 5800 and ~ 23000 Da, respectively). Interestingly, as shown in Fig. 7.1b, the presence of α -cas induces a drastic reduction of tyrosine fluorescence intensity during the fibril formation process (the initial decrease in the fluorescence signal is due to the thermalization of the sample, from room temperature to 60°C , which lowers the quantum yield of tyrosine independently from the fibrillation process). The different levels of tyrosine fluorescence quenching indicates that the presence of α -cas not only strongly delays the fibrillation process, but also drives it toward different structures, which are probably characterized by a different solvent exposure of insulin tyrosine residues within the fibrils. The tyrosine fluorescence signal in Fig. 7.1b appears to diminish even before ThT fluorescence increase (Fig. 7.1a) especially for the sample at the highest α -cas concentration. This could indicate the presence of conformational changes preceding the aggregation.

We also investigated the changes in the tertiary structure of insulin during the fibrillation process by means of near UV Circular Dichroism (CD) spectroscopy, both in the absence and in the presence of 1:100 molar ratio of α -cas (Fig. 7.2, a and b respectively). Before the aggregation both samples display similar spectra (red curves in Fig. 7.2). However, the spectral alterations due to the fibrillation process are completely different in the two cases, thus confirming that the fibers formed in the presence of α -cas are different from those formed by insulin alone. The insert in Fig. 7.2b again puts in evidence the ~ 10 -fold difference in the duration of the lag-phase, also evidencing that for both samples only negligible conformational changes seem to occur before aggregation. The morphology of the obtained fibrils was investigated by means of AFM microscopy (Fig. 7.2 c and d).

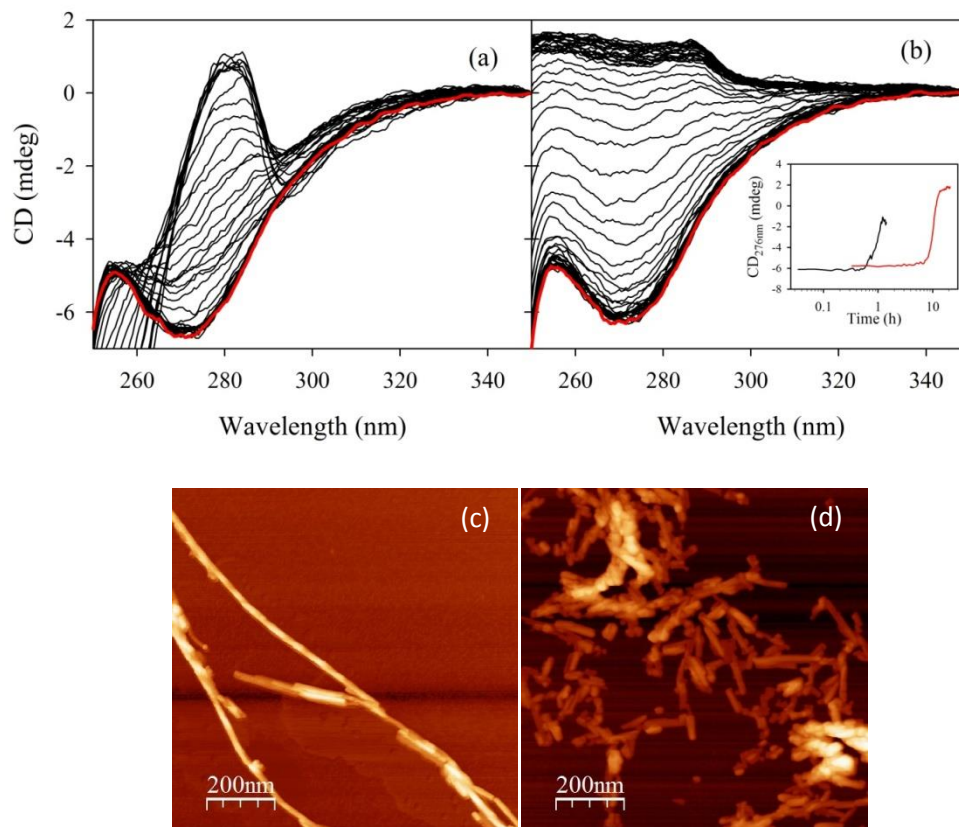


Figure 7.2 Panels a and b: **Near UV Circular Dichroism spectra at different times during fibril formation of insulin** (1 mg/ml), at 60 °C. (a) No casein; (b) casein 1:100 (mol:mol). The insert in panel (b) shows the CD signal at 276 nm as a function of time for insulin alone (black) and for the sample with α -cas 1:100 (red). Panels c and d: **AFM images at the end of the fibril formation kinetics**. (c) Insulin alone (after 1.5 h); (d) α -cas 1:100 (after 8 h).

Fibrils formed (after 8 h) in the presence of α -cas appear shorter, less ordered, and with a stronger propensity to stick together. The polymorphism of insulin fibrils is a well-known phenomenon. Depending even on fine details of external parameters, insulin is able to form fibrils with different topology and properties [7.14, 7.15, 7.10, 7.16-7.19], which, in addition, seem to be able to self-propagate in an amyloid strain mode [7.20-7.21]. In such conditions, it is perfectly reasonable that α -cas, by affecting the initial nucleation stages of the process, also preferentially selects pathways to specific polymorphs. Furthermore, two insulin fibril polymorphs with unambiguously different surface exposure of tyrosine

residues have been observed [7.22-7.24], which can help to explain the difference in the tyrosine fluorescence signal between our samples (Fig. 7.1b).

To clarify the mechanisms of action of α -cas, we also studied its effect on the thermal conformational rearrangements of insulin molecules. Fig. 7.3a, b reports Far-UV CD spectra obtained at different temperatures, from 10 to 70 °C at a rate 20 °C/h, for insulin alone (a) and with α -cas 1:100 (b).

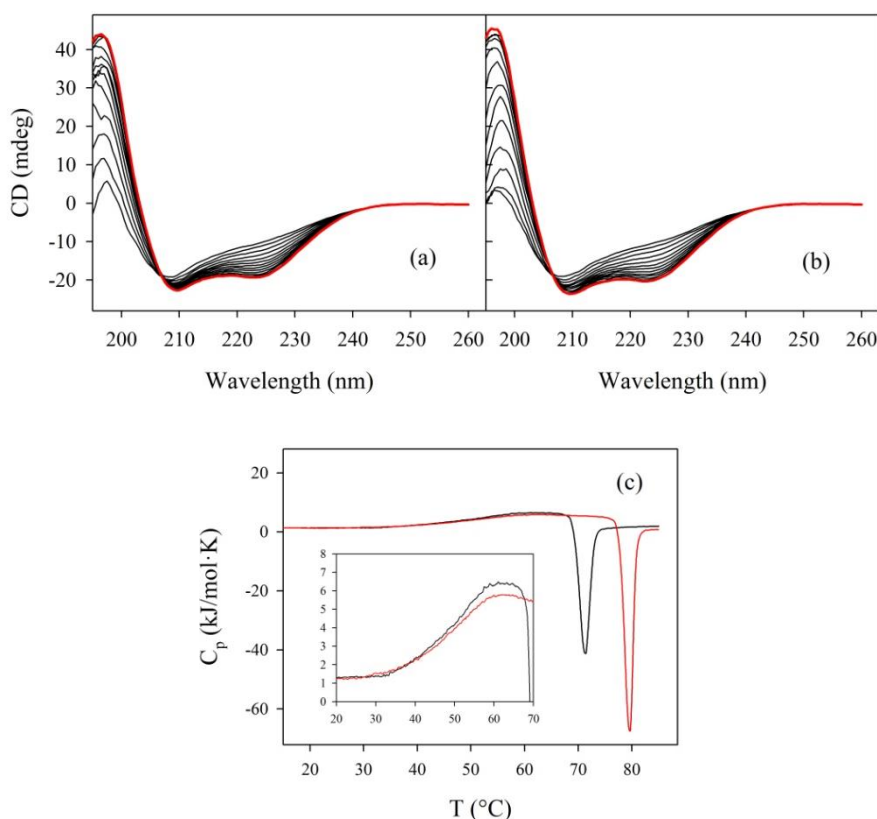


Figure 7.3 CD spectra at different temperatures, from 10 (red curve) to 70 °C, for insulin alone (a) and with α -cas 1:100 (b). (c) DSC scan for insulin alone (black) and with α -cas 1:100 (red); the insert in (c) shows the detail of the endothermic peak ascribable to conformational rearrangements. For all panels, insulin concentration is 1.0 mg/ml and scan rate is 20°C/h.

As evident, α -cas has essentially no effect at all on the temperature induced secondary structure conformational change of insulin. This finding is also supported by differential scanning calorimetry (DSC) measurements (Figure 7.3c) performed under the same conditions. The presence of α -cas shifts to higher temperatures the exothermic peak brought about by the onset of the aggregation process, confirming its inhibiting effect; it also changes the enthalpy of aggregation peak from -108 to -

-140 kJ/mol. On the contrary, in accordance with CD data (Fig. 7.3 a, b), it only slightly affects the broad endothermic peak observed at lower temperatures, which can be ascribed to temperature induced conformational changes. Also the enthalpy values for the endothermic peak are similar (11.2 kJ/mol for insulin alone and 12.7 kJ/mol for the sample with α -cas). Data reported in Fig. 7.3 indicate that α -cas has no particular stabilizing effect on isolated protein molecules. Therefore, its mechanism of action probably concerns its interaction with aggregating species than with native proteins, as previously noted [7.25].

Under our solvent conditions (HCl 25mM, NaCl 100mM, T = 60°C) and at higher concentrations, insulin is known to display a biphasic fibrillation process, the first stage being the formation of relatively small, probably off-pathway [7.10], oligomers, which successively convert to fibrils⁴ [7.9]. As a consequence, we have here the possibility to study the inhibiting effect of α -cas against aggregation, *ceteris paribus*, for two processes with completely different phenomenology, by simply increasing the concentration of protein. Accordingly, we performed analogous experiments at a concentration of 5.0 mg/ml. Fig. 7.4a clearly shows the expected biphasic behavior, which is emphasized in the log-log plot of Fig. 7.4b. Moreover, Fig. 7.4b also shows that the portion of the kinetics relative to the formation of the oligomers follows quite well the $\sim t^2$ behavior (grey line) expected for an equilibrium nucleation dependent aggregation, without any secondary nucleation pathway [7.24, 7.26, 7.27, 7.29] α -cas has essentially no effect at all on the initial oligomer formation, while, on the contrary, still sizably retards the subsequent conversion of oligomers into fibrils. This completely different effect of α -cas on the two phases of the process leads to several interesting conclusions.

⁴The formation of these oligomers proceeds immediately without any lag phase, and, at difference from the “standard” insulin amyloid fibrillation, does not show any evidence for the existence of secondary nucleation pathways.

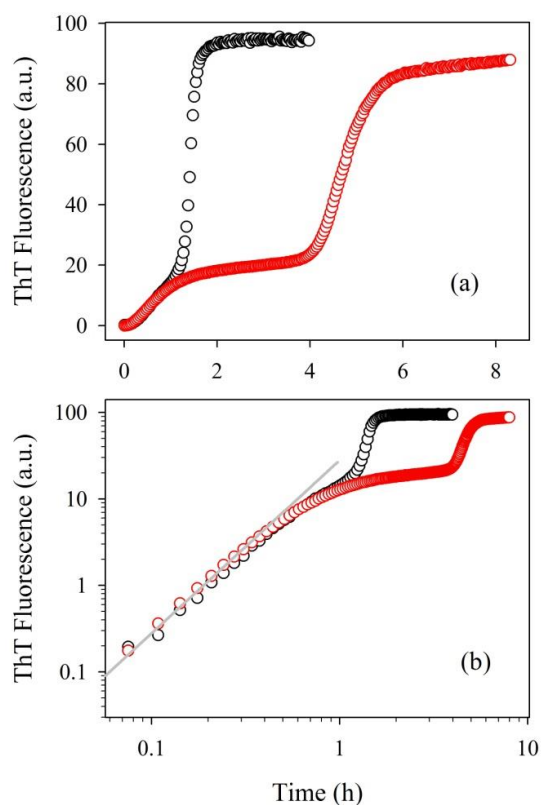


Figure 7.4 ThT fluorescence intensity as a function of time (a) for insulin at a concentration of 5 mg/ml, $T = 60^{\circ}\text{C}$. (b) Same data on a log-log scale. Black: No casein; Red: Casein 1:100 (mol:mol). The grey line in panel b represents a $\sim t^2$ behavior.

Concerning the basic mechanisms underlying insulin fibrillation, data reported in Fig. 7.4 confirm that the oligomers initially formed at high protein concentration are not on-pathway with respect to fibrils formation. The most probable scenario is that the formation of oligomers is an independent process with respect to fibril formation and that it has a much stronger concentration dependence, thus resulting negligible at low concentration and significant at high concentration. Most likely, the oligomers initially formed are in equilibrium with monomers/dimers, whose addition to them is not irreversible, and the subsequent fibril growth proceeds by monomers/dimers release from the oligomers and association into fibrils. Only this last step results to be strongly affected by the presence of α -cas, even at strongly sub-stoichiometric concentration.

The previously described results indicate that (i) the second phase of the aggregation at high insulin concentration follows the same mechanisms observed in the low concentration regime, that is, primary and secondary nucleation, and (ii) concerning the chaperone-like activity of α -cas, a strong inhibiting effect is observed only when secondary nucleation plays an important role in the aggregation kinetics. On the contrary, there is no effect on the “ordinary” association of partially unfolded protein molecules, which leads to the formation of the oligomers. These observations help to clarify the mechanisms of action of α -cas. It is an intrinsically disordered protein, [7.28, 7.29] characterized by the presence of large hydrophobic regions, which make it able to polymerize and, together with other caseins, to form micellar structures [7.30]. Because of these properties, it can be able to sequester partially unfolded protein molecules and small aggregates exposing hydrophobic regions. Hence, when the primary nucleation is very slow and the kinetics of the aggregation is essentially determined by secondary nucleation mechanisms, as it is for insulin, [7.31-7.35] the capture of the early aggregates has a very strong effect because their growing is stopped before they become able to trigger the exponential proliferation of aggregates brought about by the secondary nucleation. This fact strongly increases the duration of the lag-phase observed in the low concentration regime, in a dose-dependent way, until a number of aggregation centers sufficient to saturate α -cas molecules is reached. Given the strongly sub-stoichiometric concentration, we believe that it is more plausible that α -cas is able to sequester a small amount of aggregates before they trigger secondary nucleation rather than promote a massive formation of oligomers in solution. Importantly, a strong sub-stoichiometric effect has also been observed in the case of the A β 1-40 peptide, [7.13] whose aggregation process is characterized by the presence of secondary nucleation mechanisms [7.36]. Consistent with the previously suggested mechanism of action, negligible effects have been found on the single-molecule conformational rearrangements under destabilizing conditions (Figure 7.3). It seems reasonable to extend this mechanism of action to other systems able to exert a “chaperone-like” activity against protein aggregation in a sub-stoichiometric concentration. [7.37, 7.38, 7.39]

7.3 Conclusions

In conclusion, the study of the interactions between insulin and α -cas has shed new light both on the properties of insulin amyloid formation and on the mechanisms by which α -cas exerts its chaperone-like activity against aggregation. In particular, the connection here elucidated between the sub-stoichiometric effectiveness of α -cas and the presence of secondary nucleation pathways in the aggregation process of the target proteins may be an important and general feature in the activity of other chaperone-like molecules and could help to better understand the structural basis of the substrate binding in sHsps. Furthermore, it is worth to note that insulin, due to its use in diabetes treatments, has a considerable medical and commercial interest, and that α -cas is a quite cheap protein. Its strong effect on insulin aggregation, beyond the importance for the understanding of the molecular mechanisms of amyloid formation and its inhibition, may help to ameliorate insulin production processes, in which amyloid formation may represent a significant limit.

The major part of the results discussed in this chapter are contained in the paper: “ α -Casein inhibits insulin amyloid formation by preventing the onset of secondary nucleation processes”, by Fabio Librizzi, Rita Carrotta, Dario Spigolon, Donatella Bulone, Pier Luigi San Biagio, published in *The Journal of Physical Chemistry Letters*, 5 (2014) 3034-3038, doi: 10.1021/jz501570m.



Letter
pubs.acs.org/JPCLE

α -Casein Inhibits Insulin Amyloid Formation by Preventing the Onset of Secondary Nucleation Processes

Fabio Librizzi,* Rita Carrotta, Dario Spigolon, Donatella Bulone, and Pier Luigi San Biagio

Institute of Biophysics, UOS Palermo, National Research Council, Via Ugo La Malfa 153, Palermo 90146, Italy

Conclusions

In the last few years, chaperones appear to be emerging as a potential therapeutic strategy, particularly for the neurodegeneration field. Moreover, the growing number of diseases found to be linked to chaperone mutations, testifies to the importance of their role in the cellular protein-quality control mechanism (proteostasis).

The investigation on the biophysical features of the interactions between specific chaperones and the specific protein structures involved in disease and the study of their structural and functional properties are a crucial basic step in order to validate their role in physiological and pathological state, and for the development of effective chaperones-based approaches.

We investigated the (dis)assembly and thermal stability of chaperonins group I (mtHsp60, p-mtHsp60, GroEL) by means different biophysical techniques (DSC, ITC, CD, UV-vis, FCS, HPLC-SEC, DLS). Altogether, our findings suggest that the evolution of GroEL has generated such extreme cooperativity in unfolding in order to maximize its functional lifetime under harsh conditions. In turn, mtHsp60 is less stable than GroEL and p-mtHsp60, with a lower cooperativity in the thermal denaturation transition and a lower ΔH_d .

This is due to a more versatility and flexibility of eukaryotic (particularly mtHsp60) proteins than prokaryotic, suggesting that subunit flexibility should be closely related to the evolutionary history of a complex. Moreover, our results suggests that GroEL and Hsp60s exist in a dynamic equilibrium between monomeric/heptameric/tetradecameric rings, and that the unfolding is coupled to the dissociation of the oligomeric protein.

We believe that these studies in vitro of cooperativity, structural and thermal stability, on bacterial and human Hsp60 (across two proteins where these differences have functional relevance) could help to validate their role in physiological or pathological cases, and for the development of biomolecular nanocarriers, opening new possibilities for targeted drug delivery.

Moreover, we studied the impact of a point mutation (His147Arg) in CCT5, one of the eight subunits of the chaperonin II (the human CCT/TRiC), upon the chaperones structure and functions. The mutation is multiplied eight-fold per ring compared to

the human CCT octamer. This amplification has proved instrumental for detecting subtle effects of a mutation, such as those which are likely to occur in humans, namely mutations that cause pathology but are compatible with survival.

We observed a decreased stability and impaired chaperoning function in the hexadecamer formed by the mutant subunit and investigated on quantitative information on the loss of structural stability in the hexadecamer containing the pathogenic mutation. In conclusion, the chaperonin molecules tested (human w/wo mutation) have distinct thermodynamic profiles, showing different disassembly behavior and implying different cooperativity levels and different conformational trajectories. The pathogenic R mutant (named Pf-R) is energetically the weakest at maintaining the oligomeric complex and displays a distinct oligomeric equilibrium characterized by the lowest enthalpy of dissociation (ΔH_d). Thus, the pathogenic mutation appears to reduce the protein's stability and its capacity for self-organization. The observed differences in ATP binding provide further evidence that the R mutation in Pf-R disrupts the chaperonin's functional cycle by failing to induce the normal conformational changes. Pf-R has an exothermic ΔH (-26.8 kcal/mol) compared to the endothermic values for the wild-type humanized version Pf-H (6.5 kcal/mol).

This suggests that the pathology follows from a failure of ATP binding to induce the oligomer's closed conformation, which is required for ATP hydrolysis and the subsequent conformational cycling that underlies normal chaperonin function.

Beyond the understanding of the basic mechanisms leading to amyloid formation, considerable efforts have been dedicated also to its inhibition, which can have important implications on medical, pharmaceutical and biotechnological research. In fact, amyloid formation, further than being involved in many diseases, may also represent a limit in protein purification, production and storage.

Our results confirm the potential of molecular chaperones in interfering with the crucial molecular steps leading to amyloid aggregation in neurodegeneration and demonstrate that mtHsp60 is able to target the A β species responsible for induction of amyloid protein assembly. Due to the high grade of flexibility of the protein structure, mtHsp60 can interact with a very wide spectrum of biological molecules and protein conformations and with a high versatility of mechanisms of action,

exploiting as in the case of Hsp60 and A β oligomers, amateur, non-classical mechanisms.

Among the inhibitors, milk casein proteins have been found to exert a chaperone-like activity against aggregation. We found that an efficient inhibition of amyloid formation can be achieved by chaperone-like systems, α -Caseins, which are able to exert a stabilizing function through direct interaction (similar to small Hsps), and we evaluated the mechanism of chaperone-like activity against aggregation. Our results indicate that inhibition of amyloid formation can be achieved by chaperone-like systems by sequestering the early aggregates, before they can trigger the exponential proliferation brought about by secondary nucleation mechanisms. Investigation on its interaction mechanism could help to better understand the activity of other chaperone-like molecules and the structural basis of the substrate binding in sHsps.

Acknowledgements

This PhD would not have been possible to do without the support and guidance that I received from many people, of different nationality, becoming a truly life-changing experience for me. I would like to thank all people who made this thesis possible:

Foremost, I would like to express my sincere gratitude to my advisors and tutors Dr. Bulone Donatella (CNR-IBF, Pa), Dr. Pier Luigi San Biagio (CNR-IBF, Pa) and Dr. Maurizio Leone (Dip. Chimica e Fisica, UniPa) for the continuous support of my Ph.D study, research, for their patience, motivation, enthusiasm, and immense knowledge.

Particularly, Donatella's guidance helped me in all the time of research and writing of this thesis, and I really thank her for the useful comments, remarks, for her encouragement, insightful comments, and hard questions.

GRAZIE MILLE.

Besides my advisor, I would like to thank the rest of my thesis committee: a big thank is for all the group of the IBF of CNR (U.O.S. Palermo) where I spent most of the working time, having been given unique opportunities and taken advantage of them. In particular: Dr. Silvia Vilasi, Dr. Mariuccia Mangione, Dr. Rita Carrotta, Dr. Fabio Librizzi, Dr. Claudia Marino, Dr. Daniela Giacomazza, Dr. Alessia Provenzano, Dr. Rosina Noto, Dr. Rosa Passantino, for introducing me to the topic as well for the support on the way, leading me working on diverse exciting projects. Thanks to the Department Di.Bi.Med. of the University of Palermo, in particular to the Prof. Calogero Caruso and Dr. G. Candore.

GRAZIE A TUTTI.

My sincere thanks also goes to Dr. Adrian Velazquez Campoy for offering me the opportunities to carry out my research in his institute, BIFI (Institute for Biocomputation and Physics of Complex Systems, University of Zaragoza), for the strong support received and for the continuous collaboration during my PhD.

GRACIAS.

Special groups from Maryland, IMET (Institute of Marine and Environmental Technology, Baltimore, MD) and IBBR (Institute for Bioscience and Biotechnology Research, Rockville, MD) are not mentioned yet, because they, as well, deserve their own part: I praise the enormous amount of help and teaching by Dr. Frank Robb, Dr. Alberto J. Macario and Dr. Everly Conway de Macario throughout this last year. I greatly appreciate their support received through the collaborative work undertaken and during the months spent in USA. Thank you to those who helped and supported the project as staff and graduate students, in particular: Dr. Travis Gallagher and Dr. Jatin Narang.

THANK YOU.

Last but not least, I am greatly indebted to my family and Alessandra. Their love and support without any complaint or regret has enabled me to complete this Ph.D. project, teaching me the joy of learning, and helped me to fight for what I desire.

GRAZIE DI CUORE.

Papers and contributions during PhD:

- ✓ (Paper submitted in BBA- Molecular Basis of Disease Submit Date: Aug 23, 2016) **Dario Spigolon**, Travis Gallagher, Adrian Velazquez-Campoy, Donatello Bulone, Jatin Narang, Pier Luigi San Biagio, Francesco Cappello, MD Alberto J Macario, MD, Everly Conway de Macario, Frank T Robb, “**Diseases caused by defective molecular chaperones: Quantitative analysis of the impact of a pathogenic mutation on the CCT5 chaperonin subunit using a proxy archaeal ortholog**”.
- ✓ Emanuela F Craparo , Barbara Porsio , Domenico Schillaci , Maria G Cusimano , **Dario Spigolon** , Gaetano Giammona , Gennara Cavallaro, “**Polyanion–tobramycin nanocomplexes into functional microparticles for the treatment of Pseudomonas aeruginosa infections in cystic fibrosis**”, *Nanomedicine (Lond)*, 23 Nov 2016, doi:10.2217/nmm-2016-0262
- ✓ Mangione MR, Vilasi S, Marino C, Librizzi F, Canale C, **Dario Spigolon**, Bucchieri F, Fucarino A, Passantino R, Cappello F, Bulone D, San Biagio PL. “**Hsp60, amateur chaperone in amyloid-beta fibrillogenesis**”, *Biochim Biophys Acta*. 2016 Jul 26. pii: S0304-4165(16)30266-5. doi: 10.1016/j.bbagen.2016.07.019.
- ✓ Nicastro MC, **Spigolon D**, Librizzi F, Moran O, Ortore MG, Bulone D, Biagio PL, Carrotta R. et al., “**Amyloid β -peptide insertion in liposomes containing GM1-cholesterol domains**”, *Biophysical Chemistry, Biophys Chem*. 2015 Jul 31. pii: S0301-4622(15)30028-4. doi: 10.1016/j.bpc.2015.07.010.
- ✓ **Dario Spigolon**, Silvia Vilasi, Maria Rosalia Mangione, PierLuigi San Biagio, Donatella Bulone, “**(DIS)Assembly and Structural Stability of mtHsp60 and its Precursor Naïve Form**”, *Biophysical Journal*, Volume 108, Issue 2, Supplement 1, p502a, 27 January 2015 DOI: 10.1016/j.bpj.2014.11.2751
- ✓ Fabio Librizzi, Rita Carrotta, **Dario Spigolon**, Donatella Bulone, and Pier Luigi San Biagio., “ **α -Casein Inhibits Insulin Amyloid Formation by Preventing the Onset of Secondary Nucleation Processes**”, *The Journal of Physical Chemistry Letters*, 2014, 5, pp 3043–3048, DOI: 10.1021/jz501570m
- ✓ Maria Rosalia Mangione, **Dario Spigolon**, Rosa Passantino, Rita Carrotta, Fabio Librizzi, Caterina Ricci, Maria Grazia Ortore, Annalisa Vilasi, Vincenzo Martorana, Claudia Marino, Francesco Cappello, Pier Luigi San Biagio, Donatella Bulone, Silvia Vilasi, “**Investigation on Structural Features and Antiaggregation Properties of Chaperonins and Chaperon Like Molecules**”, *Biophysical Journal* , Volume 110, Issue 3, Supplement 1, p213a–214a, 16 February 2016, DOI: <http://dx.doi.org/10.1016/j.bpj.2015.11.1186>
- ✓ (type: proceedings) **D. Spigolon**, J. Narang, T. Gallagher, A. Velazquez Campoy, D. Bulone, F. Cappello, P.L. San Biagio, A.J.L. Macario, E. Conway de Macario, F. Robb. **Biophysical investigation on mutations in Group II chaperonins (CCT/TRiC) modeled in the thermosome of the archaeon Pyrococcus furiosus**. En: *Unfolded Proteins: From Basic to Bedside*. Stockholm, 2016
- ✓ (type: proceedings) Frank T. Robb, **Dario Spigolon**, Travis Gallagher, Donatella Bulone, Pier Luigi San Biagio, Jatin Narang , Everly Conway de Macario, Francesco

- Cappello , Alberto J.L. Macario. “**A hyperthermophile model for structural and functional analysis of a pathogenic mutation in a human protein chaperone**“, 11th International Congress on Extremophiles September 12-16, Kyoto, JAPAN
- ✓ (type: proceedings) **Spigolon D.**, Vilasi S., Velazquez-Campoy A., Mangione M.R., Passantino R., Leone M., San Biagio P. L., Bulone D., "**Thermal investigation and analysis on (dis)assembly and Structural Stability of chaperonins group I**", Conference at DCO Workshop on Extreme Biophysics Report in Washington, D.C, 14-15 November 2015
 - ✓ (type: Proceedings) **D.Spigolon**, Vilasi S., Velazquez-Campoy A., Mangione M.R., Passantino R., Leone M., San Biagio P. L., Bulone D. “**Thermal investigation and analysis on chaperonins group I**”, FisMat2015, Unipa, 28–2 Ottobre 2015.
 - ✓ (Oral p.p. Presentation) **Spigolon D**, Vilasi S., Mangione M.R., San Biagio P.L., Bulone D., “**(Dis)Assembly and Structural Stability of mtHsp60 and its precursor naïve form**”, **Biophysical Society 59th Annual Meeting**, Baltimore, Maryland, February 7-11, 2015
 - ✓ (type: Proceedings) Marino C., **Spigolon D.**, Vilasi S., Passantino R., Mangione M.R., Cappello F., Bulone D., Tagliatela G., San Biagio P.L., “**The inhibitory effect of Hsp60 on amyloid beta aggregation: a biophysical study**”, Neuroscience 2014, November 15-19, WD
 - ✓ (type: Proceedings) **D.Spigolon**, Vilasi S., Mangione M.R., San Biagio P.L., Bulone D. “**Calorimetric Investigation on SelfAssembly and Structural Stability of Conditionally Disordered Chaperonins: Hsp60 and GroEL**”, Poster Presenter at the Gordon Research Seminar and Conference on Intrinsically Disordered. Proteins (GRS) held 05/07/2014 - 11/07/2014 at Stonehill College in Easton MA United States.
 - ✓ (type: Proceedings) Vilasi S., Mangione M.R., Passantino R., Marino C., San Biagio P.L., Bulone D. **D.Spigolon** (Coauthor). “**Effect of chaperones with intrinsically disordered regions (IDRs) on the fibrillogenesis of A β amyloid peptide**”, work presented at the Gordon Research Seminar and Conference on Intrinsically Disordered. Proteins (GRS) held 05/07/2014 - 11/07/2014 at Stonehill College in Easton MA United States.
 - ✓ (lecture/abstract): **D. Spigolon**, Vilasi S, F. Cappello, San Biagio PL, Bulone D, “**Hsp60 and GroEL Chaperonins: Thermodynamic Characterization on SelfAssembly and Structural Stability, Studied by Nano DSC and Nano ITC**”: Congresso: Ricerca di base, interdisciplinare e traslazionale in ambito Biologico e Biotecnologico (II ed.), 26 e 27 Giugno 2014.
 - ✓ (type: Proceedings) Fabio Librizzi, Rita Carrotta, **Dario Spigolon**, Donatella Bulone, Pier Luigi San Biagio: **Inhibition of insulin amyloid formation by α 1-Casein: the effect on different nucleation mechanism**, XXII CONGRESSO NAZIONALE SIBPA2014 21–24 Settembre 2014.

- ✓ (type: Proceedings) M.R. Mangione, C. Marino, S. Vilasi, **D. Spigolon**, R. Passantino, C. Canale, F. Cappello, D. Bulone, P.L. San Biagio. “**Effect of HSP60 on fibrillogenesis of A β amyloid peptide**”, XXII CONGRESSO NAZIONALE SIBPA2014, 21–24 Settembre 2014.

- ✓ (type: Proceedings) M C Nicastro, **D Spigolon**, R Carrotta, F Librizzi, S Vilasi, D Bulone, PL San Biagio.. “**Influence of the liposome composition in the interaction with amyloid β -peptide**”, XXII CONGRESSO NAZIONALE SIBPA2014, 21–24 Settembre 2014.

- ✓ (Abstract) M C Nicastro, **D Spigolon**, R Carrotta, F Librizzi, S Vilasi, D Bulone, PL San Biagio. “**Influence of the liposome composition in the interaction with amyloid β -peptide**”, Congresso della Società Italiana Biomateriali 2014 (Sib 2014), Palermo. 2-4 Luglio 2014.

References

I

- [1.1] Anfinsen, C. B. Principles that govern the folding of protein chains. *Science*. 1973 Jul 20;181(4096):223-30.
- [1.2] Lindquist, S. The heat-shock response. *Annu. Rev. Biochem.* **55**, 1151–1191 (1986).
- [1.3] F.U. Hartl, A. Bracher, M. Hayer-Hartl, Molecular chaperones in protein folding and proteostasis, *Nature*, 475 (2013) 324–332, doi: 10.1146/annurev-biochem-060208-092442.
- [1.4] V.N. Uversky, Intrinsically disordered chaperones and neurodegeneration, in: S.N. Witt (Ed.) *Protein chaperones and protection from neurodegenerative diseases*, Wiley, 2011.
- [1.5] Jiang, J. *et al.* CHIP is a U-box-dependent E3 ubiquitin ligase: identification of Hsc70 as a target for ubiquitylation. *J. Biol. Chem.* **276**, 42938–42944 (2001).
- [1.6] P.J. Muchowski, J.L. Wacker, Modulation of neurodegeneration by molecular chaperones, *Nat Rev Neurosci.*, 6 (2005) 11–22, doi:10.1038/nrn1587.
- [1.7] Neil A. RANSON, Helen E. WHITE and Helen R. SAIBIL, *Chaperonins*, *Biochem. J.* (1998) 333, 233–242.
- [1.8] Vladimir Uversky *Protein Chaperones and Protection from Neurodegenerative Diseases* Copyright © 6 JUN 2011 John Wiley & Sons, Inc. DOI: 10.1002/9781118063903.
- [1.9] Lindquist, S. & Kim, G. Heat-shock protein 104 expression is sufficient for thermotolerance in yeast. *Proc. Natl Acad. Sci. USA* 93, 5301–5306 (1996).
- [1.10] Shorter, J. & Lindquist, S. Hsp104 catalyzes formation and elimination of self-replicating Sup35 prion conformers. *Science* 304, 1793–1797 (2004).
- [1.11] Smith, D. F., Whitesell, L. & Katsanis, E. Molecular chaperones: biology and prospects for pharmacological intervention. *Pharmacol. Rev.* 50, 493–514 (1998).
- [1.12] Young, J. C. & Hartl, F. U. Chaperones and transcriptional regulation by nuclear receptors. *Nature Struct. Biol.* 9, 640–642 (2002).
- [1.13] Bukau, B. & Horwich, A. L. The Hsp70 and Hsp60 chaperone machines. *Cell* 92, 351–366 (1998).
- [1.14] Tavaría, M., Gabriele, T., Kola, I. & Anderson, R. L. A hitchhiker's guide to the human Hsp70 family. *Cell Stress Chaperones* 1, 23–28 (1996).

- [1.15] Wall, D., Zylicz, M. & Georgopoulos, C. The conserved G/F motif of the DnaJ chaperone is necessary for the activation of the substrate binding properties of the DnaK chaperone. *J. Biol. Chem.* 270, 2139–2144 (1995).
- [1.16] Wall, D., Zylicz, M. & Georgopoulos, C. The NH₂-terminal 108 amino acids of the *Escherichia coli* DnaJ protein stimulate the ATPase activity of DnaK and are sufficient for lambda replication. *J. Biol. Chem.* 269, 5446–5451 (1994).
- [1.17] Minami, Y., Hohfeld, J., Ohtsuka, K. & Hartl, F. U. Regulation of the heat-shock protein 70 reaction cycle by the mammalian DnaJ homolog, Hsp40. *J. Biol. Chem.* 271, 19617–19624 (1996).
- [1.18] Clark, J. I. & Muchowski, P. J. Small heat-shock proteins and their potential role in human disease. *Curr. Opin. Struct. Biol.* 10, 52–59 (2000).
- [1.19] Bukau B, Horwich AL. 1998. The Hsp70 and Hsp60 chaperone machines. *Cell* 92: 351–366.
- [1.20] Grallert H, Buchner J. 2001. Review: a structural view of the GroE chaperone cycle. *J Struct Biol* 135: 95–103.
- [1.21] Thirumalai D, Lorimer GH. 2001. Chaperonin-mediated protein folding. *Annu Rev Biophys Biomol Struct* 30: 245–269.
- [1.22] Horwich, A. L., Low, K. B., Fenton, W. A., Hirshfeld, I. N. and Furtak, K. (1993) *Cell* 74, 909-917.
- [1.23] Cheng, M. Y., Hartl, F. U., Martin, J., Pollock, R. A., Kalousek, F., Neupert, W., Hallberg, E. M. and Horwich, A. L. (1989) *Nature (London)* 337, 620-635.
- [1.24] Maria Maguire,¹ Anthony R. M. Coates,² and Brian Henderson Chaperonin 60 unfolds its secrets of cellular communication *Cell Stress & Chaperones* (2002) 7 (4), 317–329 *Q Cell Stress Society International 2002 Article no. csac. 2002.381.*
- [1.25] Klumpp, M., Baumeister, W. and Essen, L. O. (1997) *Cell* 91, 263-270.
- [1.26] Ditzel, L., Lowe, J., Stock, D., Stetter, K. O., Huber, H., Huber, R. and Steinbacher, S. (1998) *Cell* 93, 125-138.
- [1.27] Kim, S., Willison, K. R. and Horwich, A. L. (1994) *Trends Biochem. Sci.* 19, 543-548.
- [1.28] Marco, S., Urena, D., Carrascosa, J. L., Waldmann, T., Peters, J., Hegerl, R., Pfeifer, G., Sack-Kongehl, H. and Baumeister, W. (1994) *FEBS Lett.* 341, 152-155.
- [1.29]. Iizuka, R. et al. ATP binding is critical for the conformational change from an open to closed state in archaeal group II chaperonin. *J. Biol. Chem.* 278, 44959–44965 (2003).

- [1.30]. Douglas, N. R. et al. Dual action of ATP hydrolysis couples lid closure to substrate release into the group II chaperonin chamber. *Cell*. 2011 Jan 21; 144 , 240–252, DOI: 10.1016/j.cell.2010.12.017 (2011).
- [1.31]. Zhang, J. et al. Cryo-EM structure of a group II chaperonin in the prehydrolysis ATP-bound state leading to lid closure. *Structure*. 2011 May 11; 19, 633–639, DOI: 10.1016/j.str.2011.03.005 (2011).
- [1.32]. Laksanalamai, P., Whitehead, T. A. & Robb, F. T. Minimal protein-folding systems in hyperthermophilic archaea. *Nature Rev. Microbiol.* 2, 315–324 (2004).
- [1.33] Luo, H., Laksanalamai, P. & Robb, F. T. An exceptionally stable Group II chaperonin from the hyperthermophile *Pyrococcus furiosus*. *Arch. Biochem. Biophys.* 486, 12–18 (2009).
- [1.34] Ehrnsperger, M., Graber, S., Gaestel, M. and Buchner, J. (1996) *EMBO J.* 16, 221-229.
- [1.35] Lee, G. J., Roseman, A. M., Saibil, H. R. and Vierling, E. (1997) *EMBO J.* 16, 659-671.
- [1.36] Rudiger, S., Buchberger, A. and Bukau, B. (1997) *Nat. Struct. Biol.* 4, 342-349.
- [1.37] Flaherty, K. M., DeLuca-Flaherty, C. and McKay, D. B. (1990) *Nature (London)* 346, 623-628.
- [1.38] Zhu, X. T., Zhao, X., Burkholder, W. F., Gragerov, A., Ogata, C. M., Gottesman, M. E. and Hendrickson, W. A. (1996) *Science* 272, 1606-1614.
- [1.39] Parsell, D. A., Kowal, A. S. and Lindquist, S. (1994) *J. Biol. Chem.* 269, 4480-4487.
- [1.40] Kessel, M., Wu, W. F., Gottesman, S., Kocsis, E., Steven, A. C. and Maurizi, M. R. (1996) *FEBS Lett.* 398, 274-278.
- [1.41] Chernoff, Y. O., Lindquist, S. L., Ono, B., Ingevechtomov, S. G. and Liebman, S. W. (1995) *Science* 268, 880-884.
- [1.42] Prodromou, C., Roe, S. M., O'Brien, R., Ladbury, J. E., Piper, P. W. and Pearl, L. H. (1997) *Cell*, 90, 65-75.
- [1.43] Bergeron, J. J. M., Brenner, M. B., Thomas, D. Y. and Williams, D. B. (1994) *Trends Biochem. Sci.* 19, 124-128.
- [1.44] Freedman, R. B. (1995) *Curr. Opin. Struct. Biol.* 5, 85-91.
- [1.45] Fedorov, A. N. and Baldwin, T. O. (1997) *J. Biol. Chem.* 272, 32715-32718.

- [1.46] Baker, D. and Agard, D. A. (1994) *Biochemistry* 33, 7505-7509.
- [1.47] Jackson, G. S., Staniforth, R. A., Halsall, D. J., Atkinson, T., Holbrook, J. J., Clarke, A. R. and Burston, S. G. (1993) *Biochemistry* 32, 2554-2563.
- [1.48] Kandror, O., Sherman, M., Rhode, M. and Goldberg, A. L. (1995) *EMBO J.* 14, 6021-6027.
- [1.49] Braig, K., Otwinowski, Z., Hegde, R., Boisvert, D. C., Joachimiak, A., Horwich, A. L. and Sigler, P. B. (1994) *Nature (London)* 371, 578-586.
- [1.50] Boisvert, D. C., Wang, J. M., Otwinowski, Z., Horwich, A. L. and Sigler, P. B. (1996) *Nat. Struct. Biol.*, 3, 170-177.
- [1.51] Roseman, A., Chen, S., White, H., Braig, K. and Saibil, H. (1996) *Cell* 87, 241-251.
- [1.52] Fenton, W. A., Kashi, Y., Furtak, K. and Horwich, A. L. (1994) *Nature (London)* 371, 614-619.
- [1.53] Kim, S., Willison, K. R. and Horwich, A. L. (1994) *Trends Biochem. Sci.* 19, 543-548.
- [1.54] Klumpp, M., Baumeister, W. and Essen, L. O. (1997) *Cell* 91, 263-270.
- [1.55] Ditzel, L., Lowe, J., Stock, D., Stetter, K. O., Huber, H., Huber, R. and Steinbacher, S. (1998) *Cell* 93, 125±138.
- [1.56] Frydman, J. Folding of newly translated proteins in vivo: The role of molecular chaperones. *Ann. Rev. Biochem.* 2001, 70, 603–647.
- [1.57] Lewis, V.A.; Hynes, G.M.; Zheng, D.; Saibil, H.; Willison, K. T-complex polypeptide-1 is a subunit of a heteromeric particle in the eukaryotic cytosol. *Nature* 1992, 358, 249–252.
- [1.58] Kubota, H.; Hynes, G.; Carne, A.; Ashworth, A.; Willison, K. Identification of six Tcp-1-related genes encoding divergent subunits of the TCP-1-containing chaperonin. *Curr. Biol.* 1994, 4, 89–99.
- [1.59] Leitner, A.; Joachimiak, L.A.; Bracher, A.; Monkemeyer, L.; Walzthoeni, T.; Chen, B.; Pechmann, S.; Holmes, S.; Cong, Y.; Ma, B.; et al. The molecular architecture of the eukaryotic chaperonin TRiC/CCT. *Structure* 2012, 20, 814–825.
- [1.60] Kalisman, N.; Adams, C.M.; Levitt, M. Subunit order of eukaryotic TRiC/CCT chaperonin by cross-linking, mass spectrometry, and combinatorial homology modeling. *Proc. Natl. Acad. Sci. USA* 2012, 109, 2884–2889.

[1.61]. Spiess, C.; Miller, E.J.; McClellan, A.J.; Frydman, J. Identification of the TRiC/CCT substrate binding sites uncovers the function of subunit diversity in eukaryotic chaperonins. *Mol. Cell* 2006, 24, 25–37.

[1.62] Dekker, C.; Roe, S.M.; McCormack, E.A.; Beuron, F.; Pearl, L.H.; Willison, K.R. The crystal structure of yeast CCT reveals intrinsic asymmetry of eukaryotic cytosolic chaperonins. *EMBO J.* 2011, 30, 3078–3090.

[1.63]. Munoz, I.G.; Yebenes, H.; Zhou, M.; Mesa, P.; Serna, M.; Park, A.Y.; Bragado-Nilsson, E.; Beloso, A.; de Carcer, G.; Malumbres, M.; et al. Crystal structure of the open conformation of the mammalian chaperonin CCT in complex with tubulin. *Nat. Struct. Mol. Biol.* 2011, 18, 14–19.

[1.64]. Cong, Y.; Schroder, G.F.; Meyer, A.S.; Jakana, J.; Ma, B.; Dougherty, M.T.; Schmid, M.F.; Reissmann, S.; Levitt, M.; Ludtke, S.L.; et al. Symmetry-free cryo-EM structures of the chaperonin TRiC along its ATPase-driven conformational cycle. *EMBO J.* 2012, 31, 720–730.

[1.65]. Gao, Y.; Thomas, J.O.; Chow, R.L.; Lee, G.H.; Cowan, N.J. A cytoplasmic chaperonin that catalyzes α -actin folding. *Cell* 1992, 69, 1043–1050.

[1.66]. Melki, R.; Batelier, G.; Soulie, S.; Williams, R.C., Jr. Cytoplasmic chaperonin containing TCP-1: Structural and functional characterization. *Biochemistry* 1997, 36, 5817–5826.

[1.67]. Meyer, A.S.; Gillespie, J.R.; Walther, D.; Millet, I.S.; Doniach, S.; Frydman, J. Closing the folding chamber of the eukaryotic chaperonin requires the transition state of ATP hydrolysis. *Cell* 2003, 113, 369–381.

[1.68]. Shimon, L.; Hynes, G.M.; McCormack, E.A.; Willison, K.R.; Horovitz, A. ATP-induced allostery in the eukaryotic chaperonin CCT is abolished by the mutation G345D in CCT4 that renders yeast temperature-sensitive for growth. *J. Mol. Biol.* 2008, 377, 469–477.

[1.69]. Iizuka, R.; Yoshida, T.; Ishii, N.; Zako, T.; Takahashi, K.; Maki, K.; Inobe, T.; Kuwajima, K.; Yohda, M. Characterization of archaeal group II chaperonin-ADP-metal fluoride complexes: Implications that group II chaperonins operate as a “two-stroke engine”. *J. Biol. Chem.* 2005, 280, 40375–40383.

[1.70]. Rivenzon-Segal, D.; Wolf, S.G.; Shimon, L.; Willison, K.R.; Horovitz, A. Sequential ATP-induced allosteric transitions of the cytoplasmic chaperonin containing TCP-1 revealed by EM analysis. *Nat. Struct. Mol. Biol.* 2005, 12, 233–237.

[1.71] Yao Cong^{1,4}, Gunnar F Schroder^{2,5}, Anne S Meyer^{3,6}, Joanita Jakana¹, Boxue Ma¹, Matthew T Dougherty¹, Michael F Schmid¹, Stefanie Reissmann^{3,7}, Michael Levitt², Steven L Ludtke¹, Judith Frydman³ and Wah Chiu Symmetry-free cryo-EM structures of the chaperonin TRiC along its ATPase-driven conformational cycle, *The EMBO Journal* (2012) 31, 720–730.

[1.72] Joachimiak, L.A.; Walzthoeni, T.; Liu, C.W.; Aebersold, R.; Frydman, J. The structural basis of substrate recognition by the eukaryotic chaperonin TRiC/CCT. *Cell* 2014, 159, 1042–1055.

- [1.73] Yam, A.Y.; Xia, Y.; Lin, H.T.; Burlingame, A.; Gerstein, M.; Frydman, J. Defining the TRiC/CCT interactome links chaperonin function to stabilization of newly made proteins with complex topologies. *Nat. Struct. Mol. Biol.* 2008, 15, 1255–1262.
- [1.74] Gong, Y.; Kakihara, Y.; Krogan, N.; Greenblatt, J.; Emili, A.; Zhang, Z.; Houry, W.A. An atlas of chaperone-protein interactions in *Saccharomyces cerevisiae*: Implications to protein folding pathways in the cell. *Mol. Syst. Biol.* 2009, 5.
- [1.75] Dekker, C.; Stirling, P.C.; McCormack, E.A.; Filmore, H.; Paul, A.; Brost, R.L.; Costanzo, M.; Boone, C.; Leroux, M.R.; Willison, K.R. The interaction network of the chaperonin CCT. *EMBO J.* 2008, 27, 1827–1839.
- [1.76] Freund, A.; Zhong, F.L.; Venteicher, A.S.; Meng, Z.; Veenstra, T.D.; Frydman, J.; Artandi, S.E. Proteostatic control of telomerase function through TRiC-mediated folding of TCAB1. *Cell* 2014, 159, 1389–1403.
- [1.77] Kasembeli, M.; Lau, W.C.; Roh, S.H.; Eckols, T.K.; Frydman, J.; Chiu, W.; Twardy, D.J. Modulation of STAT3 folding and function by TRiC/CCT chaperonin. *PLoS Biol.* 2014, 12, e1001844.
- [1.78] Russmann, F.; Stemp, M.J.; Monkemeyer, L.; Etchells, S.A.; Bracher, A.; Hartl, F.U. Folding of large multidomain proteins by partial encapsulation in the chaperonin TRiC/CCT. *Proc. Natl. Acad. Sci. USA* 2012, 109, 21208–21215.
- [1.79] Kalisman, N.; Levitt, M. Insights into the intra-ring subunit order of TRiC/CCT: A structural and evolutionary analysis. *Pac. Symp. Biocomput.* 2010, 252–259.
- [1.80] Kalisman, N.; Schroder, G.F.; Levitt, M. The crystal structures of the eukaryotic chaperonin CCT reveal its functional partitioning. *Structure* 2013, 21, 540–549.
- [1.81] Reissmann, S.; Joachimiak, L.A.; Chen, B.; Meyer, A.S.; Nguyen, A.; Frydman, J. A gradient of ATP affinities generates an asymmetric power stroke driving the chaperonin TRiC/CCT folding cycle. *Cell Rep.* 2012, 2, 866–877.
- [1.82] Lopez, T.; Dalton, K.; Frydman, J. The Mechanism and Function of Group II Chaperonins. *J. Mol. Biol.* 2015, 427, 2919–2930.
- [1.83] Shuvendu Biswas, Kazushi Kinbara, Tatsuya Niwa, Hideki Taguchi, Noriyuki Ishii, Sumiyo Watanabe, Kanjiro Miyata, Kazunori Kataoka, and Takuzo Aida, Biomolecular robotics for chemomechanically driven guest delivery fuelled by intracellular ATP, *NATURE CHEMISTRY*, VOL 5, 613-620, JULY 2013 DOI: 10.1038/NCHEM.1681.
- [1.84] Freitas, R. A. What is nanomedicine? *Nanomed. Nanotechnol. Biol. Med.* 1, 2–9 (2005).
- [1.85] 2. Kinbara, K. & Aida, T. Toward intelligent molecular machines: directed motions of biological and artificial molecules and assemblies. *Chem. Rev.* 105, 1377–1400 (2005).
- [1.86] 3. corpvan den Heuvel, M. G. L. & Dekker, C. Motor proteins at work for nanotechnology. *Science* 317, 333–336 (2007).
- [1.87] 4. Schliwa, M. (ed.) *Molecular Motors* (Wiley-VCH, 2003).

- [1.88] Bours, M. J. L., ;Swennen, E. L. R., Virgilio, F. D., Cronstein, B. N. & Dagnelie, P. C. Adenosine 5'-triphosphate and adenosine as endogenous signaling molecules in immunity and inflammation. *Pharmacol. Ther.* 112, 358–404 (2006).
- [1.89] Mal, N. K., Fujiwara, M. & Tanaka, Y. Photocontrolled reversible release of guest molecules from coumarin-modified mesoporous silica. *Nature* 421, 350–353 (2003).
- [1.90] Zhu, C. L., Lu, C. H., Song, X. Y., Yang, H. H. & Wang, X. R. Bioresponsive controlled release using mesoporous silica nanoparticles capped with aptamer-based molecular gate. *J. Am. Chem. Soc.* 133, 1278–1281 (2011).
- [1.91] Naito, M. et al. A phenylboronate functionalized polyion complex micelle for ATP-triggered release of siRNA. *Angew. Chem. Int. Ed.* 51, 10751–10755 (2012).
- [1.92] King, W., Pytel, N., Ng, K. & Murphy, W. Triggered drug release from dynamic microspheres via a protein conformational change. *Macromol. Biosci.* 10, 580–584 (2010).
- [1.93] Hartl, F. U., Bracher, A. & Hayer-Hartl, M. Molecular chaperones in protein folding and proteostasis. *Nature* 475, 324–332 (2011).
- [1.94] Morgan PE, Treweek TM, Lindner RA, Price WE, Carver JA. Casein proteins as molecular chaperones. *J Agric Food Chem.* 2005 Apr 6;53(7):2670-83.
- [1.95] Teresa M. Treweek, Alpha-casein as a molecular chaperone, Graduate School of Medicine - Papers (Archive), (2012). (pp. 85-119).
- [1.96] Swaisgood HE. Chemistry of the caseins. In: Fox PF. (ed.) *Advanced Dairy Chemistry- 1: Proteins*. London: Elsevier Applied Science; 1992. p63-110.
- [1.97] Fox PF, McSweeney PLH. *Dairy chemistry and biochemistry*. London: Blackie Academic and Professional; 1998.
- [1.98] Holt C, Sawyer L. Caseins as rheomorphic proteins: Interpretations of the primary and secondary structures of the alphaS1-, beta- and kappa-caseins. *Journal of the Chemical Society, Faraday Transactions* 1993; 89 2683-2692.
- [1.99] Swaisgood HE. Chemistry of the caseins. In: Fox PF, McSweeney PLH (eds.) *Advanced Dairy Chemistry – 1: Proteins*. 3rd ed., Part B. New York: Kluwer Academic/Plenum Publishers; 2003. p. 139-201.
- [1.100] Kumosinski TF, Brown FM, Farrell HMJ. Three-dimensional molecular modeling of bovine caseins: α S1-casein. *Journal of Dairy Science* 1991;74 2889-2895.
- [1.101] Kumosinski TF, King G, Farrell HMJ. An energy-minimized casein submicelle working model. *Journal of Protein Chemistry* 1994;13(8) 681-700.

- [1.102] Treweek TM, Thorn DC, Price WE, Carver JA. The chaperone action of bovine milk α S1- and α S2-caseins and their associated form α S-casein. *Archives of Biochemistry and Biophysics* 2011;510 42-52.
- [1.103] Morgan PE, Treweek TM, Lindner RA, Price WE, Carver JA. Casein proteins as molecular chaperones. *Journal of Agricultural and Food Chemistry* 2005;53(7) 2670-2683.
- [1.104] Bhattacharyya J, Das KP. Molecular chaperone-like properties of an unfolded protein, α S-casein. *Journal of Biological Chemistry* 1999;274(22) 15505-15509.
- [1.105] Zhang X, Fu X, Zhang H, Liu C, Jiao W, Chang Z. Chaperone-like activity of α S-casein. *International Journal of Biochemistry and Cell Biology* 2005;37 1232-1240.
- [1.106] Barzegar A, Yousefi R, Sharifzadeh A, Dalgalarondo M, Saboury AA, Haertle T, Moosavi-Movahedi AA. Chaperone activities of bovine and camel α S-caseins: Importance of their surface hydrophobicity in protection against alcohol dehydrogenase aggregation. *International Journal of Biological Macromolecules* 2008;42(4) 392-399.
- [1.107] Yong YH, Foegeding EA. Effects of caseins on thermal stability of bovine β -lactoglobulin. *Journal of Agricultural and Food Chemistry* 2008;56(21) 10352-10558.
- [1.108] Koudelka T, Hoffmann P, Carver JA. Dephosphorylation of α S- and α -caseins and its effect on chaperone activity: a structural and functional investigation. *Journal of Agricultural and Food Chemistry* 2009;57(13) 5956-5964.
- [1.109] Ptitsyn OB. Protein folding: Hypotheses and experiments. *Journal of Protein Chemistry* 1987;6 273-293.
- [1.110] Dunker AK, Brown CJ, Lawson JD, Iakoucheva LM, Obradovic Z. Intrinsic disorder and protein function. *Biochemistry* 2002;41(21) 6573-6582.
- [1.111] Uversky VN. What does it mean to be natively unfolded? *European Journal of Biochemistry* 2002;269(1) 2-12.
- [1.112] Alaimo MH, Farrell HMJ, Germann MW. Conformational analysis of the hydrophobic peptide α S1-casein(136-196). *Biochimica et Biophysica Acta* 1999;1431 410-420.
- [1.113] Kuwajima K. The molten globule state of β -lactalbumin. *The FASEB Journal* 1996;10 102-109.
- [1.114] Kumosinski TF, Brown EM, Farrell HMJ. Three-dimensional molecular modeling of bovine caseins: a refined, energy-minimized α -casein structure. *Journal of Dairy Science* 1993;76(9) 2507-2520.
- [1.115] Kumosinski TF, Brown FM, Farrell HMJ. Three-dimensional molecular modeling of bovine caseins: α S1-casein. *Journal of Dairy Science* 1991;74 2889-2895.

[1.116] Kumosinski TF, King G, Farrell HMJ. An energy-minimized casein submicelle working model. *Journal of Protein Chemistry* 1994;13(8) 681-700.

[1.117] Thorn DC, Ecroyd H, Carver JA. The two-faced nature of milk casein proteins: amyloid fibril formation and chaperone-like activity. *Australian Journal of Dairy Technology* 2009;64(1) 34-40.

[1.118] Farrell HMJ, Qi PX, Brown EM, Cooke PH, Tunick MH, Wickham ED, Unruh JJ. Molten globule structures in milk proteins: implications for potential new structurefunction relationships. *Journal of Dairy Science* 2002;85 459-471.

II

- [2.1] Temussi PA, Masino L, Pastore A. From Alzheimer to Huntington: why is a structural understanding so difficult? *Embo J* 2003;22:355–61.
- [2.2] Bates G. Huntingtin aggregation and toxicity in Huntington's disease. *Lancet* 2003;361:1642–4.
- [2.3] Stefani M, Dobson CM. Protein aggregation and aggregate toxicity: new insights into protein folding, misfolding diseases and biological evolution. *J Mol Med* 2003, in press.
- [2.4] Sakahira H, Breuer P, Hayer-Hartl MK, Hartl FU. Molecular chaperones as modulators of polyglutamine protein aggregation and toxicity. *Proc Natl Acad Sci USA* 2002;99(Suppl 4):16412–8.
- [2.5] Caughey B, Lansbury PT. Protofibrils, pores, fibrils, and neurodegeneration: separating the responsible protein aggregates from the innocent bystanders. *Annu Rev Neurosci* 2003;26: 267–98.
- [2.6] Chiti F, Bucciantini M, Capanni C, Taddei N, Dobson CM, Stefani M. Solution conditions can promote formation of either amyloid protofilaments or mature fibrils from the HypF N-terminal domain. *Protein Sci* 2001;10:2541–7.f.
- [2.7] Taylor JP, Tanaka F, Robitschek J, Sandoval CM, Taye A, Markovic-Plese S, et al. Aggresomes protect cells by enhancing the degradation of toxic polyglutamine-containing protein. *Hum Mol Genet* 2003;12:749–57.
- [2.8] Mishra RS, Bose S, Gu Y, Li R, Singh N. Aggresome formation by mutant prion proteins: the unfolding role of proteasomes in familial prion disorders. *J Alzheimers Dis* 2003;5:15–23.
- [2.9] McNaught KS, Shashidharan P, Perl DP, Jenner P, Olanow CW. Aggresome-related biogenesis of Lewy bodies. *Eur J Neurosci* 2002;16:2136–48.
- [2.10] Kopito RR, Sitia R. Aggresomes and Russell bodies. Symptoms of cellular indigestion? *EMBO Rep* 2000;1:225–31.
- [2.11] Broadley SA1, Hartl FU. The role of molecular chaperones in human misfolding diseases, *FEBS Lett.* 2009 Aug 20;583(16):2647-53. doi: 10.1016/j.febslet.2009.04.029. Epub 2009 Apr 23.
- [2.12] José M Barral, Sarah A Broadley, Gregor Schaffar, F.Ulrich Hartl, Roles of molecular chaperones in protein misfolding diseases, *Seminars in Cell & Developmental Biology* Volume 15, Issue 1, February 2004, Pages 17–29.
- [2.13] Dobson CM. Protein misfolding, evolution and disease. *Trends Biochem Sci* 1999;24:329–32.

[2.14] Radford SE. Protein folding: progress made and promises ahead. *Trends Biochem Sci* 2000;25:611–8.

[2.15] Muchowski PJ, Ning K, D'Souza-Schorey C, Fields S. Requirement of an intact microtubule cytoskeleton for aggregation and inclusion body formation by a mutant huntingtin fragment. *Proc Natl Acad Sci USA* 2002;99:727–32.

[2.16] Saudou F, Finkbeiner S, Devys D, Greenberg ME. Huntingtin acts in the nucleus to induce apoptosis but death does not correlate with the formation of intranuclear inclusions. *Cell* 1998;95:55–66.

[2.17] Warrick JM, Chan HY, Gray-Board GL, Chai Y, Paulson HL, Bonini NM. Suppression of polyglutamine-mediated neurodegeneration in *Drosophila* by the molecular chaperone HSP70. *Nat Genet* 1999;23:425–8.

[2.18] Klement IA, Skinner PJ, Kaytor MD, Yi H, Hersch SM, Clark HB, et al. Ataxin-1 nuclear localization and aggregation: role in polyglutamine-induced disease in SCA1 transgenic mice. *Cell* 1998;95:41–53.

[2.19] Walsh DM, Klyubin I, Fadeeva JV, Cullen WK, Anwyl R, Wolfe MS, et al. Naturally secreted oligomers of amyloid beta protein potently inhibit hippocampal long-term potentiation in vivo. *Nature* 2002;416:535–9.

[2.20] Scherzinger E, Sittler A, Schweiger K, Heiser V, Lurz R, Hasenbank R, et al. Self-assembly of polyglutamine-containing huntingtin fragments into amyloid-like fibrils: implications for Huntington's disease pathology. *Proc Natl Acad Sci USA* 1999;96:4604–9.

[2.21] Yang W, Dunlap JR, Andrews RB, Wetzel R. Aggregated polyglutamine peptides delivered to nuclei are toxic to mammalian cells. *Hum Mol Genet* 2002;11:2905–17.

[2.22] Sanchez I, Mahlke C, Yuan J. Pivotal role of oligomerization in expanded polyglutamine neurodegenerative disorders. *Nature* 2003;421:373–9.

[2.23] Schaffar G, Boteva R, Behrends C, Tzvetkoff N, Sakahira H, Siegers K, et al. Dissecting the mechanism of transcription factor deactivation by a polyglutamine disease protein. *Embo J*, submitted for publication.

[2.24] Michalik A, Van Broeckhoven C. Pathogenesis of polyglutamine disorders: aggregation revisited. *Hum Mol Genet* 2003;12(Suppl 2):R173–86.

[2.25] Volles MJ, Lee SJ, Rochet JC, Shtilerman MD, Ding TT, Kessler JC, et al. Vesicle permeabilization by protofibrillar alpha-synuclein: implications for the pathogenesis and treatment of Parkinson's disease. *Biochemistry* 2001;40:7812–9.

[2.26] Kagan BL, Hirakura Y, Azimov R, Azimova R. The channel hypothesis of Huntington's disease. *Brain Res Bull* 2001;56:281–4.

- [2.27] Monoi H, Futaki S, Kugimiya S, Minakata H, Yoshihara K. Poly-l-glutamine forms cation channels: relevance to the pathogenesis of the polyglutamine diseases. *Biophys J* 2000;78:2892–9.
- [2.28] Frydman J, Hartl FU. Principles of chaperone-assisted protein folding: differences between in vitro and in vivo mechanisms. *Science* 1996;272:1497–502.
- [2.29] D. J. Selkoe, “Cell biology of protein misfolding: the examples of Alzheimer’s and Parkinson’s diseases,” *Nature Cell Biology*, vol. 6, no. 11, pp. 1054–1061, 2004.
- [2.30] C. Dickey, C. Kraft, U. Jinwal et al., “Aging analysis reveals slowed tau turnover and enhanced stress response in a mouse model of tauopathy,” *The American Journal of Pathology*, vol. 174, no. 1, pp. 228–238, 2009.
- [2.31] Q.-L. Ma, X. Zuo, F. Yang et al., “Curcumin suppresses soluble tau dimers and corrects molecular chaperone, synaptic, and behavioral deficits in aged human tau transgenic mice,” *The Journal of Biological Chemistry*, vol. 288, no. 6, pp. 4056–4065, 2013.
- [2.32] S. A. Frautschy, W. Hu, P. Kim et al., “Phenolic anti-inflammatory antioxidant reversal of A β -induced cognitive deficits and neuropathology,” *Neurobiology of Aging*, vol. 22, no. 6, pp. 993–1005, 2001.
- [2.33] F. Yang, G. P. Lim, A. N. Begum et al., “Curcumin inhibits formation of amyloid beta oligomers and fibrils, binds plaques, and reduces amyloid in vivo. *J Biol Chem*. 2005 Feb 18; 280(7):5892-901. Epub 2004 Dec 7.
- [2.34] Y. Yang, R. S. Turner, and J. R. Gaut, “The chaperone BiP/GRP78 A β 42 secretion,” *The Journal of Biological Chemistry*, vol. 273, no. 40, pp. 25552–25555, 1998.
- [2.35] F. Dou, W. J. Netzer, K. Tanemura et al., “Chaperones increase association of tau protein with microtubules,” *Proceedings of the National Academy of Sciences of the United States of America*, vol. 100, no. 2, pp. 721–726, 2003.
- [2.36] R. L. Matts, G. E. L. Brandt, Y. Lu et al., “A systematic protocol for the characterization of Hsp90 modulators,” *Bioorganic and Medicinal Chemistry*, vol. 19, no. 1, pp. 684–692, 2011.
- [2.37] L. Petrucelli, D. Dickson, K. Kehoe et al., “CHIP and Hsp70 regulate tau ubiquitination, degradation and aggregation,” *Human Molecular Genetics*, vol. 13, no. 7, pp. 703–714, 2004.
- [2.38] Muchowski PJ, Schaffar G, Sittler A, Wanker EE, Hayer-Hartl MK, Hartl FU. Hsp70 and hsp40 chaperones can inhibit self-assembly of polyglutamine proteins into amyloid-like fibrils. *Proc Natl Acad Sci USA* 2000;97:7841–6.
- [2.39] Hansen JJ, Dürr A, Cournu-Rebeix I, Georgopoulos C, Ang D, Nielsen MN, Davoine CS, Brice A, Fontaine B, Gregersen N, Bross P. Hereditary spastic paraplegia SPG13 is

associated with a mutation in the gene encoding the mitochondrial chaperonin Hsp60. *Am J Hum Genet.* 2002; 70:1328–1332. [PubMed: 11898127].

[2.40] Fink JK. Hereditary spastic paraplegia: the pace quickens. *Ann Neurol.* 2002; 51:669–672. [PubMed: 12112070].

[2.41] Stone DL, Slavotinek A, Bouffard GG, Banerjee-Basu S, Baxevanis AD, Barr M, Biesecker LG. Mutation of a gene encoding a putative chaperonin causes McKusick–Kaufman syndrome. *Nat Genet.* 2000; 25:79–82. [PubMed: 10802661].

[2.42] Slavotinek AM, Stone EM, Mykytyn K, Heckenlively JR, Green JS, Heon E, Musarella MA, Parfrey PS, Sheffield VC, Biesecker LG. Mutations in MKKS cause Bardet–Biedl syndrome. *Nat Genet.* 2000; 26:15–16. [PubMed: 10973238].

[2.43] Litt M, Kramer P, LaMorticella DM, Murphey W, Lovrien EW, Weleber RG. Autosomal dominant congenital cataract associated with a missense mutation in the human alpha crystalline gene CRYAA. *Hum Mol Genet.* 1998; 7:471–474. [PubMed: 9467006].

[2.44] Vicart P, Caron A, Guicheney P, Li Z, Prévost MC, Faure A, Chateau D, Chapon F, Tomé F, Dupret JM, Paulin D, Fardeau M. A missense mutation in the alphaB-crystallin chaperone gene causes a desmin-related myopathy. *Nat Genet.* 1998; 20:92–95. [PubMed: 9731540].

[2.45] Djabali K, de Nechaud B, Landon F, Portier MM. AlphaB-crystallin interacts with intermediate filaments in response to stress. *J Cell Sci.* 1997; 110:2759–2769. [PubMed: 9427392] *Molecules.* 2010; 15:6885.

[2.46] Parvari R, Hershkovitz E, Grossman N, Gorodischer R, Loeys B, Zecic A, Mortier G, Gregory S, Sharony R, Kambouris M, Sakati N, Meyer BF, Al Aqeel AI, Al Humaidan AK, Al Zahrani F, Al Swaid A, Al Othman J, Diaz GA, Weiner R, Khan KTS, Gordon R, Gelb BD. Mutation of TBCE causes hypoparathyroidism-retardation-dysmorphism and autosomal recessive Kenny–Caffey syndrome. *Nat Genet.* 2002; 32:448–452. [PubMed: 12389028].

[2.47] Engert JC, Bérubé P, Mercier J, Doré C, Lepage P, Ge B, Bouchard JP, Mathieu J, Melançon SB, Schalling M, Lander ES, Morgan K, Hudson TJ, Richter A. ARSACS, a spastic ataxia common in northeastern Quebec, is caused by mutations in a new gene encoding an 11.5-kb ORF. *Nat Genet.* 2000; 24:120–125. [PubMed: 10655055].

[2.48] Takiyama Y. Sacsinopathies: saccin-related ataxia. *Cerebellum.* 2007; 6:353–359.

[2.49] Balch, W.E.; Morimoto, R.I.; Dillin, A.; Kelly, J.W. Adapting proteostasis for disease intervention. *Science* 2008, 319, 916–919.

[2.50] Morimoto, R.I. Proteotoxic stress and inducible chaperone networks in neurodegenerative disease and aging. *Genes Dev.* 2008, 22, 1427–1438.

- [2.51] Calderwood, S.K.; Khaleque, M.A.; Sawyer, D.B.; Ciocca, D.R. Heat shock proteins in cancer: Chaperones of tumorigenesis. *Trends Biochem. Sci.* 2006, 31, 164–172.
- [2.52] Santagata, S.; Hu, R.; Lin, N.U.; Mendillo, M.L.; Collins, L.C.; Hankinson, S.E.; Schnitt, S.J.; Whitesell, L.; Tamimi, R.M.; Lindquist, S.; et al. High levels of nuclear heat-shock factor 1 (HSF1) are associated with poor prognosis in breast cancer. *Proc. Natl. Acad. Sci. USA* 2011, 108, 18378–18383.
- [2.53] Ciocca, D.R.; Calderwood, S.K. Heat shock proteins in cancer: Diagnostic, prognostic, predictive, and treatment implications. *Cell Stress Chaperones* 2005, 10, 86–103.
- [2.54] Leu, J.I.; Pimkina, J.; Frank, A.; Murphy, M.E.; George, D.L. A small molecule inhibitor of inducible heat shock protein 70. *Mol. Cell* 2009, 36, 15–27.
- [2.55] Francesco Cappello, Everly Conway de Macario, Lorenzo Marasà, Giovanni Zummo & Alberto J. L. Macario Hsp60 expression, new locations, functions, and perspectives for cancer diagnosis and therapy, *Cancer Biology & Therapy* 7:6, 801-809; June 2008.
- [2.56] Chandra D, Choy G, Tang DG. Cytosolic accumulation of HSP60 during apoptosis with or without apparent mitochondrial release: evidence that its pro-apoptotic or pro-survival functions involve differential interactions with caspase-3. *J Biol Chem* 2007; 282:31289-301.
- [2.57]. Soltys BJ, Gupta RS. Cell surface localization of the 60 kDa heat shock chaperonin protein (hsp60) in mammalian cells. *Cell Biol Int* 1997; 21:315-20.
- [2.58] Piselli P, Vendetti S, Vismara D, Cicconi R, Poccia F, et al. Different expression of CD44, ICAM-1 and HSP60 on primary tumor and metastases of a human pancreatic carcinoma growing in scid mice. *Anticancer Res* 2000; 20:825-31.
- [2.59] Feng H, Zeng Y, Graner MW, Katsanis E. Stressed apoptotic tumor cells stimulate dendritic cells and induce specific cytotoxic T cells. *Blood* 2002; 100:4108-15.
- [2.60] Shin BK, Wang H, Yim AM, Le Naour F, Brichory F, Jang JH, et al. Global profiling of the cell surface proteome of cancer cells uncovers an abundance of proteins with chaperone function. *J Biol Chem* 2003; 278:7607-16.
- [2.61] Osterloh A, Meier Stiegen F, Veit A, Fleischer B, von Bonin A, Breloer M. Lipopolysaccharidefree heat shock protein 60 activates T cells. *J Biol Chem* 2004; 279:47906-11.
- [2.62] Barazi HO, Zhou L, Templeton NS, Krutzsch HC, Roberts DD. Identification of heat shock protein 60 as a molecular mediator of alpha-3-beta-1 integrin activation. *Cancer Res* 2002; 62:1541-8.

- [2.63] Laad AD, Thomas ML, Fakih AR, Chiplunkar SV. Human gamma-delta T cells recognize heat shock protein-60 on oral tumor cells. *Int J Cancer* 1999; 80:709-14.
- [2.64] Chen W, Wang J, Shao C, Liu S, Yu Y, et al. Efficient induction of antitumor T cell immunity by exosomes derived from heat-shocked lymphoma cells. *Eur J Immunol* 2006; 36:1598-607.
- [2.65] Gupta S, Knowlton AA. Hsp60 trafficking in adult cardiac myocytes: role of exosomal pathway. *Am J Physiol Heart Circ Physiol* 2007; 292:3052-6.
- [2.66] Pockley AG, Muthana M, Calderwood SK. The dual immunoregulatory roles of stress proteins. *Trends Biochem Sci* 2008; 33:71-9.
- [2.67] Steinhoff U, Brinkmann V, Klemm U, Aichele P, Seiler P, Brandt U, et al. Autoimmune intestinal pathology induced by hsp60-specific CD8 T cells. *Immunity* 1999; 11:349-58.
- [2.68] Pockley AG, Fairburn B, Mirza S, Slack LK, Hopkinson K, Muthana M. A non-receptormediated mechanism for internalization of molecular chaperones. *Methods* 2007; 43:238-44.
- [2.69] Tsan MF, Gao B. Heat shock protein and innate immunity. *Cell Mol Immunol* 2004; 1:274-9.
- [2.70] Cappello F, Czarnecka AM, La Rocca G, Di Stefano A, Zummo G, Macario AJ. Hsp60 and Hsp10 as antitumor molecular agents. *Cancer Biol Ther* 2007; 6:487-9.
- [2.71] Calderwood, S.K.; Khaleque, M.A.; Sawyer, D.B.; Ciocca, D.R. Heat shock proteins in cancer: Chaperones of tumorigenesis. *Trends Biochem. Sci.* 2006, 31, 164–172.
- [2.72] Kasembeli, M.; Lau, W.C.; Roh, S.H.; Eckols, T.K.; Frydman, J.; Chiu, W.; Tweardy, D.J. Modulation of STAT3 folding and function by TRiC/CCT chaperonin. *PLoS Biol.* 2014, 12, e1001844.
- [2.73] Leu, J.I.; Pimkina, J.; Frank, A.; Murphy, M.E.; George, D.L. A small molecule inhibitor of inducible heat shock protein 70. *Mol. Cell* 2009, 36, 15–27.
- [2.74] Guest, S.T.; Kratche, Z.R.; Bollig-Fischer, A.; Haddad, R.; Ethier, S.P. Two members of the TRiC chaperonin complex, CCT2 and TCP1 are essential for survival of breast cancer cells and are linked to driving oncogenes. *Exp. Cell Res.* 2015, 332, 223–235.
- [2.75] Sergeeva, O.A.; Chen, B.; Haase-Pettingell, C.; Ludtke, S.J.; Chiu, W.; King, J.A. Human CCT4 and CCT5 chaperonin subunits expressed in escherichia coli form biologically active homo-oligomers. *J. Biol. Chem.* 2013, 288, 17734–17744.

[2.76] Yam, A.Y.; Xia, Y.; Lin, H.T.; Burlingame, A.; Gerstein, M.; Frydman, J. Defining the TRiC/CCT interactome links chaperonin function to stabilization of newly made proteins with complex topologies. *Nat. Struct. Mol. Biol.* 2008, 15, 1255–1262.

[2.77] Saegusa, K.; Sato, M.; Sato, K.; Nakajima-Shimada, J.; Harada, A.; Sato, K. *Caenorhabditis elegans* chaperonin CCT/TRiC is required for actin and tubulin biogenesis and microvillus formation in intestinal epithelial cells. *Mol. Biol. Cell* 2014, 25, 3095–3104.

[2.78] Melville, M.W.; McClellan, A.J.; Meyer, A.S.; Darveau, A.; Frydman, J. The Hsp70 and TRiC/CCT chaperone systems cooperate in vivo to assemble the von Hippel-Lindau tumor suppressor complex. *Mol. Cell Biol.* 2003, 23, 3141–3151.

[2.79] McClellan, A.J.; Scott, M.D.; Frydman, J. Folding and quality control of the VHL tumor suppressor proceed through distinct chaperone pathways. *Cell* 2005, 121, 739–748.

[2.80] Trinidad, A.G.; Muller, P.A.; Cuellar, J.; Klejnot, M.; Nobis, M.; Valpuesta, J.M.; Vousden, K.H. Interaction of p53 with the CCT complex promotes protein folding and wild-type p53 activity. *Mol. Cell* 2013, 50, 805–817.

[2.81] Rivlin, N.; Katz, S.; Doody, M.; Sheffer, M.; Horesh, S.; Molchadsky, A.; Koifman, G.; Shetzer, Y.; Goldfinger, N.; Rotter, V.; et al. Rescue of embryonic stem cells from cellular transformation by proteomic stabilization of mutant p53 and conversion into WT conformation. *Proc. Natl. Acad. Sci. USA* 2014, 111, 7006–7011.

III

- [3.1] Min W., Angileri F., Luo H., Lauria A., Shanmugasundaram M., Almerico A.M., Cappello F., Conway de Macario E., Lednev I.K., Macario A.J.L., Robb F.T. A human CCT5 gene mutation causing distal neuropathy impairs hexadecamer assembly in an archaeal model. *Sci. Rep.* (2014) 4:6688. DOI: 10.1038/srep06688.
- [3.2] Y. Fezoui, D.M. Hartley, J.D. Harper, R. Khurana, D.M. Walsh, M.M. Condron, D.J. Selkoe, P.T. Lansbury, A.L. Fink, D.B. Teplow, An improved method of preparing the amyloid beta-protein for fibrillogenesis and neurotoxicity experiments, *Amyloid*, 7 (2000) 166-178, doi: [http://dx.doi.org/10.1016/S0197-4580\(00\)82569-5](http://dx.doi.org/10.1016/S0197-4580(00)82569-5).
- [3.3] Luke K., Apiyo D., Wittung-Stafshede P. Dissecting homo-heptamer thermodynamics by isothermal titration calorimetry: entropy-driven assembly of co-chaperonin protein 10. *Biophys. J.* (2005) Nov; 89(5):3332-6. Epub 2005 Aug 12. PMID: 16100270.
- [3.4] Barranco-Medina S., Kakorin S., Lázaro J.J., Dietz K.J. Thermodynamics of the dimer-decamer transition of reduced human and plant 2-cys peroxiredoxin. *Biochemistry.* (2008) Jul 8;47(27):7196-204. doi: 10.1021/bi8002956. Epub 2008 Jun 14. PMID: 18553980.
- [3.5] Matthew W. Freyer, Edwin A. Lewis, *Isothermal Titration Calorimetry: Experimental Design, Data Analysis, and Probing Macromolecule/Ligand Binding and Kinetic Interactions*, *Methods in Cell Biology* Volume 84, 2008, Pages 79–113.
- [3.6] Sreerama N, Woody RW. Estimation of protein secondary structure from circular dichroism spectra: comparison of CONTIN, SELCON, and CDSSTR methods with an expanded reference set. *Anal. Biochem.* (2000) Dec 15;287(2):252-60. PMID: 11112271.
- [3.7] Silvia Vilasi, Rita Carrotta et al., Human Hsp60 with Its Mitochondrial Import Signal Occurs in Solution as Heptamers and Tetradecamers Remarkably Stable over a Wide Range of Concentrations, *May* (2014), Volume 9, Issue 5 , e97657.

IV

- [4.1] Dario Spigolon, Silvia Vilasi, Maria Rosalia Mangione, PierLuigi San Biagio, Donatella Bulone, “(DIS)Assembly and Structural Stability of mtHsp60 and its Precursor Naïve Form”, *Biophysical Journal* Volume 108, Issue 2, Supplement 1, p502a, 27 January 2015 DOI: <http://dx.doi.org/10.1016/j.bpj.2014.11.2751>.
- [4.2] Ellis RJ, 2007, Protein misassembly: macromolecular crowding and molecular chaperones *Adv Exp Med Biol.*, 594: 1-13. DOI: 10.1007/978-0-387-39975-11.
- [4.3] Jonathan D. Localization of Mitochondrial 60-kD Heat Shock Chaperonin Protein (Hsp60) in Pituitary Growth Hormone Secretory Granules and Pancreatic Zymogen Granules, *Journal of Histochemistry & Cytochemistry*, Volume 48(1): 45–56, 2000, doi: 10.1177/002215540004800105.
- [4.4] Chandra D, Choy G, Tang DG. Cytosolic accumulation of HSP60 during apoptosis with or without apparent mitochondrial release: evidence that its pro-apoptotic or pro-survival functions involve differential interactions with caspase-3. *J Biol Chem* 2007; 282:31289-301.
- [4.5] Parnas, A., Nisemlat, S., Weiss, C., Levy-Rimler, G., Pri-Or, A., Zor, T., Lund, P. A., Bross, P. & Azem, A. Identification of Elements That Dictate the Specificity of Mitochondrial Hsp60 for Its Co-Chaperonin (2012). *PLoS One*, 7, e50318.
- [4.6] *Acta Crystallogr F Struct Biol Commun.* 2014 Jan;70(Pt 1):116-9. doi: 10.1107/S2053230X1303389X. Epub 2013 Dec Crystallization and structure determination of a symmetrical 'football' complex of the mammalian mitochondrial Hsp60-Hsp10 chaperonins. Nisemlat S1, Parnas A1, Yaniv O2, Azem A1, Frolow F2.
- [4.7] Surin 1999 *Russian Journal of Bioorganic Chemistry*, Vol. 25, No. 5, 1999, pp. 314-320.
- [4.8] Residual Structure in Urea-Denatured Chaperonin GroEL Gorovits, B. M., Seale, J. W., and Horowitz, P. M. (1995) *Biochemistry*, 34, 13928-13933.
- [4.9] Denaturation and reassembly of chaperonin GroEL studied by solution X-ray scattering Arai, M., Inobe, T., Maki, K., Ikura, T., Kihara, H., Amemiya, Y., and Kuwajima, K. (2003) *Protein Sci.*, 12, 672-680.
- [4.10] Ryabova N. A., Marchenkov V. V., Marchenkova S. Y., Kotova N. V. and Semisotnov G. V. (2013) Molecular chaperone GroEL/ES: unfolding and refolding processes. *Biochemistry* 78, 1405–1414.
- [4.11] P.L. Privalov, A. D. (2007). Microcalorimetry of biological macromolecules. *Biophys. Chem.*, 126.

- [4.12] Freire, E. "Statistical thermodynamic analysis of the heat capacity function associated with protein folding-unfolding transitions". *Comm. Mol. Cell. Biophys*; (1989), 6, 123±140.
- [4.13] Cortajarena AL. and Regan L." Calorimetric study of a series of designed repeat proteins: Modular structure and modular folding "*Protein Sci.* 2011 Feb;20(2):336-40.
- [4.14] 2A Cortajarena AL, Regan L (2010) *The folding of repeat proteins.* Oxford: Elsevier Science.
- [4.15] 15A Cortajarena AL, Mochrie SG, Regan L (2008) Mapping the energy landscape of repeat proteins using NMR-detected hydrogen exchange. *J Mol Biol* 379:617–626.
- [4.16] 22. Cziepluch C, Kordes E, Poirey R, Grewenig A, Rommelaere J, Jauniaux J (1998) Identification of a novel cellular TPR-containing protein, SGT, that interacts with the nonstructural protein NS1 of parvovirus H-1. *J Virol* 72:4149–4159.
- [4.17] 56 Creighton, T. E. (1979) *J. Mol. Biol.*, 129, 235-264.
- [4.18] Mendoza JA1, Martinez JL, Horowitz PM. Tetradecameric chaperonin 60 can be assembled in vitro from monomers in a process that is ATP independent. *Biochim Biophys Acta.* (1995) Mar 15;1247(2):209-14.
- [4.19] Sanchez-Ruiz JM, Theoretical analysis of Lumry-Eyring models in differential scanning calorimetry, *Biophys J.* (1992) Apr;61(4):921-35.
- [4.20] TIM J. AHERN et al., Control of oligomeric enzyme thermostability by protein engineering *Proc Natl Acad Sci U S A.* (1987) Feb; 84(3): 675–679.
- [4.21] Rufus Lumry , Henry Eyring, Conformation Changes of Proteins, *J. Phys. Chem.*, (1954), 58 (2), pp 110–120 DOI: 10.1021/j150512a005.
- [4.22] Privalov, P. L. (1982). Stability of proteins. Proteins which do not present a single cooperative system. *Adv. Protein Chem.* 35:1-104.
- [4.23] L.V. Medved', S.V. Litvinovich and P.L. Privalov. Domain organization of the terminal parts in the fibrinogen molecule. Published by Elsevier Science Publishers B. V. (Biomedical Division) 1986, Volume 202, number 2.
- [4.24] Manly, S. P., K. S. Matthews, and J. M. Sturtevant. 1985. Thermal denaturation of the core protein of lac repressor. *Biochemistry.* 24:3842-3846.
- [4.25] Ricci C, Ortore MG, Vilasi S, Carrotta R, Mangione MR, Bulone D, Librizzi F, Spinozzi F, Burgio G, Amenitsch H, San Biagio PL. Stability and disassembly properties of human native Hsp60 and bacterial GroEL chaperonins, *Biophys Chem.* 2016 Jan;208:68-75. doi: 10.1016/j.bpc.2015.07.006.

[4.26] Mendoza JA, Demeler B, Horowitz PM (1994) Alteration of the quaternary structure of cpn60 modulates chaperonin- assisted folding. Implications for the mechanism of chaperonin action. *J. Biol. Chem.* 269: 2447–2451.

[4.27] Gorovits B, Raman CS, Horowitz PM (1995) High hydrostatic pressure induces the dissociation of cpn60 tetradecamers and reveals a plasticity of the monomers. *J. Biol. Chem.* 270: 2061–2066.

[4.28] Ybarra J, Horowitz PM (1995) Inactive GroEL monomers can be isolated and reassembled to functional tetradecamers that contain few bound peptides. *J. Biol. Chem.* 270: 22962–22967.

[4.29] Horovitz A, Bochkareva ES, Girshovich AS (1993) The N terminus of the molecular chaperonin GroEL is a crucial structural element for its assembly. *J. Biol. Chem.* 268: 9957–9959.

[4.30] Parnas A, Nadler M, Nisemblat S, Horovitz A, Mandel H, et al. (2009) The MitCHAP-60 disease is due to entropic destabilization of the human mitochondrial Hsp60 oligomer. *J. Biol. Chem.* 284: 28198–28203.

[4.31] Kathryn Luke et al. Bioche (2005)“Dissecting Homo-Heptamer Thermodynamics by Isothermal Titration Calorimetry: Entropy- Driven Assembly of Co-Chaperonin Protein 10”, *Biophysical Journal* Volume 89 November. Bioche, 3332–3336.

V

- [5.1] H. Saibil, Chaperone machines for protein folding, unfolding and disaggregation, *Nat Rev Mol Cell Biol.*, 14 (2013) 630-642, doi: 10.1038/nrm3658.
- [5.2] B. Kalmar, C.H. Lu, L. Greensmith, The role of heat shock proteins in Amyotrophic Lateral Sclerosis: The therapeutic potential of Arimoclomol, *Pharmacol Ther.*, 141 (2014) 40-54, doi: 10.1016/j.pharmthera.2013.08.003.
- [5.3] J.D. West, Y. Wang, K.A. Morano, Small molecule activators of the heat shock response: chemical properties, molecular targets, and therapeutic promise, *Chem. Res Toxicol.*, 25 (2012) 2036-2053, doi: 10.1021/tx300264x.
- [5.4] P.T. White, C. Subramanian, Q. Zhu, H. Zhang, H. Zhao, R. Gallagher, B.N. Timmermann, B.S. Blagg, M.S. Cohen, Novel HSP90 inhibitors effectively target functions of thyroid cancer stem cell preventing migration and invasion, *Surgery*, 6060 (2015) 00741-00742, doi: 10.1016/j.surg.2015.07.050.
- [5.5] L.M. Butler, R. Ferraldeschi, H.K. Armstrong, M.M. Centenera, P. Workman, Maximizing the therapeutic potential of HSP90 inhibitors, *Mol Cancer Res.*, (2015) 1445-1451, doi: 10.1158/1541-7786.MCR-15-0234.
- [5.6] R.U. Bodani, U. Sengupta, D.L. Castillo-Carranza, M.J. Guerrero-Muñoz, J.E. Gerson, J. Rudra, R. Kaye, Antibody against small aggregated peptide specifically recognizes toxic A β -42 oligomers in Alzheimer's Disease, *ACS Chem Neurosci.*, (2015) 1981-9, doi: 10.1021/acchemneuro.5b00231.
- [5.7] M.J. Guerrero-Muñoz, D.L. Castillo-Carranza, R. Kaye, Therapeutic approaches against common structural features of toxic oligomers shared by multiple amyloidogenic proteins, *Biochemical Pharmacology*, 88 (2014) 468-478, doi: 10.1016/j.bcp.2013.12.023.
- [5.8] S.I. Cohen, P. Arosio, J. Presto, F.R. Kurudenkandy, H. Biverstål, L. Dolfe, C. Dunning, X. Yang, B. Frohm, M. Vendruscolo, J. Johansson, C.M. Dobson, A. Fisahn, T.P. Knowles, S. Linse, A molecular chaperone breaks the catalytic cycle that generates toxic A β oligomers, *Nat Struct Mol Biol.*, 22 (2015) 207-213.
- [5.9] C. Månsson, P. Arosio, R. Hussein, H.H. Kampinga, R.M. Hashem, W.C. Boelens, C.M. Dobson, T.P. Knowles, S. Linse, C. Emanuelsson, Interaction of the molecular chaperone DNAJB6 with growing amyloid-beta 42 (A β 42) aggregates leads to substoichiometric inhibition of amyloid formation, *J Biol Chem.*, 289 (2014) 31066-31076, doi: 10.1038/nsmb.2971.
- [5.10] V.N. Uversky, Intrinsically disordered chaperones and neurodegeneration, in: S.N. Witt (Ed.) *Protein chaperones and protection from neurodegenerative diseases*, Wiley, 2011.

[5.11] S. Vilasi, R. Carrotta, M.R. Mangione, C. Campanella, F. Librizzi, L. Randazzo, V. Martorana, A. Marino Gammazza, M. Ortore, A. Vilasi, G. Pocsfalvi, G. Burgio, D. Corona, A. Palumbo Piccionello, G. Zummo, D. Bulone, E. Conway de Macario, A.J. Macario, P.L. San Biagio, F. Cappello, Human Hsp60 with its mitochondrial import signal occurs in solution as heptamers and tetradecamers remarkably stable over a wide range of concentrations, *PLoS One*, 9 (2014) e97657, doi: 10.1371/journal.pone.0097657.

[5.12] K.L. Nielsen, N.J. Cowan, A single ring is sufficient for productive chaperonin-mediated folding in vivo, *Molecular Cell*, 2 (1998) 93-99, [http://dx.doi.org/10.1016/S10972765\(00\)80117-3](http://dx.doi.org/10.1016/S10972765(00)80117-3).

[5.13] G. Levy-Rimler, P. Viitanen, C. Weiss, R. Sharkia, A. Greenberg, A. Niv, A. Lustig, Y. Delarea, A. Azem, The effect of nucleotides and mitochondrial chaperonin 10 on the structure and chaperone activity of mitochondrial chaperonin 60, *European Journal of Biochemistry*, 268 (2001) 3465-3472, doi: 10.1046/j.1432-1327.2001.02243.x.

[5.14] A. Parnas, M. Nadler, S. Nisemlat, A. Horovitz, H. Mandel, A. Azem, The MitCHAP-60 disease is due to entropic destabilization of the human mitochondrial Hsp60 oligomer, *Journal of Biological Chemistry*, 284 (2009) 28198-28203, doi: 10.1074/jbc.M109.031997.

[5.15] C. Ricci, M.G. Ortore, S. Vilasi, R. Carrotta, M.R. Mangione, D. Bulone, F. Librizzi, F. Spinozzi, G. Burgio, H. Amenitsch, P.L. San Biagio, Stability and disassembly properties of human naïve Hsp60 and bacterial GroEL chaperonins, *Biophys Chem.*, 4622 (2015) 3002430027, doi: 10.1016/j.bpc.2015.07.006.

[5.16] D. Chandra, G. Choy, D.G. Tang, Cytosolic accumulation of HSP60 during apoptosis with or without apparent mitochondrial release: evidence that its pro-apoptotic or pro-survival functions involve differential interactions with caspase-3, *J Biol Chem.*, 282 (2007) 3128931301, doi: 10.1074/jbc.M702777200.

[5.17] C. Campanella, F. Rappa, C. Sciumè, A. Marino Gammazza, R. Barone, F. Bucchieri, S. David, G. Curcurù, C. Caruso Bavisotto, A. Pitruzzella, G. Geraci, G. Modica, F. Farina, G. Zummo, S. Fais, E. Conway de Macario, A.J. Macario, F. Cappello, Heat shock protein 60 levels in tissue and circulating exosomes in human large bowel cancer before and after ablative surgery, *Cancer*, 121 (2015) 3230-3239, doi: 10.1002/cncr.29499.

[5.18] K.C. Walls, P. Coskun, J.L. Gallegos-Perez, N. Zadourian, K. Freude, S. Rasool, M. Blurton-Jones, K.N. Green, F.M. LaFerla, Swedish Alzheimer mutation induces mitochondrial dysfunction mediated by HSP60 mislocalization of amyloid precursor protein (APP) and beta amyloid, *J Biol Chem.*, 287 (2012) 30317-30327, doi: 10.1074/jbc.M112.365890.

[5.19] F. Edenhofer, R. Rieger, M. Famulok, W. Wendler, S. Weiss, E.L. Winnacker, Prion protein PrPc interacts with molecular chaperones of the Hsp60 family, *J Virol.*, 70 (1996) 4724-4728.

- [5.20] M. Yagi-Utsumi, T. Kuniyama, T. Nakamura, Y. Uekusa, K. Makabe, K. Kuwajima, K. K., NMR characterization of the interaction of GroEL with amyloid β as a model ligand, *FEBS Lett.*, 587 (2013) 1605-1609, doi: 10.1016/j.febslet.2013.04.007.
- [5.21] J. Chen, H. Yagi, P. Sormanni, M. Vendruscolo, K. Makabe, T. Nakamura, Y. Goto, K. Kuwajima, Fibrillogenic propensity of the GroEL apical domain: a Janus-faced minichaperone, *FEBS Lett.*, 586 (2012) 1120-1127, doi: 10.1016/j.febslet.2012.03.019.
- [5.22] D.E. Dunstan, P. Hamilton-Brown, P. Asimakis, W. Ducker, J. Bertolini, Shear flow promotes amyloid- β fibrilization, *PEDS* 22 (2009) 741-746, doi: 10.1093/protein/gzp059.
- [5.23] P. Hamilton-Brown, I. Bekard, D. W.A., D.E. Dunstan, How does shear affect A β fibrillogenesis?, *J. Phys. Chem. B*, 112 (2008) 16249-16252, doi: 10.1021/jp805257n.
- [5.24] H.R. Saibil, W.A. Fenton, D.K. Clare, A.L. Horwich, Structure and allostery of the chaperonin GroEL, *J Mol Biol.*, 425 (2013) 1476-1487, doi: 10.1016/j.jmb.2012.11.028.
- [5.25] I. Coluzza, S.M. van der Vies, D. Frenkel, Translocation boost protein-folding efficiency of double-barreled chaperonins, *Biophys J.*, 90 (2006) 3375-3381, doi: <http://dx.doi.org/10.1529/biophysj.105.074898>
- [5.26] K.L. Nielsen, N.J. Cowan, A single ring is sufficient for productive chaperonin-mediated folding in vivo, *Mol Cell.*, 2 (1998) 93-99, doi: [http://dx.doi.org/10.1016/S1097-2765\(00\)801173](http://dx.doi.org/10.1016/S1097-2765(00)801173).
- [5.27] S.R. Krystek, W.J. Metzler, J. Novotny, Hydrophobicity profiles for protein sequence analysis, *Curr Protoc Protein Sci.*, (2001) doi: 10.1002/0471140864.ps0202s00.
- [5.28] V.N. Uversky, Mysterious oligomerization of the amyloidogenic proteins, *FEBS Journal* 277 (2010) 2940-2953, doi: 10.1111/j.1742-4658.2010.07721.x.
- [5.29] R. Carrotta, C. Canale, A. Diaspro, A. Trapani, P.L. Biagio, D. Bulone, Inhibiting effect of a(s1)-casein on A β (1-40) fibrillogenesis, *Biochim Biophys Acta*, 1820 (2012) 124-132, doi: 10.1016/j.bbagen.2011.11.010.
- [5.30] F. Librizzi, R. Carrotta, D. Spigolon, D. Bulone, P.L. San Biagio, a-Casein inhibits insulin amyloid formation by preventing the onset of secondary nucleation processes, *J Phys Chem Lett.*, 5 (2014) 3034-3038 doi: 10.1021/jz501570m.
- [5.31] J. Stöhr, J.C. Watts, Z.L. Mensinger, A. Oehler, S.K. Grillo, S.J. DeArmond, S.B. Prusiner, K. Giles, Purified and synthetic Alzheimer's amyloid beta (A β) prions, *Proc Natl Acad Sci U S A*, 109 (2012) 11025-11030, doi: 10.1073/pnas.1206555109.
- [5.32] M.M. Wilhelmus, R.M. de Waal, M.M. Verbeek, Heat shock proteins and amateur chaperones in amyloid-Beta accumulation and clearance in Alzheimer's disease, *Mol Neurobiol.*, 35 (2007) 203-216, doi: 10.1007/s12035-007-0029-7.

VI

- [6.1] Shendure J., Akey J.M. The origins, determinants, and consequences of human mutations. *Science*. 349, (2015), 1478-83. DOI: 10.1126/science.aaa9119.
- [6.2] Macario, A.J.L., Conway de Macario, E. Sick chaperones, cellular stress and disease. *New Eng. J. Med.* 353, (2005), 1489-1501. DOI: 10.1056/NEJMra050111.
- [6.3] Joachimiak L.A., Walzthoeni T., Liu Corey W., Aebersold R., Frydman J. The structural basis of substrate recognition by the eukaryotic chaperonin TRiC/CCT. *Cell*. 159, (2014), 1042–1055. DOI: 10.1016/j.cell.2014.10.042.
- [6.4] Lopez T., Dalton K., Frydman J. The mechanism and function of Group II Chaperonins. *J. Mol. Biol.* 427, (2015), 2919–2930. DOI: 10.1016/j.jmb.2015.04.013.
- [6.5] Macario A.J.L, Conway de Macario, E., Cappello, F. The Chaperonopathies. Diseases with Defective Molecular Chaperones. Springer Dordrecht-Heidelberg-New York-London. (2013). DOI: 10.1007/978-94-007-4667-1.
- [6.6] Rommelaere H., Van Troys M., Gao Y., Melki R., Cowan N.J., Vandekerckhove J., Ampe C. Eukaryotic cytosolic chaperonin contains t-complex polypeptide 1 and seven related subunits. *Proc. Natl. Acad. Sci. USA*. 90, (1993), 11975–11979. DOI: 10.1073/pnas.90.24.11975.
- [6.7] Chen X., Sullivan D.S., Huffaker T.C. Two yeast genes with similarity to TCP-1 are required for microtubule and actin function in vivo. *Proc. Natl. Acad. Sci. USA* 91, (1994), 9111–9115. DOI: 10.1073/pnas.91.19.9111.
- [6.8] Thulasiraman V., Yang C.F., Frydman J. In vivo newly translated polypeptides are sequestered in a protected folding environment. *EMBO J.* 18, (1999), 85–95. DOI: 10.1093/emboj/18.1.85.
- [6.9] Spiess C., Meyer A.S., Reissmann S., Frydman J. Mechanism of the eukaryotic chaperonin: protein folding in the chamber of secrets. *Trends Cell Biol.* 14, (2004), 598–604. DOI: 10.1016/j.tcb.2004.09.015.
- [6.10] Yam A.Y., Xia Y., Lin H.T., Burlingame A, Gerstein M, Frydman J. Defining the TRiC/CCT interactome links chaperonin function to stabilization of newly made proteins with complex topologies. *Nat. Struct. Mol. Biol.* (2008) Dec;15(12):1255-62. doi: 10.1038/nsmb.1515. Epub 2008 Nov 16. PMID: 19011634.
- [6.11] Amit M., Weisberg S.J., Nadler-Holly M., McCormack E.A., Feldmesser. E., Kaganovich D., Willison K.R., Horovitz A. Equivalent mutations in the eight subunits of the chaperonin CCT produce dramatically different cellular and gene expression phenotypes. *J. Mol. Biol.* (2010) Aug 20;401(3):532-43. doi: 10.1016/j.jmb.2010.06.037. Epub 2010 Jun 25. PMID: 20600117.

- [6.12] Kitamura A., Kubota H., Pack C.G., Matsumoto G., Hirayama S., Takahashi Y., Kimura H., Kinjo M., Morimoto R.I., Nagata K. Cytosolic chaperonin prevents polyglutamine toxicity with altering the aggregation state. *Nat. Cell Biol.* (2006) Oct;8(10):1163-1170. DOI: 10.1038/ncb1478. Epub 2006 Sep 17. PMID: 16980958.
- [6.13] Shahmoradian SH, Galaz-Montoya JG, Schmid MF, Cong Y, Ma B, Spiess C, Frydman J, Ludtke SJ, Chiu W. TRiC's tricks inhibit huntingtin aggregation. *Elife.* (2013) Jul 9;2:e00710. doi: 10.7554/eLife.00710. PMID: 23853712.
- [6.14] Gregersen N., Bross P., Jorgensen M.M., Corydon T.J., Andresen B.S. Defective folding and rapid degradation of mutant proteins is a common disease mechanism in genetic disorders. *J. Inherit. Metab. Dis.* 23, (2000), 441–447. DOI:10.1023/A:1005663728291.
- [6.15] Dobson C.M. Principles of protein folding, misfolding and aggregation. *Semin. Cell Dev. Biol.* 15, (2004), 3–16. DOI: 10.1016/j.semcdb.2003.12.008.
- [6.16] Meyer A.S., Gillespie J.R., Walther D., Millet I.S., Doniach S., Frydman J. Closing the folding chamber of the eukaryotic chaperonin requires the transition state of ATP hydrolysis. *Cell.* 113, (2003), 369–381. DOI: 10.1016/S0092-8674(03)00307-6.
- [6.17] Min W., Angileri F., Luo H., Lauria A., Shanmugasundaram M., Almerico A.M., Cappello F., Conway de Macario E., Lednev I.K., Macario A.J.L., Robb F.T. A human CCT5 gene mutation causing distal neuropathy impairs hexadecamer assembly in an archaeal model. *Sci. Rep.* (2014) 4:6688. DOI: 10.1038/srep06688.
- [6.18] Bouhouche, A., Benomar, A., Bouslam, N., Chkili, T., Yahyaoui, M. Mutation in the epsilon subunit of the cytosolic chaperonin-containing t-complex peptide-1 (Cct5) gene causes autosomal recessive mutilating sensory neuropathy with spastic paraplegia. *J. Med. Genet.* 43, (2006), 441-443. DOI: 10.1136/jmg.2005.039230.
- [6.19] Cappello F., Marino Gammazza A., Palumbo Piccionello A., Campanella C., Pace A., Conway de Macario E., Macario A.J.L.. Hsp60 chaperonopathies and chaperonotherapy: targets and agents. *Exp. Op. Ther. Targets* (2014), 18: 185-208. On line first, November 29, 2013. DOI:10.1517/14728222.2014.856417.
- [6.20] Luo, H., Laksanalamai, P., Robb, F.T. An exceptionally stable Group II chaperonin from the hyperthermophile *Pyrococcus furiosus*. *Arch. Biochem. Biophys.* 486, (2009), 12-18. DOI: 10.1016/j.abb.2009.03.005.
- [6.21] Freire E. Statistical thermodynamic analysis of the heat capacity function associated with protein folding-unfolding transitions. *Comm. Mol. Cell. Biophys.* 6, (1989), 123±140.
- [6.22] Cohen S.S., Riven I., Cortajarena A.L., De Rosa L., D'Andrea L.D., Regan L., Haran G. Probing the molecular origin of native-state flexibility in repeat proteins. *J. Am. Chem. Soc.* 137(32), (2015) 10367-73. DOI: 10.1021/jacs.5b06160.

- [6.23] Barranco-Medina S., Kakorin S., Lázaro J.J., Dietz K.J. Thermodynamics of the dimer-decamer transition of reduced human and plant 2-cys peroxiredoxin. *Biochemistry*. (2008) Jul 8;47(27):7196-204. doi: 10.1021/bi8002956. Epub 2008 Jun 14. PMID: 18553980.
- [6.24] Privalov P.L., Dragan A.I. Microcalorimetry of biological macromolecules. *Biophys. Chem.* 126(1-3), (2007), 16-24. DOI: 10.1016/j.bpc.2006.05.004.
- [6.25] Lakshminarayanan R., Fan D., Du C., and Moradian-Oldak J. The role of secondary structure in the entropically driven amelogenin self-assembly. *Biophys. J.* 93, (2007), 3664–3674. DOI: 10.1529/biophysj.107.113936.
- [6.26] Abraham T., Lewis R.N, Hodges R.S., and McElhaney R.N. Isothermal titration calorimetry studies of the binding of a rationally designed analogue of the antimicrobial peptide gramicidin S to phospholipid bilayer membranes. *Biochemistry*. 44, (2005), 2103–2112. DOI: 10.1021/bi048077d.
- [6.27] Barisas B. G., Gill S, J. Microcalorimetry of Biological Systems, *Ann. Rev. Physical Chem.*, 29, (1978), 141-166. DOI: 10.1146/annurev.pc.29.100178.001041.
- [6.28] Cong Y., Schroder F. G., Meyer A. S., Jakana J., Ma B., Dougherty M. T., Schmid M. F., Reissmann S., Levitt M., Ludtke S. L., Frydman J., Chiu W. Symmetry-free cryo-EM structures of the chaperonin TRiC along its ATPase-driven conformational cycle. *The EMBO J.* 31, (2011) 720–730. DOI: 10.1038/emboj.2011.366.
- [6.29] Reissmann, S.; Parnot, C.; Booth, C.R.; Chiu, W.; Frydman, J. Essential function of the built-in lid in the allosteric regulation of eukaryotic and archaeal chaperonins. *Nat. Struct. Mol. Biol.* 14, (2007), 432–440. DOI: 10.1038/nsmb1236.
- [6.30] Sreerama N, Woody RW. Estimation of protein secondary structure from circular dichroism spectra: comparison of CONTIN, SELCON, and CDSSTR methods with an expanded reference set. *Anal. Biochem.* (2000) Dec 15;287(2):252-60. PMID: 11112271.

VII

- [7.1] Brange, J.; Andersen, L.; Laursen, E. D.; Meyn, G.; Rasmussen, E. Toward Understanding Insulin Fibrillation. *J. Pharm. Sci.* 1997, 86, 517–525.
- [7.2] Waugh, D. F. A Fibrous Modification of Insulin. I. The Heat Precipitation of Insulin. *J. Am. Chem. Soc.* 1946, 68, 247–250.
- [7.3] Waugh, D. F.; Wilhelmson, D. F.; Commerford, S. L.; Sackler, M. L. Studies on the Nucleation and Growth Reactions of Selected Types of Insulin Fibrils. *J. Am. Chem. Soc.* 1953, 75, 2592–2600.
- [7.4] Nielsen, L.; Khurana, R.; Coats, A.; Frokjaer, S.; Brange, J.; Vyas, S.; Uversky, V. N.; Fink, A. L. Effect of Environmental Factors on the Kinetics of Insulin Fibril Formation: Elucidation of the Molecular Mechanism. *Biochemistry* 2001, 40, 6036–6046.
- [7.5] Nielsen, L.; Frokjaer, S.; Brange, J.; Uversky, V. N.; Fink, A. L. Probing the Mechanism of Insulin Fibril Formation with Insulin Mutants. *Biochemistry* 2001, 40, 8397–8409.
- [7.6] Ivanova, M. I.; Sievers, S. A.; Sawaya, M. R.; Wall, J. S.; Eisenberg, D. Molecular Basis for Insulin Fibril Assembly. *Proc. Natl. Acad. Sci. U.S.A.* 2009, 106, 18990–18995.
- [7.7] Ferrone, F. A.; Hofrichter, J.; Eaton, W. A. Kinetics of Sickle Hemoglobin Polymerization. II. A Double Nucleation Mechanism. *J. Mol. Biol.* 1985, 183, 611–631.
- [7.8] Ferrone, F. A. Analysis of Protein Aggregation Kinetics. *Methods Enzymol.* 1999, 309, 256–274.
- [7.9] Foderà, V.; Cataldo, S.; Librizzi, F.; Pignataro, B.; Spiccia, P.; Leone, M. Self-Organization Pathways and Spatial Heterogeneity in Insulin Amyloid Fibril Formation. *J. Phys. Chem. B* 2009, 113, 10830–10837.
- [7.10] Grudzielanek, S.; Smirnovas, V.; Winter, R. Solvation-Assisted Pressure Tuning of Insulin Fibrillation: From Novel Aggregation Pathways to Biotechnological Applications. *J. Mol. Biol.* 2006, 356, 497–509.
- [7.11] Levine, H. Quantification of β -Sheet Amyloid Structures with Thioflavin T. *Methods Enzymol.* 1999, 309, 256–274.
- [7.12] Foderà, V.; Groenning, M.; vetri, V.; Librizzi, F.; Spagnolo, S.; Cornett, C.; Olsen, L.; van de Weert, M.; Leone, M.; Thioflavin, T. Hydroxylation at Basic Ph and Its Effect on Amyloid Fibril Detection. *J. Phys. Chem. B* 2008, 112, 15174–15181.
- [7.13] Carrotta, R.; Canale, C.; Diaspro, A.; Trapani, A.; San Biagio, P. L.; Bulone, D. Inhibiting Effect of α s1-Casein on A β 1–40 Fibrillogenesis. *Biochim. Biophys. Acta* 2012, 1820, 124–132.

[7.14] Jansen, R.; Dzwolak, W.; Winter, R. Amyloidogenic Self-Assembly of Insulin Aggregates Probed by High Resolution Atomic Force Microscopy. *Biophys. J.* 2005, 88, 1344–1353.

[7.15] Thorn, D. C.; Ecroyd, H.; Carver, J. A. The Two-Faced Nature of Milk Casein Proteins: Amyloid Fibril Formation and Chaperone- Like Activity. *Austr. J. Dairy. Technol.* 2009, 64, 34–40.

[7.16] Dzwolak, W.; Jansen, R.; Smirnovas, V.; Lokszejn, A.; Porowski, S.; Winter, R. Template-Controlled Conformational Patterns of Insulin fibrillar Self-Assembly Reflect History of Solvation of the Amyloid Nuclei. *Phys. Chem. Chem. Phys.* 2005, 7, 1349–1351.

[7.17] Foderà, V.; Pagliara, S.; Otto, O.; Keyser, U. F.; Donald, A. M. Microfluidics Reveals a Flow-Induced Large-Scale Polymorphism of Protein Aggregates. *J. Phys. Chem. Lett.* 2012, 3, 2803–2807.

[7.18] Rogers, S. S.; Krebs, M. R. H.; Bromley, E. H. C.; van der Linden, E.; Donald, A. M. Optical Microscopy of Growing Insulin Amyloid Spherulites on Surfaces in Vitro. *Biophys. J.* 2006, 90, 1043–1054.

[7.19] Smirnovas, V.; Winter, R. Revealing Different Aggregation Pathways of Amyloidogenic Proteins by Ultrasound Velocimetry. *Biophys. J.* 2008, 90, 3241–3246.

[7.20] Dzwolak, W.; Smirnovas, V.; Jansen, R.; Winter, R. Insulin Forms Amyloid in a Strain-Dependent Manner: An Ft-Ir Spectroscopic Study. *Protein Sci.* 2004, 13, 1927–1932.

[7.21] Dzwolak, W.; Grudzielanek, S.; Smirnovas, V.; Ravindra, R.; Nicolini, C.; Jansen, R.; Lokszejn, A.; Porowski, S.; Winter, R. Ethanol-Perturbed Amyloidogenic Self-Assembly of Insulin: Looking for Origins of Amyloid Strains. *Biochemistry* 2005, 44, 8948–8958.

[7.22] Kurouski, D.; Deckert-Gaudig, T.; Deckert, V.; Lednev, I. K. Structure and Composition of Insulin Fibril Surfaces Probed by Ters. *J. Am. Chem. Soc.* 2012, 134, 13323–13329.

[7.23] Kurouski, D.; Dukor, R. K.; Lu, X.; Nafie, L. A.; Lednev, I. K. Normal and Reversed Supramolecular Chirality of Insulin Fibrils Probed by Vibrational Circular Dichroism at the Protofilament Level of Fibril Structure. *Biophys. J.* 2012, 103, 522–531.

[7.24] Kurouski, D.; Deckert-Gaudig, T.; Deckert, V.; Lednev, I. K. Surface Characterization of Insulin Protofilaments and Fibril Polymorphs Using Tip-Enhanced Raman Spectroscopy [TERS]. *Biophys. J.* 2014, 106, 263–271.

[7.25] Treweek, T. M. Alpha-Casein as a Molecular Chaperone. In *Milk Protein*; Hurley, W. L., Ed.; InTech: Rijeka, Croatia, 2012; pp 85– 119.

- [7.26] Flyvbjerg, H.; Jobs, E.; Leibler, S. Kinetics of Self-Assembling Microtubules: An “Inverse Problem” in Biochemistry. *Proc. Natl. Acad. Sci. U.S.A.* 1996, 93, 5975–5979.
- [7.27] Oosawa, F.; Asakura, S. *Thermodynamics of the Polymerization of Proteins*; Academic Press: New York, 1975.
- [7.28] Morgan, P. E.; Treweek, T. M.; Lindner, R. A.; Price, W. E.; Carver, J. A. Casein Proteins as Molecular Chaperones. *J. Agric. Food. Chem.* 2005, 53, 2670–2683.
- [7.29] Foderà, V.; van de Weert, M.; Vestergaard, B. Large-Scale Polymorphism and Auto-Catalytic Effect in Insulin Fibrillogenesis. *Soft Matter* 2010, 6, 4416–4419.
- [7.30] Horne, D. S. Casein Micelle Structure: Models and Muddles. *Curr. Opin. Interface Sci.* 2006, 11, 148–153.
- [7.31] Librizzi, F.; Rischel, C. The Kinetic Behavior of Insulin Fibrillation Is Determined by Heterogeneous Nucleation Pathways. *Protein Sci.* 2005, 14, 3129–3134.
- [7.32] Manno, M.; Craparo, E. F.; Martorana, V.; Bulone, D.; San Biagio, P. L. Kinetics of Insulin Aggregation: Disentanglement of Amyloid Fibrillation from Large-Size Cluster Formation. *Biophys. J.* 2006, 90, 4585–4591.
- [7.33] Librizzi, F.; Foderà, V.; Vetri, V.; Lo Presti, C.; Leone, M. Effects of Confinement on Insulin Amyloid Fibrils Formation. *Eur. Biophys. J.* 2007, 36, 711–715.
- [7.34] Manno, M.; Craparo, E. F.; Podestà, A.; Bulone, D.; Carrotta, R.; Martorana, V.; Tiana, G.; San Biagio, P. L. Kinetics of Different Processes in Human Insulin Amyloid Formation. *J. Mol. Biol.* 2007, 366, 258–274.
- [7.35] Foderà, V.; Librizzi, F.; Groenning, M.; van de Weert, M.; Leone, M. Secondary Nucleation and Accessible Surface in Insulin Amyloid Fibril Formation. *J. Phys. Chem. B* 2008, 112, 3853–3858.
- [7.36] Meisl, G.; Yang, X.; Hellstrand, E.; Frohm, B.; Kirkegaard, J. B.; Cohen, S. I. A.; Dobson, C. M.; Linse, S.; Knowles, P. J. Differences in Nucleation Behavior Underlie the Contrasting Aggregation Kinetics of the A β 40 and A β 42 Peptides. *Proc. Natl. Acad. Sci. U.S.A.* 2014, 111, 9384–9389.
- [7.37] Knight, S. D.; Presto, J.; Linse, S.; Johansson, J. The BRICHOS Domain, Amyloid Fibril Formation, and Their Relationship. *Biochemistry* 2013, 52, 7523–7531.
- [7.38] Hard, T. Amyloid Fibrils: Formation, Polymorphism, and Inhibition. *J. Phys. Chem. Lett.* 2014, 5, 607–614.
- [7.39] Lowe, T. L.; Strzelec, A.; Kiessling, L. L.; Murphy, R. M. Structure-Function Relationships for Inhibitors of β -Amyloid Toxicity Containing the Recognition Sequence KLVFF. *Biochemistry* 2001, 40, 7882–7889.

Appendix

Supplementary data

A.1 FASTA sequences

Pyrococcus furiosus (archaeal) CCT subunit: FASTA sequences

Pyrococcus furiosus chaperonin (the archaeal Pf-Cpn). Ile (I) at position 138.

>gi|18978346|ref|NP_579703.1| thermosome, single subunit [*Pyrococcus furiosus* DSM 3638].

Name: Pf-Cpn (549 amino acids). **Note:** this molecule was not studied in the work presented but it is shown here because it is the master molecule from which all studied mutants are derived.

MAQLAGQPILILPEGTQRYVGRDAQRMNILAARIVAETIRTTLGPKGMDKMLVDSLGDIVI
TNDGATILDEMDIQHPAAKMMVEVAKTQDKEAGDGTTTAVVIAGELLRKAEEELLDQNIH
PSIIKGYTLAAQKAQEILENIAKEVKPDDEEILLKAAMTSITGKAAEEEREYLAKLAVEAV
KLVAEKEDGKYKVDIDNIKLEKKEGGSVRDTQLIRGVVIDKEVVHPGMPKRVEKAKIALI
NDALEVKETETDAEIRITSPEQLQAFLEQEERMLREMVEKIKEVGANVVFVQKGIDDLAQ
HYLAKYGIMAVRRVKKSDMEKLAKATGAKIVTNIRDLTPEDLGYAELVEERKVAGESMI
FVEGCQNPKAVTILIRGGTEHVVDEVERALEDAIKVVKDILEDGKILAGGGAPEIELAIRLD
EYAKEVGGKEQLAIEAFAEALKVIPRTLAENAGLDPIETLVKVIAAAHKEKGPTIGVDVYEG
EPADMLERGVIEPLRVKKQAIKSASEAAIMILRIDDVIAASKLEKEKEKEGEKGGGSEDF
SSDLLD

Mutants studied

Pyrococcus furiosus chaperonin Pf-Cpn mutant CD1, namely the wild type without the last 22 amino acids

Name: Pf-CD1. (527 amino acids).

MAQLAGQPILILPEGTQRYVGRDAQRMNILAARIVAETIRTTLGPKGMDKMLVDSLGDIVI
TNDGATILDEMDIQHPAAKMMVEVAKTQDKEAGDGTTTAVVIAGELLRKAEEELLDQNIH
PSIIKGYTLAAQKAQEILENIAKEVKPDDEEILLKAAMTSITGKAAEEEREYLAKLAVEAV
KLVAEKEDGKYKVDIDNIKLEKKEGGSVRDTQLIRGVVIDKEVVHPGMPKRVEKAKIALI
NDALEVKETETDAEIRITSPEQLQAFLEQEERMLREMVEKIKEVGANVVFVQKGIDDLAQ
HYLAKYGIMAVRRVKKSDMEKLAKATGAKIVTNIRDLTPEDLGYAELVEERKVAGESMI
FVEGCQNPKAVTILIRGGTEHVVDEVERALEDAIKVVKDILEDGKILAGGGAPEIELAIRLD
EYAKEVGGKEQLAIEAFAEALKVIPRTLAENAGLDPIETLVKVIAAAHKEKGPTIGVDVYEG
EPADMLERGVIEPLRVKKQAIKSASEAAIMILRIDDVIAASKL

***Pyrococcus furiosus* chaperonin Pf-Cpn mutant CD1, namely the wild type without the last 22 amino acids, with His (H) instead of Ile at position 138 (Ile138His).**

Name: Pf-CD1 His 138; Pf-H in short. (527 amino acids).

MAQLAGQPILILPEGTQRYVGRDAQRMNILAARIVAETIRTTLGPKGMDKMLVDSLGDIVI
TNDGATILDEMDIQHPAAKMMVEVAKTQDKEAGDGTAVVIAGELLRKAEEELLDQNIH
PSIIKGYTLAAQKAQEHLENIAKEVKPDDEEILLKAAMTSITGKAAEEEREYLAKLAVEA
VKLVAEKEDGKYKVDIDNIKLEKKEGGSVRDTQLIRGVVIDKEVVHPGMPKRVEKAKIAL
INDALEVKETETDAEIRITSPEQLQAFLEQEERMLREMVEKIKEVGANVVFVQKGIDDLAQ
HYLAKYGIMAVRRVKKSDMEKLAKATGAKIVTNIRDLTPEDLGYAELVEERKVAGESMI
FVEGCQNPKA V TILIRGGTEHVVDEVERALEDAIKVVKDILEDGKILAGGGAPEIELAIRLD
EYAKEVGGKEQLAIEFAEALKVIPRTLAENAGLDPIETLVKVIAAAHKEKGP TIGVDVYEG
EPADMLERGVIEPLRVKKQAIKSASEAAIMILRIDDVIAASKL

***Pyrococcus furiosus* chaperonin Pf-Cpn mutant CD1, namely the wild type without the last 22 amino acids, with Arg (R) instead of Ile or His at position 138 (Ile148Arg).**

Name: Pf-CD1 Arg 138; Pf-R in short. (527 amino acids).

MAQLAGQPILILPEGTQRYVGRDAQRMNILAARIVAETIRTTLGPKGMDKMLVDSLGDIVI
TNDGATILDEMDIQHPAAKMMVEVAKTQDKEAGDGTAVVIAGELLRKAEEELLDQNIH
PSIIKGYTLAAQKAQERLENIAKEVKPDDEEILLKAAMTSITGKAAEEEREYLAKLAVEA
VKLVAEKEDGKYKVDIDNIKLEKKEGGSVRDTQLIRGVVIDKEVVHPGMPKRVEKAKIAL
INDALEVKETETDAEIRITSPEQLQAFLEQEERMLREMVEKIKEVGANVVFVQKGIDDLAQ
HYLAKYGIMAVRRVKKSDMEKLAKATGAKIVTNIRDLTPEDLGYAELVEERKVAGESMI
FVEGCQNPKA V TILIRGGTEHVVDEVERALEDAIKVVKDILEDGKILAGGGAPEIELAIRLD
EYAKEVGGKEQLAIEFAEALKVIPRTLAENAGLDPIETLVKVIAAAHKEKGP TIGVDVYEG
EPADMLERGVIEPLRVKKQAIKSASEAAIMILRIDDVIAASKL

A.2 Nucleotide effect on Pf-CD1, Pf-H, Pf-R

Secondary structure composition and assignments from Circular Dichroism spectra for native and upon the binding with ATP

